UNIVERSIDADE FEDERAL DE SÃO CARLOS
CENTRO DE CIÊNCIAS E TECNOLOGIA PARA A SUSTENTABILIDADE
PROGRAMA DE PÓS-GRADUAÇÃO EM CIÊNCIA DOS MATERIAIS

Samir Leite Mathias

MODIFICAÇÃO QUÍMICA DE QUITOSANA COM ETOXIMETILENOS: OTIMIZAÇÃO REACIONAL, CARACTERIZAÇÃO E APLICAÇÃO NA ADSORÇÃO DE CRISTAL VIOLETA E DICLOFENACO.

Sorocaba

2026

UNIVERSIDADE FEDERAL DE SÃO CARLOS
CENTRO DE CIÊNCIAS E TECNOLOGIA PARA A SUSTENTABILIDADE
PROGRAMA DE PÓS-GRADUAÇÃO EM CIÊNCIA DOS MATERIAIS

Samir Leite Mathias

MODIFICAÇÃO QUÍMICA DE QUITOSANA COM ETOXIMETILENOS: OTIMIZAÇÃO REACIONAL, CARACTERIZAÇÃO E APLICAÇÃO NA ADSORÇÃO DE CRISTAL VIOLETA E DICLOFENACO.

Tese apresentada ao Programa de Pós-Graduação em Ciência dos Materiais (PPGCM), como parte dos requisitos para obtenção do título de Doutor em Ciência dos Materiais da Universidade Federal de São Carlos.
Área de concentração: Materiais Funcionais e Polímeros de Fontes Renováveis

Orientação: Prof. Dr. Aparecido Junior de Menezes
Coorientação: Prof. Dr. Alain Dufresne
Financiamento: Fundação Coordenação de Aperfeiçoamento de Pessoal de Nível Superior (CAPES) – 001

Sorocaba

2026

Mathias, Samir Leite

Modificação química de quitosana com etoximetilenos: otimização reacional, caracterização e aplicação na adsorção de cristal violeta e diclofenaco / Samir Leite Mathias -- 2026.

158f.

Tese de Doutorado - Universidade Federal de São Carlos, campus Sorocaba, Sorocaba

Orientador (a): Aparecido Júnior de Menezes

Banca Examinadora: Douglas Cardoso Dragunski, Farayde Matta Fakhouri, Gean Henrique Marcatto de Oliveira, Jorge Augusto de Moura Delezuk

Bibliografia

1. Modificação química. 2. Adsorção de corantes e fármacos. I. Mathias, Samir Leite. II. Título.

Ficha catalográfica desenvolvida pela Secretaria Geral de Informática (SIn)

DADOS FORNECIDOS PELO AUTOR

Bibliotecário responsável: Maria Aparecida de Lourdes Mariano - CRB/8 6979

UFSCar

UNIVERSIDADE FEDERAL DE SÃO CARLOS

Centro de Ciências e Tecnologia para a Sustentabilidade

Programa de Pós-Graduação em Ciência dos Materiais

Folha de Aprovação

Defesa de Tese de Doutorado do candidato Samir Leite Mathias, realizada em 31/03/2026.

Comissão Julgadora:

Prof. Dr. Aparecido Junior de Menezes (UFSCar)

Prof. Dr. Douglas Cardoso Dragunski (Unioeste)

Profa. Dra. Farayde Matta Fakhouri (UPC/ BarcelonaTech)

Prof. Dr. Gean Henrique Marcatto de Oliveira (TU GRAZ)

Prof. Dr. Jorge Augusto de Moura Delezuk (IFSP)

O Relatório de Defesa produzido pelos membros da Comissão Julgadora encontra-se arquivado junto ao Programa de Pós-Graduação.

AGRADECIMENTOS

À minha avó, Luzinete (*in memoriam*), que me deu seu amor incondicional em todos os momentos possíveis e impossíveis.

Aos meus avôs, Salvador (*in memoriam*) e Salustiano (*in memoriam*), que, com suas vidas, me mostraram que podemos sempre recomeçar, às vezes do zero, às vezes com ajuda, ou às vezes não, mas que desistir não é uma opção.

Ao meu pai, Dário (*in memoriam*), que nos deixou muito cedo, mas que me ensinou resiliência e que, às vezes, fazer apenas o que você gosta, e não o que você deve fazer, é necessário.

À minha mãe, Maria Neuza, e ao meu irmão, Peterson, que, mesmo com todas as dificuldades, conseguiram me oferecer os meios para que eu pudesse estudar.

À Jéssika, minha esposa, pelo apoio incondicional durante toda a minha trajetória acadêmica e pela companhia de vida.

Ao Jorge, pelas grandes discussões pertinentes durante toda a vida acadêmica, pela companhia e conversas e pela rivalidade amigável.

Aos amigos Henrique e Fernanda, pela companhia e apoio durante a maior parte do doutorado.

Aos professores Aparecido Junior de Menezes, Robson Valentim Pereira e Alain Dufresne, pelas ricas discussões, pelo apoio e pelo grande auxílio na condução da pesquisa.

Aos amigos Vitor e Marcus, pelo companheirismo, colaborações e experiências vividas durante o curso.

Ao LGP^2, ao LabEx Tec 21 (Investissements d'Avenir n° ANR-11-LABX-0030) e ao PolyNat Carnot Institut (Investissements d'Avenir n° ANR-11-CARN-030-01), pelo suporte financeiro.

À equipe do LGP^2, por todo o auxílio durante os dez meses de doutorado sanduíche na França, em especial à Cécile Silard.

O presente trabalho foi realizado com apoio da Coordenação de Aperfeiçoamento de Pessoal de Nível Superior - Brasil (CAPES) - Código de Financiamento 001.

RESUMO

A presença crescente de contaminantes orgânicos em ambientes aquáticos tem despertado grande interesse no desenvolvimento de novos materiais adsorventes capazes de remover esses compostos de forma eficiente. Entre os materiais investigados para essa finalidade, a quitosana destaca-se como um biopolímero promissor devido à sua abundância, biodegradabilidade e presença de grupos funcionais reativos ao longo de sua cadeia polimérica. No entanto, as propriedades adsorptivas da quitosana podem ser significativamente ampliadas por meio de modificações químicas que permitam alterar sua estrutura e propriedades de superfície. Nesse contexto, este projeto teve como objetivo desenvolver derivados funcionalizados de quitosana por meio de reações de substituição nucleofílica vinílica utilizando derivados alcoximetilênicos contendo diferentes grupos substituintes e investigar a influência da natureza eletrônica e da densidade desses grupos funcionais sobre o desempenho adsorptivo do material. Inicialmente, foi investigada a modificação da quitosana utilizando Etoximetilenomalononitrila, permitindo estabelecer as condições reacionais para a funcionalização do polímero por meio da formação de estruturas enaminas conjugadas, alcançando grau de substituição de até 0,91. Posteriormente, novos derivados de quitosana foram sintetizados utilizando Dietiletoximetilenomalonato e Etil 2-ciano-3-etoxiacrilato (Etil (etoximetileno)cianoacetato), contendo grupos diéster e éster-nitrila, respectivamente. Para esses sistemas, as condições de reação foram otimizadas por meio de planejamento experimental, visando maximizar o grau de funcionalização do polímero. Os materiais obtidos foram caracterizados por diferentes técnicas, permitindo avaliar as modificações estruturais e físico-químicas decorrentes da introdução dos grupos funcionais. O desempenho adsorptivo dos derivados sintetizados foi investigado na remoção de contaminantes orgânicos modelo em solução aquosa, incluindo o corante cristal violeta e o fármaco diclofenaco. Os resultados demonstraram que a modificação química da quitosana promoveu alterações significativas nas propriedades de superfície do material, influenciando diretamente sua capacidade de adsorção. Observou-se que o aumento da densidade de grupos funcionais ao longo da cadeia polimérica contribuiu para o aumento da afinidade entre o material adsorvente e os contaminantes estudados, atingindo capacidade máxima de adsorção da ordem de 219 $mg.g^{-1}$ para diclofenaco e 383 $mg.g^{-1}$ para cristal violeta. De maneira geral, os resultados desta tese demonstram que a modificação da quitosana por meio de reações de substituição nucleofílica vinílica

constitui uma estratégia eficiente para o desenvolvimento de novos materiais adsorventes baseados em biopolímeros. Além de ampliar o desempenho adsorptivo da quitosana, essa abordagem sintética também abre novas perspectivas para o desenvolvimento de materiais poliméricos funcionalizados com propriedades ajustáveis para diferentes aplicações ambientais.

Palavras-chave: quitosana, modificação química, substituição nucleofílica vinílica, adsorção, contaminantes orgânicos.

ABSTRACT

The increasing presence of organic contaminants in aquatic environments has stimulated significant interest in the development of new adsorbent materials capable of efficiently removing these compounds from water. Among the materials investigated for this purpose, chitosan stands out as a promising biopolymer due to its abundance, biodegradability, and the presence of reactive functional groups along its polymeric backbone. However, the adsorption performance of chitosan can be significantly enhanced through chemical modifications that alter its structure and surface properties. In this context, the aim of this project was to develop functionalized chitosan derivatives through nucleophilic vinylic substitution reactions using alkoxymethylene derivatives bearing different substituent groups, and to investigate how the electronic nature and density of these functional groups influence the adsorption performance of the material. Initially, chitosan was modified using (Ethoxymethylene)malononitrile, allowing the establishment of suitable reaction conditions for polymer functionalization through the formation of conjugated enamine structures, achieving a degree of substitution of up to 0.91. Subsequently, new chitosan derivatives were synthesized using Diethylethoxymethylenemalonate and Ethyl 2-cyano-3-ethoxyacrylate (Ethyl (ethoxymethylene)cyanoacetate), introducing diester and ester–nitrile groups, respectively. For these systems, reaction conditions were optimized using a design of experiments approach in order to maximize the degree of polymer functionalization. The obtained materials were characterized by different analytical techniques to evaluate the structural and physicochemical modifications resulting from the introduction of these functional groups. The adsorption performance of the synthesized derivatives was evaluated for the removal of model organic contaminants from aqueous solutions, including the dye crystal violet and the pharmaceutical compound diclofenac. The results demonstrated that chemical modification of chitosan significantly altered the surface properties of the material, directly influencing its adsorption capacity. An increase in the density of functional groups along the polymer chain led to enhanced affinity between the adsorbent material and the investigated contaminants, reaching a maximum adsorption capacity on the order of 219 $mg.g^{-1}$ for diclofenac and 383 $mg.g^{-1}$ for violet crystal. Overall, the results obtained in this thesis demonstrate that the chemical modification of chitosan through nucleophilic vinylic substitution reactions represents an efficient strategy for the development of new biopolymer-based adsorbent materials. In

addition to improving the adsorption performance of chitosan, this synthetic approach also opens new perspectives for the development of functional polymeric materials with tunable properties for environmental applications.

Keywords: chitosan, chemical modification, nucleophilic vinylic substitution, adsorption, organic contaminants.

SUMÁRIO

1. INTRODUÇÃO

1.1. CONTAMINAÇÃO AMBIENTAL POR POLUENTES ORGÂNICOS

O crescimento populacional, a intensificação das atividades industriais e o aumento do consumo de produtos químicos nas últimas décadas têm contribuído significativamente para a introdução contínua de contaminantes orgânicos em ambientes aquáticos. Esses compostos são frequentemente detectados em rios, lagos, águas subterrâneas e efluentes de estações de tratamento, representando um desafio relevante para a qualidade dos recursos hídricos e para a saúde dos ecossistemas aquáticos. Entre os diferentes grupos de contaminantes, corantes sintéticos e fármacos têm recebido atenção especial devido à sua elevada estabilidade no meio ambiente, complexidade estrutural e resistência aos processos convencionais de tratamento de água (Ahmed et al., 2021; Rodriguez-Narvaez et al., 2022; Rout et al., 2021).

Os corantes sintéticos são amplamente utilizados em diversas indústrias, incluindo os setores têxtil, farmacêutico, cosmético, alimentício e de papel. Estima-se que milhares de toneladas desses compostos sejam produzidas anualmente em escala global, sendo que uma fração significativa acaba sendo liberada em efluentes industriais durante processos de fabricação e aplicação (Aijaz; Shafi and; Shahid, 2025). Muitos desses corantes apresentam estruturas aromáticas altamente conjugadas, frequentemente associadas a grupos cromóforos e auxocrômicos que conferem elevada estabilidade química e resistência à degradação natural (Islam et al., 2022). Como consequência, a presença desses compostos em corpos d'água pode provocar alterações na penetração da luz, afetar processos fotossintéticos e causar impactos negativos em organismos aquáticos (Sudarshan et al., 2023).

Além dos corantes industriais, os fármacos têm emergido como uma classe particularmente preocupante de contaminantes ambientais. O aumento da produção e do consumo de medicamentos, associado ao descarte inadequado e à excreção de metabólitos ativos por organismos humanos e animais, tem resultado na presença contínua desses compostos em sistemas aquáticos (Rodriguez-Narvaez et al., 2022). Entre os diferentes grupos farmacêuticos, os anti-inflamatórios não esteroidais (AINEs) estão entre os mais frequentemente detectados em efluentes urbanos e em águas superficiais. Dentre esses compostos, o diclofenaco destaca-se pela elevada taxa de consumo global e pela sua persistência ambiental, sendo frequentemente identificado em concentrações detectáveis

mesmo após processos convencionais de tratamento de águas residuais (Alessandretti et al., 2021; Warren-Vega et al., 2023).

A presença de fármacos em ambientes aquáticos tem sido associada a diversos efeitos ecotoxicológicos, incluindo alterações fisiológicas em organismos aquáticos, bioacumulação e possíveis impactos na saúde humana através da cadeia alimentar (Rodriguez-Narvaez et al., 2022). Além disso, muitos desses compostos apresentam elevada estabilidade química e baixa biodegradabilidade, dificultando sua remoção por processos biológicos convencionais empregados em estações de tratamento de efluentes (Rout et al., 2021).

1.2. TECNOLOGIAS PARA REMOÇÃO DE CONTAMINANTES ORGÂNICOS EM ÁGUA

A presença persistente de contaminantes orgânicos em sistemas aquáticos tem impulsionado o desenvolvimento de diferentes tecnologias destinadas à sua remoção em processos de tratamento de água e efluentes. De maneira geral, essas tecnologias podem ser classificadas em processos biológicos, processos físico-químicos e métodos baseados em separação ou adsorção, cada um apresentando características operacionais e níveis de eficiência distintos dependendo da natureza do contaminante (Ahmed et al., 2021).

Os processos biológicos constituem a base da maioria das estações de tratamento de efluentes, sendo amplamente utilizados para a remoção de matéria orgânica biodegradável por meio da atividade metabólica de microrganismos. Sistemas como lodos ativados e reatores anaeróbios apresentam elevada eficiência para compostos facilmente degradáveis. No entanto, muitos poluentes orgânicos modernos apresentam estruturas químicas complexas e elevada estabilidade molecular, o que limita sua degradação biológica. Como consequência, diferentes classes de contaminantes orgânicos podem persistir após o tratamento biológico convencional. Entre esses compostos destacam-se corantes sintéticos amplamente utilizados em processos industriais, como o cristal violeta, bem como fármacos frequentemente detectados em ambientes aquáticos, como o diclofenaco (Vide Figura 1) (Alessandretti et al., 2021; Rout et al., 2021).

Figura 1 - Fármaco (diclofenaco de sódio) e corante (cristal violeta) utilizados como contaminantes orgânicos modelo.

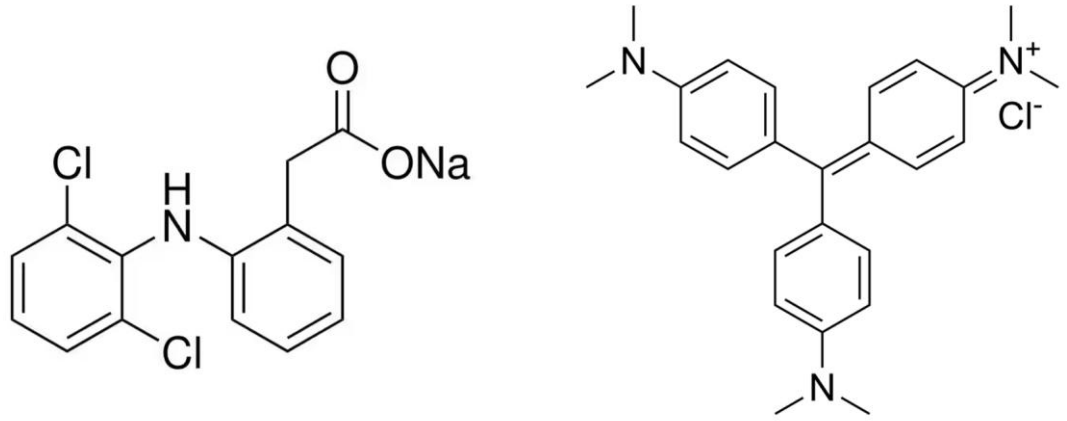

Diclofenaco de sódio Cristal violeta

Fonte: Próprio autor

Para superar essas limitações, diversos processos físico-químicos têm sido investigados, incluindo oxidação avançada, fotocatálise, coagulação-floculação e separação por membranas. Processos de oxidação avançada, por exemplo, baseiam-se na geração de espécies altamente reativas capazes de degradar moléculas orgânicas complexas. Embora eficientes em determinadas condições, esses métodos frequentemente requerem elevado consumo energético e podem gerar subprodutos intermediários cuja toxicidade deve ser cuidadosamente avaliada (Ahmed et al., 2021).

Tecnologias baseadas em membranas, como nanofiltração e osmose reversa, também apresentam elevada eficiência na remoção de contaminantes dissolvidos. Entretanto, limitações relacionadas ao custo operacional, fouling das membranas e necessidade de tratamento do concentrado gerado durante o processo ainda restringem sua aplicação em larga escala (Rout et al., 2021).

Nesse contexto, a adsorção tem se destacado como uma alternativa particularmente promissora para o tratamento de águas contaminadas por compostos orgânicos. Esse processo baseia-se na transferência de espécies presentes em solução para a superfície de um material sólido, denominado adsorvente, por meio de interações físico-químicas que podem envolver forças eletrostáticas, interações dipolares, ligações de hidrogênio ou interações π-π (Aijaz; Shafi and; Shahid, 2025). Entre suas principais

vantagens destacam-se a simplicidade operacional, a elevada eficiência para diferentes classes de contaminantes e a possibilidade de regeneração dos materiais adsorventes.

1.3. BIOPOLÍMEROS COMO MATERIAIS ADSORVENTES

O desempenho de processos de adsorção está diretamente relacionado às propriedades físico-químicas do material adsorvente. Parâmetros como área de superfície específica, porosidade, distribuição de sítios ativos e natureza dos grupos funcionais presentes na superfície desempenham papel fundamental na determinação da capacidade e seletividade de adsorção. Tradicionalmente, materiais como carvão ativado, sílicas modificadas, zeólitas e diversos materiais carbonáceos têm sido amplamente utilizados para a remoção de contaminantes orgânicos em água devido à sua elevada área de superfície específica e capacidade de interação com diferentes espécies químicas (Kowanga; Nyairo, 2025).

Apesar de sua eficiência, muitos desses materiais apresentam limitações relacionadas ao custo de produção, à dificuldade de regeneração e ao impacto ambiental associado à sua síntese ou descarte. Nesse cenário, biopolímeros naturais têm emergido como candidatos promissores para o desenvolvimento de novos materiais adsorventes (El-Araby et al., 2023). Esses materiais apresentam vantagens significativas, como abundância, biodegradabilidade e elevada densidade de grupos funcionais capazes de interagir com diferentes espécies químicas em solução.

Biopolímeros são macromoléculas produzidas por organismos vivos ou obtidas a partir de recursos naturais renováveis (Vide Figura 2). Entre os exemplos mais estudados encontram-se a celulose, o alginato, a lignina, a quitina e a quitosana. Esses materiais apresentam uma característica particularmente interessante para aplicações em adsorção: a presença de diferentes grupos funcionais ao longo de suas cadeias poliméricas, como hidroxilas, aminas e grupos carboxílicos. Tais funcionalidades conferem aos biopolímeros a capacidade de estabelecer diferentes tipos de interações com espécies químicas presentes em solução, incluindo interações eletrostáticas, ligações de hidrogênio, interações dipolares e forças de van der Waals (Wang et al., 2023).

Figura 2 - Exemplos de biopolímeros naturais.

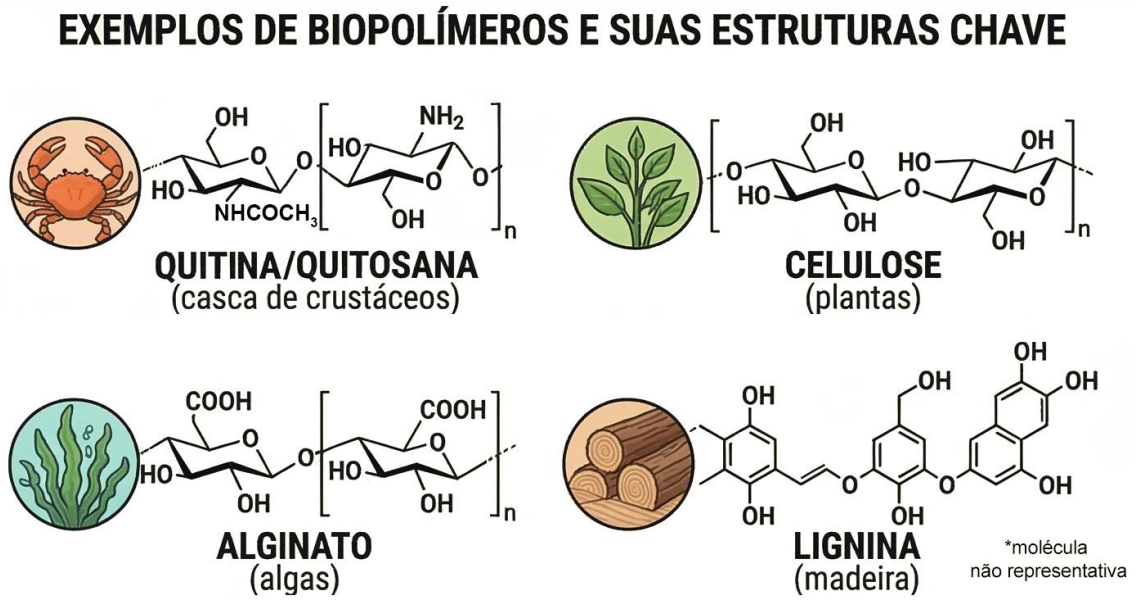

Fonte: Próprio autor

Outra vantagem significativa desses materiais reside na possibilidade de modificação química de suas estruturas. A introdução de novos grupos funcionais ao longo da cadeia polimérica permite ajustar propriedades como polaridade de superfície, densidade de carga, hidrofobicidade e afinidade química com diferentes contaminantes. Dessa forma, a modificação química de biopolímeros tem sido amplamente explorada como estratégia para aumentar a eficiência de adsorção e ampliar o espectro de contaminantes que podem ser removidos a partir de soluções aquosas (Lehocký, 2025).

Diversos estudos têm demonstrado o potencial de biopolímeros na remoção de diferentes classes de poluentes orgânicos, incluindo corantes industriais e compostos farmacêuticos. Corantes catiônicos, como o cristal violeta, apresentam elevada estabilidade estrutural e são frequentemente utilizados como moléculas modelo em estudos de adsorção devido à sua forte coloração e facilidade de detecção espectrofotométrica (Ahmad; Ejaz, 2023). De forma semelhante, compostos farmacêuticos amplamente utilizados, como o diclofenaco, têm sido investigados como contaminantes modelos em estudos voltados ao desenvolvimento de novos materiais adsorventes, especialmente devido à sua ocorrência frequente em ambientes aquáticos (Alessandretti et al., 2021; Firmansyah; Alwan; Ullah, 2025).

1.4. QUITOSANA: ESTRUTURA, PROPRIEDADES E APLICAÇÕES

Entre os biopolímeros investigados para aplicações ambientais, a quitosana destaca-se como um dos materiais mais versáteis, principalmente devido à presença de grupos amina reativos ao longo de sua cadeia polimérica. Esses grupos funcionais não apenas contribuem para as propriedades adsorptivas intrínsecas do material, mas também possibilitam uma ampla variedade de modificações químicas capazes de alterar sua reatividade, polaridade e comportamento interfacial (Lehocký, 2025).

A quitosana é obtida a partir da desacetilação da quitina, um polissacarídeo natural amplamente distribuído na natureza e considerado o segundo polímero natural mais abundante no planeta, ficando atrás apenas da celulose (Vide

Figura 3) (Wang et al., 2023). A quitina é encontrada principalmente nos exoesqueletos de crustáceos, na cutícula de insetos e na parede celular de fungos. A conversão da quitina em quitosana ocorre por meio da remoção parcial dos grupos acetil presentes na estrutura do polímero, geralmente através de tratamento alcalino, resultando em uma cadeia polimérica composta predominantemente por unidades de β-(1→4)-2-amino-2-desoxi-D-glicose (El-Araby et al., 2023).

Figura 3 - Fontes naturais de quitina e sua rota de conversão química (desacetilação) para a obtenção de quitosana.

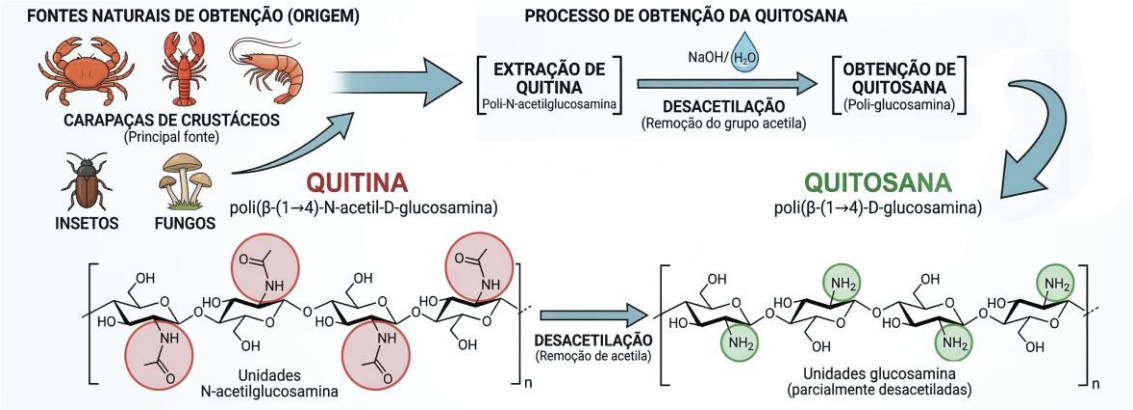

Fonte: Próprio autor

A estrutura química da quitosana é caracterizada pela presença de dois principais grupos funcionais reativos: grupos hidroxila localizados nas posições C_3 e C_6 da unidade glicosídica e grupos amina primários na posição C_2. Entre esses grupos, os grupos amina desempenham papel particularmente importante, pois podem ser protonados em meio ácido, conferindo ao polímero comportamento catiônico em solução aquosa. À medida

que o pH do meio aumenta, ocorre a desprotonação dos grupos amina, reduzindo a carga positiva da superfície e alterando o comportamento interfacial do material. Essa característica distingue a quitosana da maioria dos polissacarídeos naturais, que geralmente apresentam caráter neutro ou aniônico (Salama; Hesemann, 2025).

Além das propriedades ácido-base, outros parâmetros estruturais influenciam significativamente as propriedades da quitosana, incluindo o grau de desacetilação, o peso molecular e o grau de cristalinidade do polímero. O grau de desacetilação, em particular, determina a quantidade de grupos amina disponíveis ao longo da cadeia polimérica, influenciando diretamente propriedades como solubilidade, reatividade química e capacidade de interação com diferentes espécies químicas (Shukla et al., 2013).

Devido à presença desses grupos funcionais reativos, a quitosana pode ser submetida a diversas transformações químicas que permitem ajustar suas propriedades estruturais e de superfície. Entre as estratégias mais exploradas encontram-se reações de acilação, alquilação, formação de bases de Schiff, enxertia de cadeias poliméricas e funcionalização com diferentes grupos orgânicos. Essas modificações podem alterar propriedades como polaridade de superfície, hidrofobicidade, densidade de carga e distribuição de sítios ativos, ampliando o potencial de aplicação da quitosana em diferentes áreas, incluindo biomedicina, agricultura, indústria alimentícia e tratamento de águas (Haj; Mohammed; Mohammood, 2020; Lehocký, 2025; Paula et al., 2020; Piegat et al., 2020).

No contexto de aplicações ambientais, a quitosana e seus derivados têm sido amplamente investigados como materiais adsorventes para a remoção de diferentes classes de contaminantes, incluindo corantes sintéticos, compostos farmacêuticos e metais pesados. A combinação entre alta densidade de grupos funcionais, possibilidade de modificação química e origem renovável torna esse biopolímero uma plataforma particularmente promissora para o desenvolvimento de novos materiais adsorventes (Kowanga; Nyairo, 2025).

1.5. ESTRATÉGIAS DE MODIFICAÇÃO QUÍMICA DA QUITOSANA

Entre as diferentes estratégias de modificação, muitas abordagens baseiam-se na formação de materiais compósitos ou na introdução de estruturas poliméricas adicionais capazes de aumentar a área de superfície ou melhorar a estabilidade estrutural do material. Embora esses sistemas frequentemente apresentem bom desempenho adsorptivo, eles

podem envolver processos sintéticos relativamente complexos ou a incorporação de múltiplos componentes na estrutura do adsorvente (El-Araby et al., 2023).

Como alternativa, abordagens baseadas na modificação direta da cadeia polimérica da quitosana têm atraído crescente interesse, uma vez que permitem ajustar propriedades eletrônicas e interfaciais do material sem a necessidade de arquiteturas estruturais complexas. Nesse tipo de estratégia, a introdução de substituintes orgânicos específicos ao longo da cadeia do polímero pode promover alterações na distribuição eletrônica da matriz polimérica, influenciando propriedades como polaridade da superfície do material, equilíbrio de protonação e natureza das interações adsorptivas (Lehocký, 2025).

Entre as diferentes classes de reagentes utilizados para esse tipo de funcionalização, os derivados alcoximetileno representam um grupo particularmente interessante. Esses compostos apresentam sistemas vinílicos ativados capazes de reagir com aminas por meio de mecanismos de substituição nucleofílica vinílica, resultando na formação de ligações enaminas conjugadas. Esse tipo de reação permite a introdução de diferentes substituintes orgânicos diretamente na cadeia polimérica da quitosana, possibilitando a modulação de propriedades eletrônicas e estruturais do material (Lu et al., 2022).

A natureza dos grupos substituintes introduzidos ao longo da cadeia polimérica pode exercer forte influência sobre as propriedades do material resultante. Substituintes com diferentes características eletrônicas, como grupos éster ou nitrila, podem alterar a distribuição de densidade eletrônica da matriz polimérica e modificar as propriedades de superfície do adsorvente. Essas alterações podem, por sua vez, influenciar os mecanismos de interação entre o material adsorvente e diferentes contaminantes orgânicos presentes em solução (Salama; Hesemann, 2025).

Nesse contexto, o desenvolvimento de derivados de quitosana contendo substituintes com diferentes características eletrônicas constitui uma abordagem promissora para a investigação da relação entre estrutura química e desempenho adsorptivo. A introdução sistemática de grupos funcionais ao longo da cadeia do polímero permite avaliar como fatores como densidade de substituição e natureza eletrônica dos substituintes influenciam propriedades como carga superficial, polaridade e heterogeneidade energética dos sítios de adsorção (Firmansyah; Alwan; Ullah, 2025).

1.6. DERIVADOS ALCOXIMETILENO E SUBSTITUIÇÃO NUCLEOFÍLICA VINÍLICA

Entre as diferentes estratégias de funcionalização de aminas orgânicas, reações envolvendo derivados alcoximetileno têm recebido atenção significativa devido à sua elevada reatividade frente a nucleófilos nitrogenados. Esses compostos apresentam sistemas vinílicos ativados por grupos eletronegativos, o que torna o carbono β altamente suscetível ao ataque nucleofílico (Vide Figura 4). Como consequência, aminas primárias podem reagir com esses substratos por meio de mecanismos de substituição nucleofílica vinílica, resultando na formação de estruturas enaminas conjugadas (Lu et al., 2022; Santilli; Bruce; Osdene, 1964).

Derivados alcoximetileno contendo grupos fortemente eletronegativos, como nitrilas ou ésteres, apresentam elevada ativação eletrônica da dupla ligação carbono-carbono, favorecendo a ocorrência desse tipo de reação. Durante o processo, o ataque nucleofílico do nitrogênio amínico ocorre no carbono vinílico eletrofílico, seguido pela eliminação do grupo alcóxi, levando à formação de uma nova ligação C–N conjugada ao sistema insaturado. Esse tipo de transformação permite a introdução direta de substituintes orgânicos contendo diferentes grupos funcionais ao longo de cadeias contendo aminas primárias (Lu et al., 2022; Molander; Singaram; Brown, 1984a).

Figura 4 – Sistematização da reação nucleofílica vinílica (adição-eliminação conjugada).

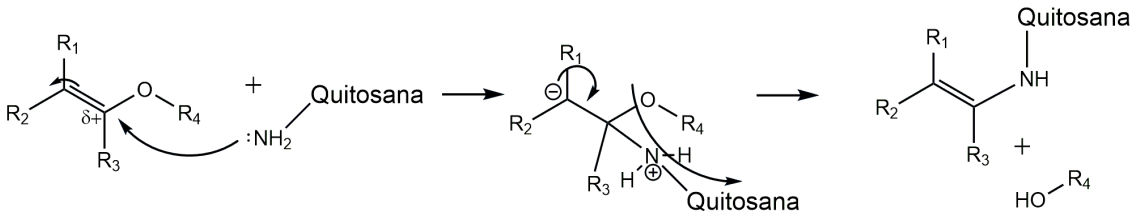

Fonte: Próprio autor

No caso da quitosana, a presença de grupos amina primários na posição C_2 das unidades glicosídicas torna o polímero particularmente adequado para esse tipo de funcionalização. A reação entre a quitosana e derivados alcoximetilênicos possibilita a introdução de diferentes substituintes orgânicos diretamente na cadeia polimérica, resultando na formação de derivados contendo estruturas enaminas conjugadas ligadas ao esqueleto do biopolímero (Figura 5) (Lehocký, 2025; Salama; Hesemann, 2025).

Figura 5 - Representação da quitosana e os derivados que foram sintetizados neste trabalho.

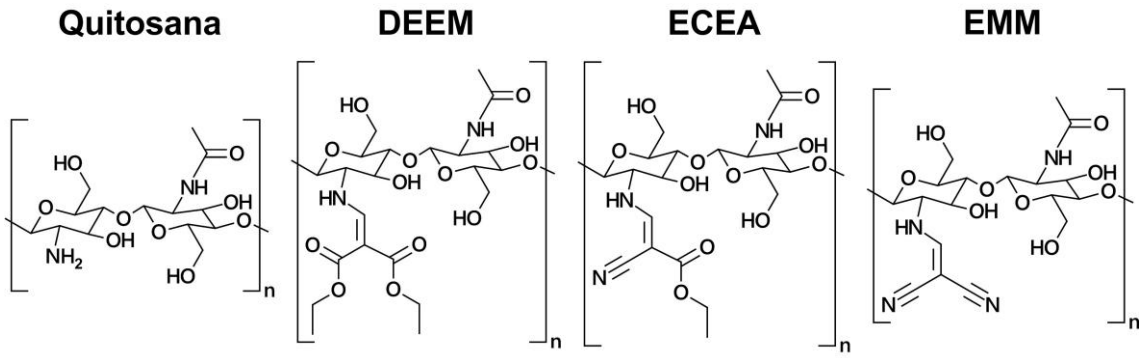

Fonte: Próprio autor

Uma característica importante dessa estratégia sintética é a possibilidade de modular as propriedades do material resultante por meio da escolha apropriada do reagente eletrofílico utilizado na reação. Diferentes derivados alcoximetilênicos podem introduzir grupos funcionais com distintas características eletrônicas, permitindo alterar propriedades como polaridade da superfície, densidade de dipolos e distribuição eletrônica ao longo da cadeia polimérica (Kowanga; Nyairo, 2025).

No contexto de materiais adsorventes, a introdução de grupos funcionais contendo átomos altamente eletronegativos pode modificar significativamente o ambiente interfacial do polímero. Grupos como ésteres e nitrilas apresentam forte caráter retirador de elétrons e elevada polaridade, o que pode favorecer interações específicas com diferentes espécies químicas presentes em solução. Essas interações podem envolver mecanismos como estabilização íon-dipolo, ligações de hidrogênio ou interações dipolares, dependendo da natureza do contaminante e das condições do meio (Misra; Bhattacharyya, 2018; Pereira; Garcia Ferreira; Gehlen, 2005; Salama; Hesemann, 2025).

Além disso, a densidade de substituintes introduzidos ao longo da cadeia polimérica pode desempenhar papel importante na determinação do comportamento adsorptivo do material. A variação do grau de substituição permite controlar a quantidade de grupos funcionais presentes no polímero, influenciando diretamente propriedades como heterogeneidade energética da superfície, afinidade por diferentes moléculas adsorvidas e mecanismos de interação envolvidos no processo de adsorção (Firmansyah; Alwan; Ullah, 2025).

2. HIPÓTESE DA TESE

A eficiência de materiais adsorventes baseados em biopolímeros está fortemente associada às propriedades estruturais e eletrônicas da superfície do material. No caso da quitosana, embora a presença de grupos amina e hidroxila proporcione capacidade de interação com diferentes espécies químicas em solução, a natureza e a densidade desses grupos funcionais podem limitar o desempenho adsorptivo do material frente a determinados contaminantes orgânicos.

Nesse contexto, estratégias de modificação química da quitosana que permitam alterar a distribuição eletrônica da matriz polimérica e introduzir novos grupos funcionais representam uma abordagem promissora para otimizar suas propriedades adsorptivas. A incorporação de substituintes com diferentes características eletrônicas pode modificar o ambiente interfacial do polímero, influenciando propriedades como polaridade de superfície, densidade de dipolos e natureza das interações intermoleculares entre o adsorvente e as moléculas adsorvidas.

Dessa forma, parte-se da hipótese de que a modificação da quitosana por meio da introdução de substituintes orgânicos contendo grupos fortemente eletronegativos pode alterar significativamente as propriedades eletrônicas e interfaciais do material. Essas alterações são esperadas influenciar os mecanismos de interação entre o adsorvente e contaminantes orgânicos presentes em solução, afetando parâmetros como capacidade de adsorção, afinidade entre adsorvente e adsorbato e comportamento cinético do processo.

Além disso, considera-se que a densidade de substituintes introduzidos ao longo da cadeia polimérica desempenha papel fundamental na determinação dessas propriedades. O aumento do grau de substituição pode levar à formação de uma superfície adsorvente com maior densidade de sítios polares capazes de interagir com diferentes espécies químicas, favorecendo mecanismos de interação intermolecular como interações dipolares, ligações de hidrogênio e estabilização íon-dipolo.

Assim, propõe-se que a introdução sistemática de grupos funcionais com diferentes características eletrônicas na cadeia da quitosana permite modular as propriedades da superfície do material e, consequentemente, influenciar seu desempenho adsorptivo frente a diferentes classes de contaminantes orgânicos.

A investigação dessa hipótese foi realizada por meio da síntese de derivados de quitosana funcionalizados com substituintes contendo grupos diester, ester-nitrila e

dinitrila, permitindo avaliar como a natureza eletrônica e a densidade desses grupos influenciam o comportamento adsorptivo do material em sistemas contendo contaminantes orgânicos modelos, como o corante cristal violeta e o fármaco diclofenaco.

3. OBJETIVOS

3.1. OBJETIVO GERAL

Desenvolver derivados funcionalizados de quitosana por meio de reações de substituição nucleofílica vinílica utilizando derivados alcoximetilênicos contendo diferentes grupos substituintes, e investigar como a natureza eletrônica e a densidade desses grupos funcionais influenciam as propriedades estruturais e o desempenho adsorptivo do material na remoção de contaminantes orgânicos em meio aquoso.

3.2. OBJETIVOS ESPECÍFICOS

- Sintetizar derivados de quitosana funcionalizados por meio da reação com diferentes derivados alcoximetilênicos contendo grupos diéster, éster-nitrila e dinitrila.
- Caracterizar estrutural e fisicoquimicamente os materiais obtidos, avaliando propriedades como grau de substituição, estrutura química e alterações nas propriedades do biopolímero após a modificação.
- Investigar a influência das condições reacionais na funcionalização da quitosana, visando otimizar a síntese e o grau de modificação do polímero.
- Avaliar o desempenho adsorptivo dos materiais desenvolvidos na remoção de contaminantes orgânicos modelo em solução aquosa.
- Estudar o comportamento de adsorção frente a diferentes classes de contaminantes orgânicos, incluindo corantes catiônicos e compostos farmacêuticos.
- Analisar a relação entre natureza eletrônica dos substituintes introduzidos, grau de funcionalização do polímero e propriedades adsorptivas dos materiais obtidos.
- Investigar os possíveis mecanismos de interação envolvidos no processo de adsorção entre os derivados de quitosana e os contaminantes orgânicos estudados.

4. ESTRUTURA DA TESE

Esta tese está organizada no formato de coletânea de artigos científicos, nos quais são apresentados os principais resultados obtidos ao longo do desenvolvimento deste trabalho. A estrutura foi organizada de modo a refletir a progressão das etapas de investigação, desde o desenvolvimento da estratégia de modificação química da quitosana até a avaliação do desempenho adsorptivo dos materiais obtidos.

O Capítulo 1 apresenta a introdução geral do trabalho, abordando o contexto da contaminação ambiental por poluentes orgânicos, as principais tecnologias utilizadas para sua remoção, o uso de biopolímeros como materiais adsorventes e o potencial da quitosana como plataforma para modificação química. Nesse capítulo também são discutidos os fundamentos da funcionalização da quitosana por meio de reações envolvendo derivados alcoximetileno e sua relação com o desempenho adsorptivo de materiais poliméricos funcionalizados.

O Capítulo 2 apresenta o primeiro artigo desta tese, no qual é descrita a aplicação da reação de substituição nucleofílica vinílica para a modificação da quitosana utilizando o reagente Etoximetilenomalononitrila (EMM), contendo grupos dinitrila. Este estudo representa a prova de conceito da estratégia sintética adotada ao longo da tese, sendo investigados parâmetros reacionais como meio de reação, razão molar entre reagente e unidades repetitivas da quitosana e tempo de reação. O derivado obtido foi caracterizado por diferentes técnicas com o objetivo de avaliar suas propriedades estruturais e físico-químicas.

No Capítulo 3 é apresentado o segundo artigo da tese, no qual é investigada a modificação da quitosana utilizando Dietiletoximetilenomalonato (DEEM), um derivado contendo grupos diéster. Neste trabalho, as condições de reação foram otimizadas por meio de uma abordagem baseada em planejamento experimental (design de experimentos), permitindo avaliar a influência de diferentes variáveis sintéticas sobre o grau de funcionalização do polímero. O material obtido foi posteriormente caracterizado quanto às suas propriedades estruturais e físico-químicas.

O Capítulo 4 apresenta o terceiro artigo da tese, dedicado à síntese de um derivado de quitosana contendo grupos éster-nitrila a partir da reação com Etil 2-ciano-3-etoxiacrilato (ECEA). De maneira semelhante ao estudo anterior, a otimização das condições reacionais foi realizada utilizando ferramentas de planejamento experimental,

permitindo identificar as condições mais adequadas para a obtenção do material funcionalizado. As propriedades estruturais e físico-químicas do derivado obtido também foram investigadas por diferentes técnicas de caracterização.

O Capítulo 5 apresenta o quarto artigo da tese, no qual é avaliado o desempenho adsorptivo dos derivados de quitosana na remoção do corante cristal violeta em solução aquosa, investigando-se os mecanismos de interação envolvidos no processo de adsorção.

O Capítulo 6 apresenta o quinto artigo, no qual é investigada a influência da densidade de grupos funcionais introduzidos na quitosana sobre o desempenho adsorptivo do material na remoção do fármaco diclofenaco em solução aquosa.

Por fim, o Capítulo 7 apresenta as conclusões gerais da tese, destacando as principais contribuições científicas do trabalho, bem como perspectivas para pesquisas futuras relacionadas ao desenvolvimento de novos materiais adsorventes baseados em biopolímeros funcionalizados.

5. A NEW ROUTE TO PRODUCE CHITOSAN DERIVATIVES: NUCLEOPHILIC VINYLIC SUBSTITUTION WITH ETHOXYMETHYLENEMALONONITRILE

5.1. ABSTRACT

Chitosan (Ch) is a polysaccharide obtained from chitin: a renewable, non-toxic, biocompatible biomolecule that constitutes the second most abundant natural polymer on the planet. The presence of amino groups in the chitosan polymers chain allows change the physicochemical properties of the natural polymer. In this work, we prepared a chitosan derivative (ChMM) with ethoxymethylenemalononitrile (EMM) through a nucleophilic vinylic substitution (S_NV), changing the experimental conditions as stoichiometry, solvent (ethanol, DMSO) and reaction time (3 and 6 hours). ChMM was characterized by Fourier Transform Infrared Spectroscopy (FTIR), Solid State ^{13}C Nuclear Magnetic Resonance (^{13}C NMR), Elemental Analysis (EA), Thermogravimetry (TG), Scanning Electron Microscopy (SEM) and X-Ray Diffraction (XRD). The FTIR and ^{13}C NMR results confirms the success of the reaction, showing a sharp peak at 2213 cm^{-1} corresponding to the stretching of the CN bond and additional signals at 52 and 166 ppm, respectively. The degree of substitution (DS) was calculated from EA and the results obtained show that sample modified with 1:2 molar ratio of [Ch]/[EMM] over 3 hours in DMSO presented the better result (DS= 0.91). ChMM did not show a considerable change in morphology (SEM) and thermal stability (TG). The insertion of methylenemalononitrile groups led to a decrease in the crystallinity index of chitosan derivatives (XRD). ChMM showed good ability to remove dyes in acidic and basic medium (pH 5, 7, 9), and for crystal violet and safranin dyes the removal percentage surpassed 70%.

5.2. INTRODUCTION

Chitin is a natural polymer corresponding to the second most abundant natural polymer on the planet after cellulose and can be extracted from animal/marine, and fungal sources 1,2. In the latter case, chitin can be obtained from agricultural residues in mushroom farms where losses can reach 5 to 20 % of the total production 2. Other important sources of chitin are the exoskeleton of crustaceans and the cuticle of insects which contain approximately 36% chitin3. However, in some species of lobster such as *Nephrops* sp. and *Homarus* sp. this percentage can reach up to 75% 4. Chitin is classified as a polysaccharide whose chemical structure is constituted by monomeric units of β-(1-

4)-2-amino-2-deoxy-D-glucose and β-(1-4)-2-acetamide-2-deoxy-D-glucose 3. Chitin, in most applications, is used as chitosan (Ch), which is formed by monomeric units of β-(1-4)-2-amino-2-deoxy-D-glucose and obtained by alkaline or enzymatic treatment of chitin 4. Historically, chitosan was first characterized by Charles Rouget in 1859 by heating chitin in the presence of potassium hydroxide 5.

Like cellulose, chitosan has renewable and biodegradable source, biocompatibility and non-toxicity allowing applications in medicine 1,6,7 (biomaterials, anti-diabetic, anticancer), pharmacy 8–10 (drug delivery, bioadhesives, adjuvant for vaccine delivery) and nutrition 11,12 (encapsulating agent, nanoemulsion).

The presence of reactive amino groups in the chitosan polymer chain allows numerous chemical modifications such as grafting onto copolymerization 13, thiolated 14, alkylated 15, Schiff bases 16, phosphorylation 17, triazolyl 18, N-heterocyclic 19, sulfoethylation 20, carboxymethylation, quaternization, coupling with cyclodextrins 21,22, allowing to change the physicochemical and biological properties of the polymer. For example, the introduction of a phosphate 17,23 and sulfate 24 groups make chitosan water soluble while functionalization with N-(Thiophene-2-acetyl) leads to a hydrophobic modification in the polymer chain 25. The chemical modification of chitosan also leads to an increase in applications of this polymer in the areas of food and health 26,27.

In addition, chitosan and its derivatives are also used in other areas such as environmental 28,29, electrochemistry 30,31 (sensor, corrosion), agriculture 32,33 (fertilizer delivery/release, crop protection), papermaking industry 34, textiles 35, CO_2 adsorption 36. Regarding the environmental area, the main applications of chitosan and its derivatives are in the removal of organic molecules (dyes 37–39, pharmaceuticals 40,41, insecticide 42, surfactant 43), phenolic compound 44, inorganic (heavy metal) 45–47.

Alkoxymethylene derivatives (Figure 1) are a very interesting group of molecules that react with the amine group of organic molecules through a nucleophilic vinylic substitution (S_NV) mechanism 48–50 and to best of our knowledge, this is the first time that this polymer has been modified by this synthetic route.

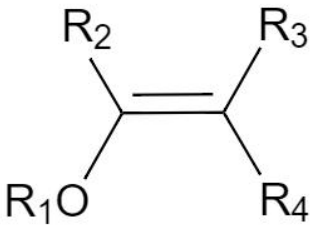

Figure 1. Chemical structure of alkoxymethylene derivatives. R1= CH_3, C_2H_5; R2= H, CH_3; R3, R4= CO_2CH_3, $CO_2C_2H_5$, CN, $COCH_3$.

Commercially are found 3-(ethoxymethylene)-2,4-pentanedione (R1=C_2H_5, R2=H, R3=R4=$COCH_3$), diethyl ethoxymethylenemalonate (R1=C_2H_5, R2=H, R3=R4=$CO_2C_2H_5$), ethyl (ethoxymethylene)cyanoacetate (R1=C_2H_5, R2=H, R_3=CN, R4=$CO_2C_2H_5$), and etoxymethylenemalononitrile (R1= C_2H_5, R2= H, R3= R4= CN), besides these commercials one a variety of others alkoxymethylene can be synthesised. They can be prepared from propanedioic acid, 3-oxobutanoic acid and cyanoacetic acids 49.

The goal of this study was to obtained a chitosan derivative (ChMM) with ethoxymethylenemalononitrile (EMM) through a S_NV and evaluate it for potential use in dye adsorption. In relation to ethyl (ethoxymethylene)cyanoacetate we also had a successful reaction and we are working under the best experimental conditions.

5.3. EXPERIMENTALS

5.3.1. Materials

Chitosan with average molecular weight (75–85% deacetylation) and ethoxymethylenemalononitrile (98%) were purchased from Sigma-Aldrich. Crystal violet (CV, 97%), Safranin (SF, 95%), Methylene Blue (MB, 95%), NaOH (98%), KH_2PO_4 (99%), Na_2HPO_4 (98%), methanol (99.8%), ethanol (99.5%), DMSO (99.9%), were purchase from Synth. All solvents and reagents were used without further purification.

5.3.2. Functionalization of the chitosan

The ChMM was synthesized by dispersing 0.5 g of chitosan (2.50 mmol, glucosamine residue) in ethanol or DMSO at 50 °C, and placed under agitation. After that, an appropriate quantity (2.5 or 5.0 mmol) of EMM was added and allowed to react at different times (3 or 6 hours). Therefore, the Ch/EMM stoichiometry ranged from 1:1 and

1:2, respectively. After the programmed reaction time, the crude product was placed in a sintered glass funnel (nº 4) and rinsed with acetone, ethanol, methanol, and distilled water until neutral pH was reached. The sample was dried at 25 ºC in a desiccator under vacuum pressure. The degree of substitution (DS) was calculated using equation 1 51. In equation 1 DS is equal to "x".

$$\frac{C_1}{N_1}.(1-x)+\frac{C_2}{N_2}.x=\frac{C_3}{N_3}.0.803 \quad (1)$$

Where, C_1/N_1 is a value calculated from the formula of nonsubstitued chitosan, C_2/N_2 from the EMM group introduced in chitosan, and C_3/N_3 is the resulted obtained from Elementary Analysis (EA). The degree of acetylation (DA) was 0.197 and this value was calculated by FTIR using equation 2 52.

$$DA=\frac{(A_{1320}/A_{1420})-0.3822}{0.03133} \quad (2)$$

Where A_{1320}/A_{1420} is the absorbance ratio at 1320 and 1420 cm^{-1}, respectively. The degree of deacetylation (DD) was calculated from equation (3):

$$DD=1-DA \quad (3)$$

5.3.3. Characterization

5.3.3.1. Fourier Transform Infrared – FTIR

The chemical structure was examined by Fourier transform infrared spectroscopy (FTIR). The attenuated total reflectance (ATR) mode was used in the spectrophotometer (Perkin-Elmer, 100S). Samples were analyzed using IR range from 800 to 4000 cm^{-1}.

5.3.3.2. Solid State ^{13}C NMR

The solid state ^{13}C NMR analyses were performed at room temperature in a Bruker Avance III-400 operating at 9.4T magnetic field. The powdered samples were packed into a 4 mm zirconia rotor and spun at 5 kHz. The spectra were acquired using the CP-MAS-TOSS (CPMAS with total sideband suppression) with the following parameters: contact time of 1 ms, recycle delay of 4s, acquisition time of 34 ms and 1024 scans. Both spectra were processed with an exponential apodization function using a linebroadening factor of 30 Hz. TopSpin Bruker software (version 3.6.3) was used for the acquisition and processing of the NMR data.

5.3.3.3. Elementary analysis

The content of carbon (C), hydrogen (H), and nitrogen (N) in samples of pure and modified chitosan was determined by elementary analysis with a Perkin Elmer model 2400 instrument.

5.3.3.4. Thermogravimetry - TG

The thermogravimetric analysis (TG) of pure and modified chitosan was performed using a TA Instruments, model TG 550, with 50 mL.min^{-1} nitrogen flow, 25-500 °C analysis interval, and 10 °C min^{-1} heating rate.

5.3.3.5. X-Ray Diffraction - XRD

X-ray diffraction data were carried out using a DRX-6100 Shimadzu instrument and the samples were prepared by the powder method. Ni-filtered CuK α radiation (λ=1.54060 Å) generated at a voltage of 40 KV and current of 30 mA was utilized, and scan speed of 0.02°/sec and 2θ from 5° to 30° was used.

The degree of crystallinity of chitosan and its derivative were calculated by equation 4, commonly utilized on cellulose 53,54.

$$\% I_{cr} = \frac{(I_c - I_a)}{I_c} x\ 100 \qquad (4)$$

Where I_{cr} is the crystallinity index, I_a and I_c are the amorphous fraction (2θ~11°) and crystalline fraction (2θ~20°).

5.3.3.6. Scanning Electron Microscopy - SEM

Scanning electron microscopy (SEM) of Chitosan after and before chemical modification was performed with a TM300 Tabletop Scanning Electron Microscope (model Hitachi TM3000), Dual Accelerating voltages - 5kV and 15kV and low vacuum.

5.3.3.7. Zeta Potential

Zeta potential measurements were performed using an analyzer electrokinetic (SurPASS, Anton Paar). The surface zeta potential was determined in function of pH in a 0.001 M KCl electrolyte solution by varying the pH of the solution by addition of 0.05 M NaOH through the automatic titration unit of the instrument. Solid samples were equilibrated at neutral pH with various rinsing steps and then the pH was adjusted to 3, where a pH scan with 0.3 change per cycle until reaching pH 9. All experiments were carried out at 50 ºC.

5.3.3.8. Adsorption of dyes onto ChMM as a function of solution pH

Adsorption measurements were performed using erlenmeyers flasks containing 50 mL of buffered solution 0.05 M KH_2PO_4 / Na_2HPO_4 (from pH 5 to 9). Dye concentrations were 0.1 mM, and the mass of ChMM was maintained at 50 mg (C = 1 $g.L^{-1}$). The flasks were stirred at 130 rpm and 25 °C for 24 h. Dye removal percentage (R%) was calculated using equation 5 and the adsorption experiments were made in triplicate.

$$R\% = \left(\frac{C_0 - C_e}{C_0}\right) x\ 100 \quad (5)$$

Where C_0 and C_e ($mmol.L^{-1}$) are the dye solution concentrations initially and at equilibrium, respectively.

5.4. RESULTS AND DISCUSSIONS

5.4.1. Functionalization of the chitosan

The S_NV reaction between Ch and EMM is presented in figure 2. The ChMM exhibited a yellow color. The effect of stoichiometry, solvent and time on the reaction efficiency was investigated, keeping the same temperature. The best experimental condition (highest DS) for S_NV reaction were 1:2 molar ratio (Ch/EMM) and 3 and 6 hours of reaction (Table 1). All samples used in the material's characterization were performed in DMSO and the first two numbers represent the stoichiometry and the last the reaction time.

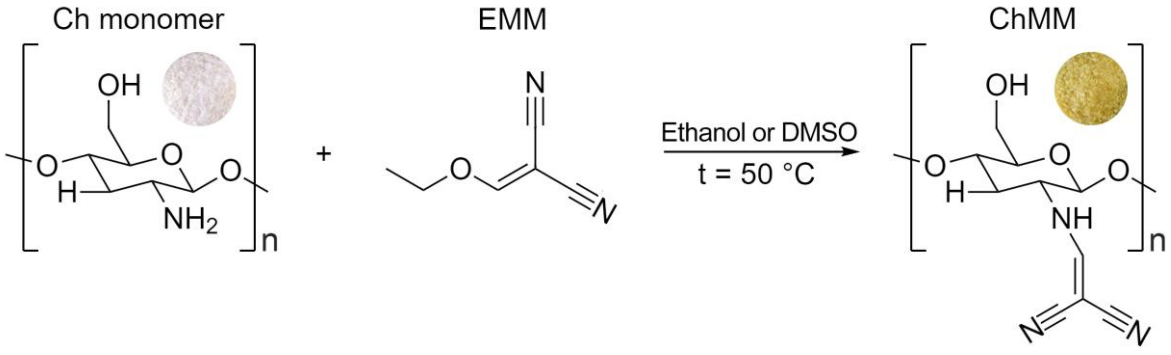

Figure 2. Chitosan (Ch) functionalization with EMM.

5.4.2. Fourier Transform Infrared – FTIR

Infrared spectroscopy (Figure 3) confirms the success of the reaction, showing a sharp peak appears at 2213 cm^{-1}, corresponding to the stretching of the CN bond 49,50.

Furthermore, the peaks around 2880 cm^{-1} are attributed to the CH and CH_2 stretch and 1623 cm^{-1} is attributed to the C=C group 55 corroborate the chemical modification.

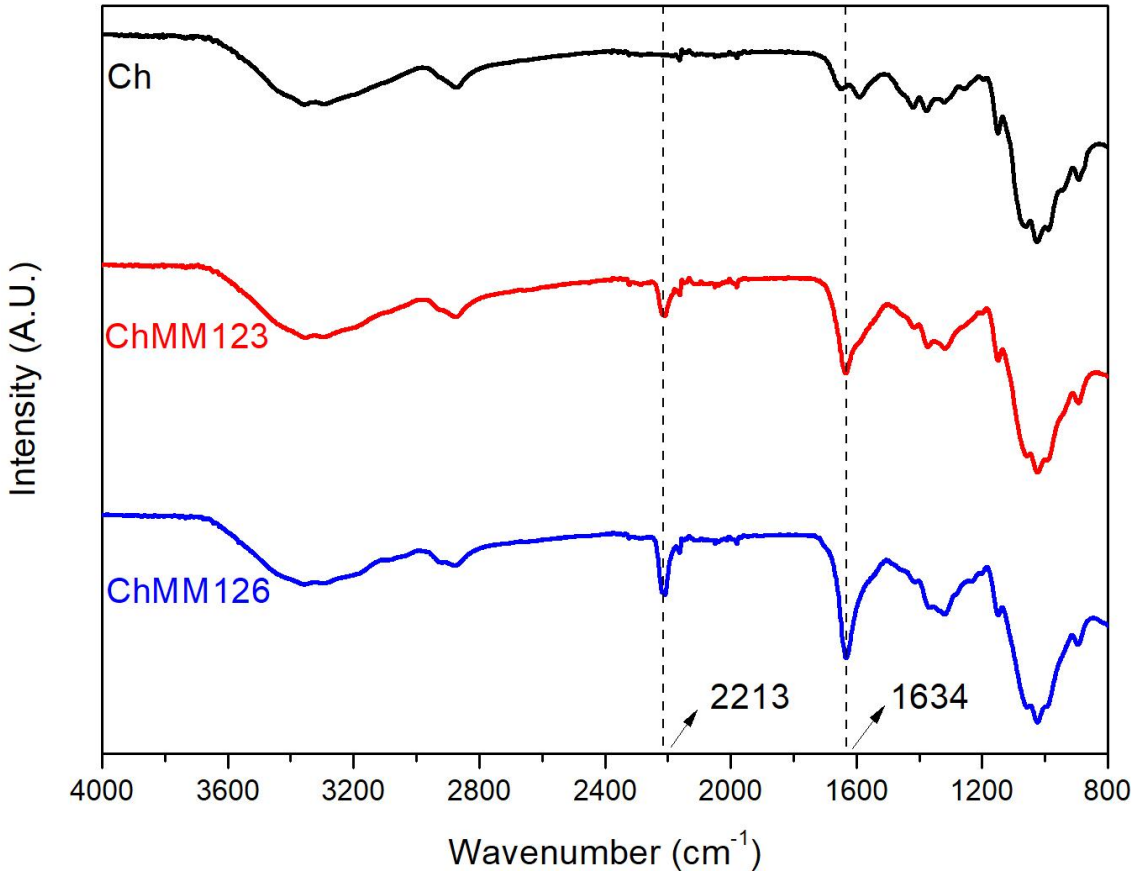

Figure 3. FTIR of chitosan pure (black line) and modified (red and blue lines).

5.4.3. Solid State ^{13}C Nuclear Molecular Resonance - NMR

The figure 4 exhibits the major signals of the chitosan in both spectra at 105, 57, 81 and 61 ppm, assigned to the C1, C2, C4 and C6 carbons, respectively. The signals at 75 ppm are related to the C3, C5 carbons and the signals at 24 and 174 ppm are assigned to methyl and carbonyl groups in the chitosan structure due to incomplete deacetylation of the chitin[56]. After the chemical modification additional signals at 52 (tertiary carbon) and 166 ppm (methylene) were observed as in the spectrum in red, corroborating the FTIR data 55,56.

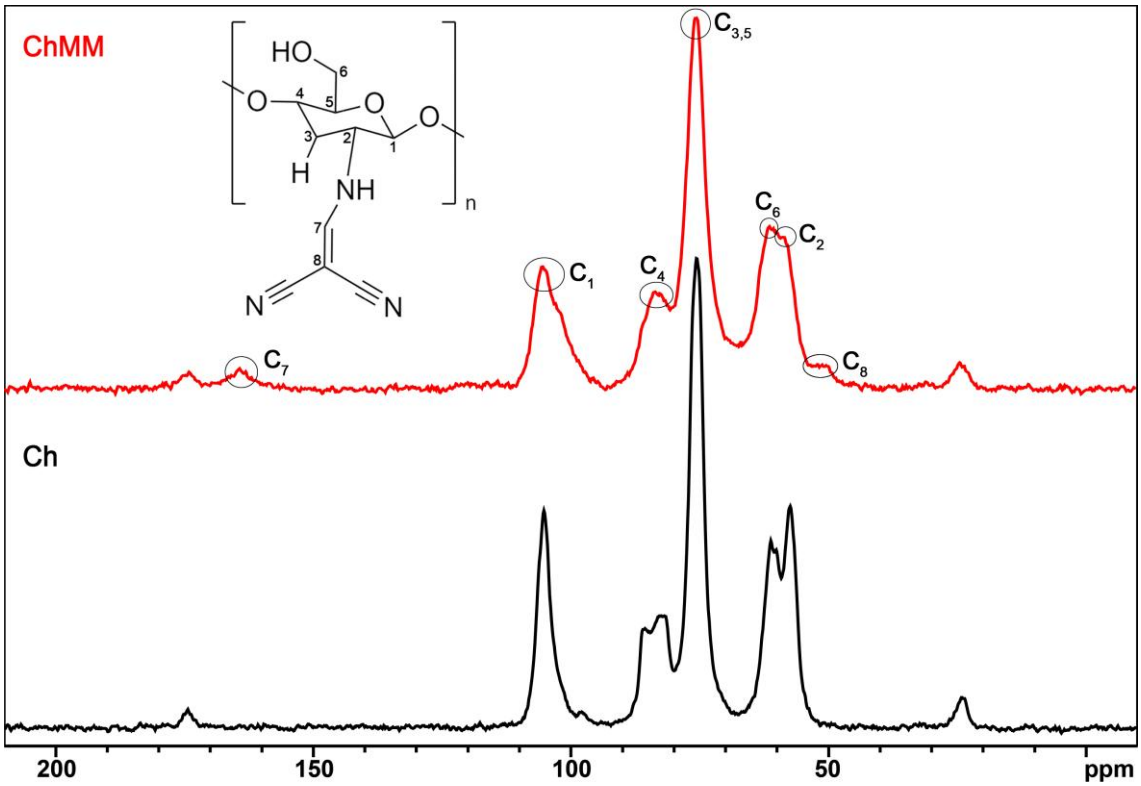

Figure 4. Solid State ^{13}C NMR of chitosan pure (black line) and modified (red line).

5.4.4. Elementary analysis – EA

Table 1 shows CHN results and DS for the functionalization of Ch with EMM. The calculated DS values (Eq. 1) indicate that the reaction was more effective in the DMSO solvent and that the highest DS value corresponds to 1:2 stoichiometry and 3 hours of reaction.

Table 1. Elementary analysis results and DS for the functionalization of Ch with EMM.

Solvent	[Ch]:[EMM]	Time (h)	%C	%N	DS
Ethanol	1:1	3	41.08	8.28	0.51
	1:1	6	42.19	8.54	0.51
	1:2	3	32.77	6.36	0.44
	1:2	6	42.38	7.99	0.38
DMSO	1:1	3	44.09	10.36	0.75
	1:1	6	43.45	10.46	0.79
	1:2	3	45.43	11.90	0.91
	1:2	6	48.06	11.72	0.81

5.4.5. Thermogravimetry – TG

Figure 5 shows the thermogravimetric analysis for pure and modified chitosan as well as the derivatives of the thermogravimetric curves. Pure and modified chitosan had a similar thermal behavior, presenting a mass loss (WL) in two thermal events, the first being related to water loss and the second being attributed to organic moiety elimination as also found in chitosan pyridine derivatives 57.

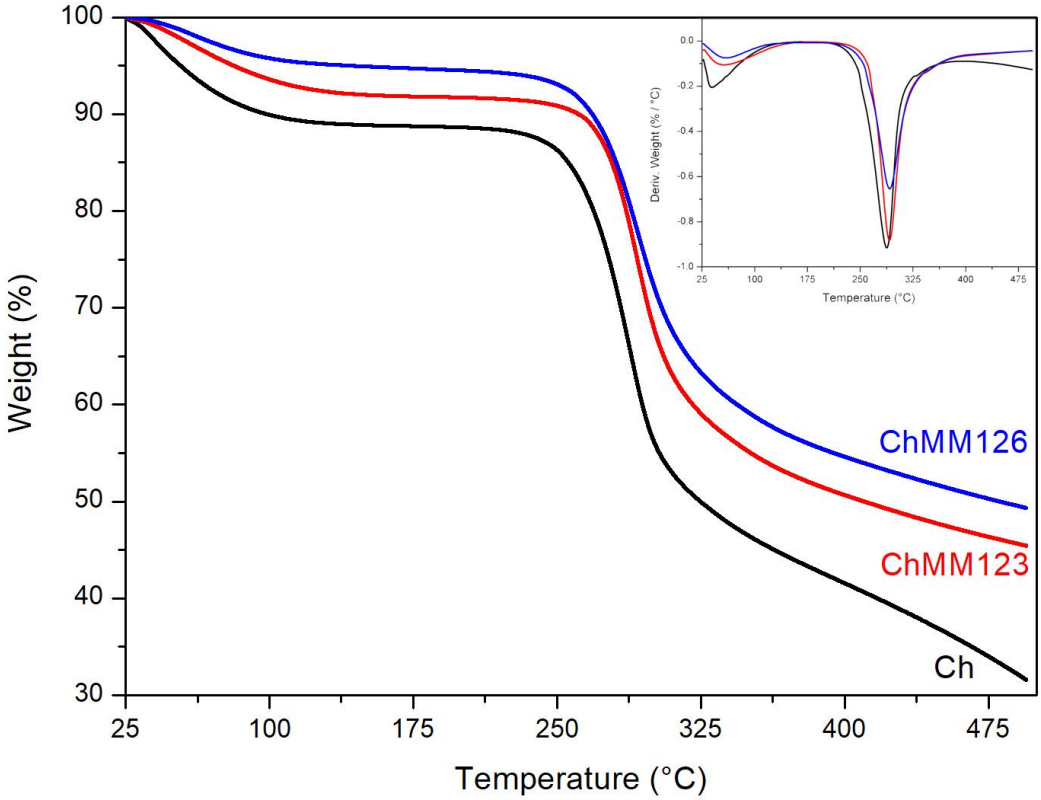

Figure 5. TG and dTG (inset) curves for chitosan pure (black line) and modified (red and blue lines).

The thermal analysis showed that the ChMM123 had a higher degradation start temperature (t_{onset}= 174.8 ºC) and a lower mass loss (WL = 35.48%) when compared to chitosan (t_{onset} = 159.0 ºC, WL = 39.42%), this also can be seen on the other reaction conditions (vide Table 2).

Table 2. Thermogravimetric data for chitosan derivatives synthesized in DMSO.

Samples	Water Evaporation				Chitosan Thermal Degradation			
	T_{onset} (°C)	T_{max} (°C)	T_{endset} (°C)	WL (%)	T_{onset} (°C)	T_{max} (°C)	T_{endset} (°C)	WL (%)
Ch	26.1	39.6	159.0	11.18	159.0	287.7	328.4	39.42
ChMM123	28.5	57.4	174.8	8.17	174.8	291.6	341.2	35.48
ChMM126	28.1	59.6	146.9	5.05	146.9	292.0	346.3	35.28

5.4.6. X-Ray Diffraction - XRD

From the X-ray diffractograms of the chitosan (Figure 6), can be observed two broad peaks approximately at 2θ to 11° and 20°, that correspond to an amorphous and crystalline region, respectively. The sample of DS equals to 0.91 showed wider and weak peaks at 11° and 20°. The degree of crystallinity of pure chitosan (66.4%) showed a decrease with the introduction of methylenemalononitrile groups (59.3%). The decrease in chitosan crystallinity is related to the insertion of functional groups in the chitosan polymer chain promoting the disruption of inter and extra molecular hydrogen bonds in the original polymeric chains 57.

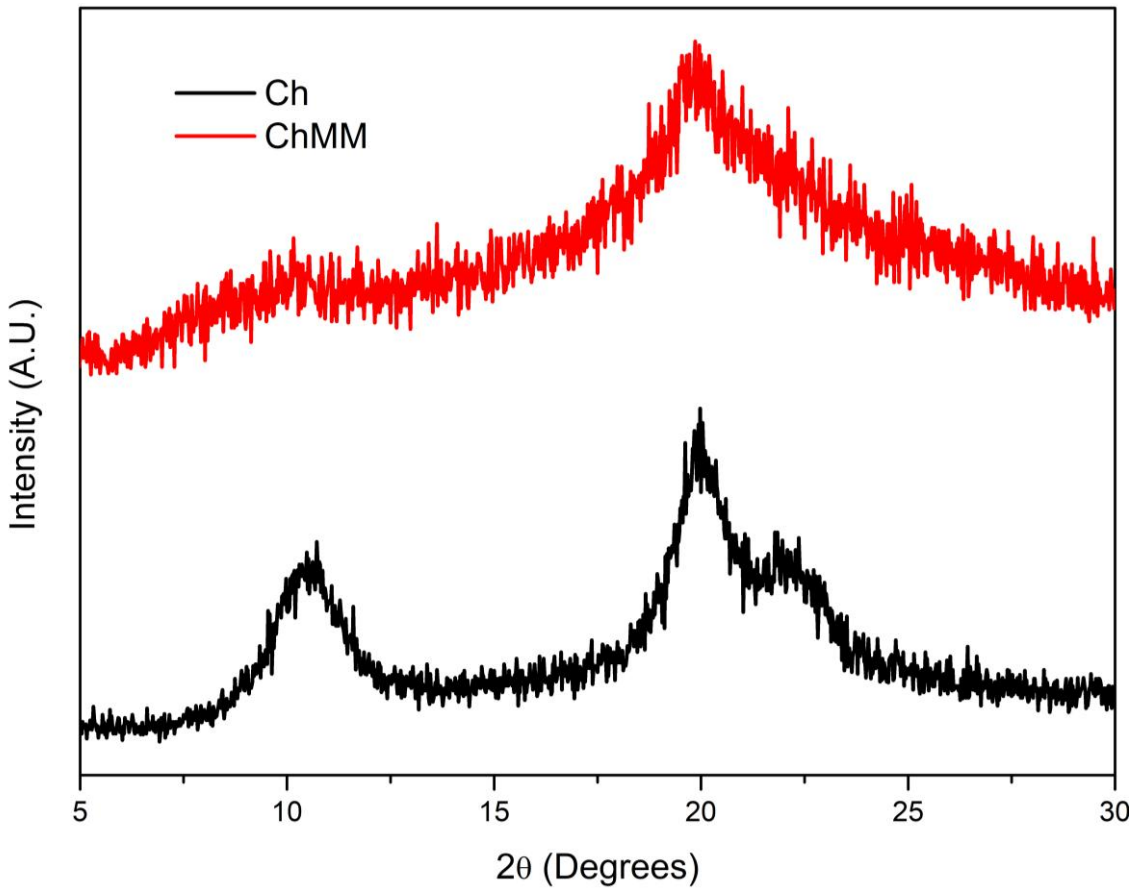

Figure 6. X-Ray diffractogram of chitosan pure (black line) and modified (red and line).

5.4.7. Scanning Electron Microscopy – SEM

SEM micrographs show that chitosan morphology before and after the chemical modification reaction was not modified (Figure 7). Fibrous morphology is observed and for some samples the length is slightly longer than diameter while for others the length is considerably longer than the diameter.

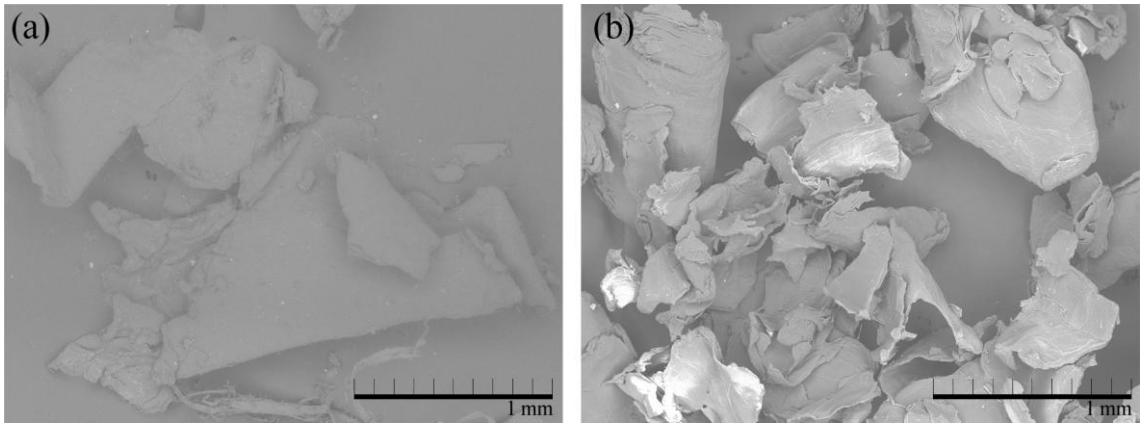

Figure 7. SEM micrographs of chitosan (a) pure and modified ChMM123 (b)

5.4.8. Zeta Potential

The zeta potential measurements of pure and modified chitosan (Figure 8) show that the total electrical charge on the surface of the ChMM becomes negative from pH = 5.61 (isoelectric point) and remains practically unchanged at pH above 8. The increase in the negative charge on the modified chitosan polymer structure may be related to the delocalization of electrons from the amino group to the cyano groups, this process being favored at pH above 5.61 by the gradual deprotonation of the amino group.

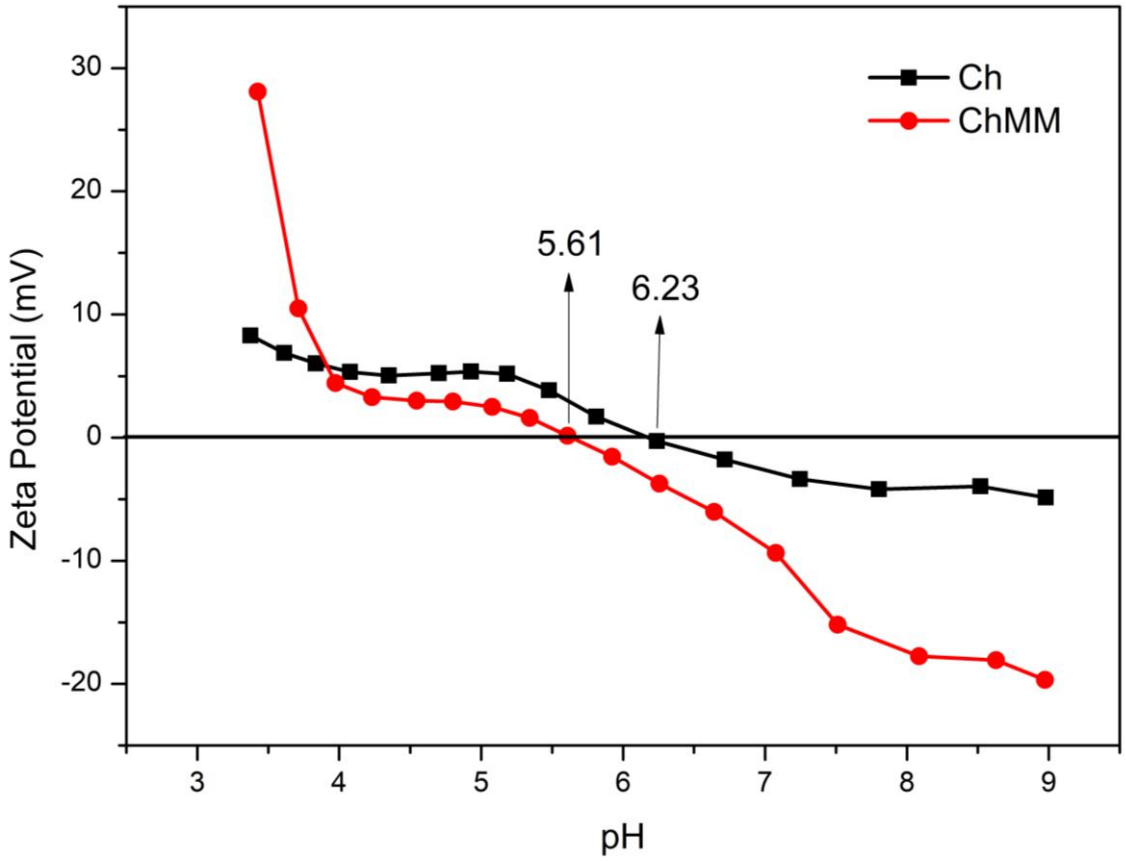

Figure 8. Zeta potential of chitosan pure (black line) and modified (red line) as a function of pH.

5.4.9. Adsorption of dyes onto ChMM as a function of solution pH

The percentage of removal by the chitosan derivative of the methylene blue, crystal violet and safranin dyes are shown in figure 9. Crystal violet and safranin dyes showed a removal percentage above 70% at pH 5, 7 and 9. On the other hand, methylene blue was able to remove only 40% at pH 7 and less than that at pH 5 and 9. These results suggest that in addition to the attraction between the dye charges and the modified

chitosan polymer chain, other types of interaction such as van der Waals, hydrogen bond, hydrophobic attraction are also important in the adsorption mechanism. Furthermore, the results showed that the adsorption of dyes, especially safranin and crystal violet, is greater than 70% at both acidic and basic pH. This efficiency may be related to the push–pull effect of the amino group and cyano groups56, which are favored at basic pH, since in this condition the transfer of electrons from the chitosan amino group to the cyano groups is favored, leaving them with a partial negative charge and favoring the interaction with the dyes.

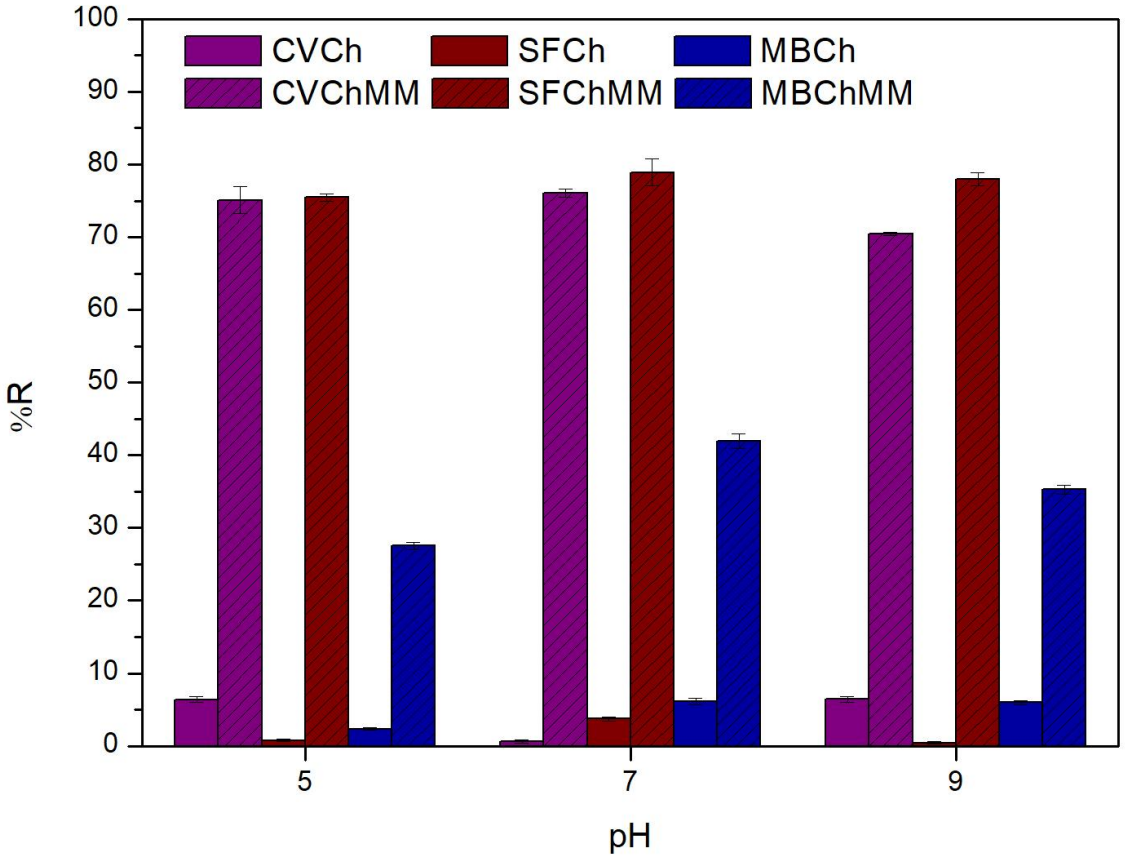

Figure 9. Effect of pH on cationic dye adsorption capacity by chitosan pure (Ch) and modified (ChMM).

5.5. CONCLUSIONS

Nucleophilic Vinylic Substitution of chitosan with EMM was successfully carried out being corroborated by the sharp and strong cyano band at 2213 cm^{-1} in the FTIR spectrum and the additional signals at 52 (tertiary carbon) and 166 ppm (methylene) in the NMR. The highest DS (0.91) was found to 1:2 molar ratio, DMSO, and 3 hours of

reaction at 50 ºC. ChMM showed a chitosan like morphology and thermal behavior while XRD showed a decrease in crystallinity with the insertion of methylenemalononitrile groups in the chitosan polymer chain. Furthermore, the inclusion of these groups led to a decrease in the isoelectric point of the material when compared to unmodified chitosan as the zeta potential analysis showed. The application of the material for dye removal proved to be promising, and the percentage of removal of crystal violet and safranin dyes was greater than 70% at pHs 5, 7 and 9.

5.6. ACKNOWLEDGEMENTS

The authors thank the financial support, FAPERJ/ Fundação de Amparo à Pesquisa do Estado do Rio de Janeiro and Program of Post-Graduation in Science of Materials - PPGCM of the Universidade Federal de São Carlos - UFSCar, campus Sorocaba.

6. SYNTHESIS OF A CHITOSAN DERIVATIVE VIA CONJUGATE ADDITION-ELIMINATION WITH DIETHYLETHOXYMETHYLENEMALONATE AND ITS PHYSICOCHEMICAL PROPERTIES

6.1. ABSTRACT

Chitin, the second most abundant natural polymer after cellulose, is mainly sourced from fungal waste and crustacean exoskeletons. It can be deacetylated to yield chitosan, a biocompatible and renewable material with versatile applications due to its reactive amino groups, allowing modifications like the one presented here, namely the synthesis of a novel chitosan derivative (ChDEEM) through a conjugate addition-elimination reaction with diethylethoxymethylenemalonate (DEEM). The reaction was conducted under various conditions to optimize the degree of substitution (DS) of the chitosan derivative (ChDEEM). Stoichiometry (1:1.5, 1:1.75, 1:2 Ch:DEEM), temperature (60, 70, and 80 °C), and reaction time (1, 2, and 3 hours) were varied. ChDEEM was characterized by a range of techniques including Fourier Transform Infrared Spectroscopy (FTIR), Carbon-13 Nuclear Magnetic Resonance (^{13}C NMR), Thermogravimetric analysis (TGA), Scanning Electron Microscopy (SEM), X-Ray Diffraction (XRD), Zeta Potential, Contact Angle (CA) and Elemental Analysis (EA). FTIR confirmed the successful modification, with a sharp peak at 805 cm^{-1} corresponding to the C=C bond stretch. ^{13}C NMR analysis showed new chemical shifts (158, 166, 87 and 11 ppm), and in combination with EA, was used to estimate the degree of substitution (DS) as 0.225 and 0.291, respectively. While SEM revealed no significant morphological changes, TGA indicated a decrease in thermal stability and Zeta Potential suggested reduced colloidal stability. Conversely, contact angle measurements showed increased hydrophobicity and decreased surface energy. Finally, XRD analysis revealed a decrease in the crystallinity index (from 79% to 38%) of ChDEEM compared to chitosan, likely due to the incorporation of methylenemalonate groups.

6.2. INTRODUCTION

Chitin, a polysaccharide composed of monomeric units of β-(1,4)-2-amino-2-deoxy-D-glucose and β-(1,4)-2-acetamido-2-deoxy-D-glucose (El Knidri et al., 2018), can be extracted from diverse sources, including fungal cell walls, arthropod and crustacean exoskeletons, and nematode eggshells (Croisier; Jérôme, 2013; Huq et al., 2022; Merzendorfer, 2006). Extraction from fungi is derived from agricultural waste in

mushroom farms (around 5-20% of the total production) (Huq et al., 2022), and the amount of chitin present in fungal cell walls varies according to species. Yeast contains the least (2%), while ascomycetes the most (42%) (Chatterjee et al., 2005; Hu et al., 1999; Ruiz-Herrera; Sentandreu, 1989; Teng et al., 2001). In animals, the main source is the waste generated by global seafood industries, approximately 2.4 million tons (Terkula Iber et al., 2022). The amount of chitin in these organisms typically ranges from 20 to 30% in crustacean exoskeletons (Yeul; Rayalu, 2013), 30 to 40% in shrimp cuticles, 5 to 25% in insect cuticles (Zainol Abidin et al., 2020), and can reach up to 75% in some lobster species (Maleki; Woltering; Mozafari, 2022).

In the majority of applications, chitin is utilized in the form of chitosan, which is formed from monomeric units of β-(1-4)-2-amino-2-deoxy-D-glucose and is obtained through alkaline or enzymatic treatment of chitin (Kou; Peters; Mucalo, 2021). Like cellulose, chitosan is a renewable and biodegradable source, biocompatible and non-toxic, allowing it to be used as antimicrobial, mucoadhesive, hemostasis, antitumor and antioxidant (Hemmami et al., 2024; Zhao et al., 2018), as well as for the removal of dyes and heavy metals (Chen et al., 2022; Hameed et al., 2022; Salehi et al., 2022).

The versatility of chitosan stems from the presence of reactive amino groups along its polymer chain. These amino groups enable a wide range of chemical modifications, including acylation (Nanda et al., 2019; Niemczyk et al., 2019; Piegat et al., 2020), carboxylation (Chen et al., 2004; Na et al., 2010), alkylation (Sun et al., 2021; Zhang et al., 2019a), quaternization (Luan et al., 2018; Zhang et al., 2018), sulfonation (Qiu et al., 2020; Schatz et al., 2005), phosphorylation (Han et al., 2020), thiolation (Prabahar; Udhumansha; Qushawy, 2020), graft copolymerization (Bratskaya et al., 2019), Schiff base formation (Cao et al., 2021), and many others.

Chitin, a ubiquitous natural polymer, has garnered significant attention due to its biocompatibility, biodegradability, and abundance. While chitosan, its deacetylated derivative, has found diverse applications, further modifications are necessary to optimize its properties for specific uses. This study hypothesizes that the introduction of alkoxymethylene groups to chitosan through reaction with diethylethoxymethylenemalonate (DEEM) will yield a novel derivative with significantly lower solubility and stability, enabling efficient adsorption of dyes, organic molecules, and heavy metals. The reduced solubility is expected to facilitate material recovery and reuse. This approach is novel as it explores a new class of modifying agents for chitosan.

The alkoxymethylene groups are anticipated to contribute to increased hydrophobicity and reduced hydrogen bonding, thereby decreasing solubility (Pereira et al., 2023). By developing a highly efficient and reusable material for pollutant removal, this research contributes to addressing critical environmental challenges and promoting sustainable practices.

6.3. EXPERIMENTAL

6.3.1. Materials

Chitosan (Ch) with average molecular weight (80% deacetylation degree (DD) ~ AGU molar mass of 169.57 $g.mol^{-1}$), Diethyl ethoxymethylenemalonate (99%) (DEEM) were purchased from Merck Chemicals, dimethyl sulfoxide (DMSO) (99.5%) and acetone (99.8%) were purchased from Roth. All solvents and reagents were used without further purification.

6.3.2. Methods

6.3.2.1. Functionalization of chitosan

This study explored the synthesis of ChDEEM using different reaction conditions. For this, 0.5 g of chitosan (~2.7 mmol) was dispersed in DMSO at three temperatures: 60, 70, and 80 °C. DEEM was added to chitosan at stoichiometric ratios ranging from 1:1.5 to 1:2, followed by continuous magnetic stirring for 1, 2, and 3 hours. After completing the programmed reaction time, the crude product was isolated by Soxhlet extraction with acetone for 4 hours to remove any unreacted starting material. The extracted product was then dried and stored in a desiccator.

6.3.2.2. Design of Experiments (DoE)

A Box-Behnken design (BBD) was employed to investigate the influence of three factors: temperature, time, and molar ratio, on the response variable, mass gain. The mass gain was defined as the percentage ratio between the mass of the chitosan derivative (ChDEEM) and the unmodified chitosan. The BBD consisted of 13 runs. The coded level for each factor was [-1, 0, +1]. The design matrix is presented in Table 1.

Table 1 – BBD design.

Run	Temperature (°C)	Time (h)	Molar ratio [1]:[X]
#1	60 (-1)	1 (-1)	1.75 (0)
#2	80 (+1)	1 (-1)	1.75 (0)
#3	60 (-1)	3 (+1)	1.75 (0)
#4	80 (+1)	3 (+1)	1.75 (0)
#5	60 (-1)	2 (0)	1.5 (-1)
#6	80 (+1)	2 (0)	1.5 (-1)
#7	60 (-1)	2 (0)	2.0 (+1)
#8	80 (+1)	2 (0)	2.0 (+1)
#9	70 (0)	1 (-1)	1.5 (-1)
#10	70 (0)	3 (+1)	1.5 (-1)
#11	70 (0)	1 (-1)	2.0 (+1)
#12	70 (0)	3 (+1)	2.0 (+1)
#13	70 (0)	2 (0)	1.75 (0)

Response data were analyzed using statistical software (Minitab®). A quadratic (second-order) polynomial model for three explanatory variables was fitted to the data, and model adequacy was assessed through residual analysis and diagnostic checks. The significance of individual factor effects and their interactions were evaluated using analysis of variance (ANOVA).

6.3.2.3. Fourier-transform infrared spectroscopy (FTIR)

The samples were prepared as KBr discs (1/99), analyzed on a Perkin Elmer Spectrum 65 equipment within 4000-600 cm^{-1} range at 4 cm^{-1} resolution with 16 scans, and data were processed after standard background correction and averaging. The degree of deacetylation (DD) of chitosan was determined using the cited technique following the adapted Equation 1 (Brugnerotto et al., 2001).

$$DD = 100 - \frac{\frac{A_{1320}}{A_{1420}} - 0.3822}{0.03133} \quad (1)$$

Where A_{1320}/A_{1420} is the absorbance ratio at 1320 and 1420 cm^{-1}.

Although Brugnerotto et al. (2001) employed a different resolution (2 cm^{-1}) and number of scans (64) for their analysis, Equation 1 was adopted as it represents a correlation derived from their experimental dataset, and its applicability has been demonstrated in the present study.

6.3.2.4. Field Emission Scanning Electron Microscopy (FESEM)

The surface morphology was analyzed by Field Emission Scanning Electron Microscopy (FESEM), before and after the modification process. Micrographs were obtained using a FEI QUANTA-FEG 250 microscope at magnifications of 60x, 1000x, and 5000x.

6.3.2.5. X-ray Diffraction (XRD)

Powder samples were analyzed using a PANalytical X'Pert Pro MPD diffractometer operated in reflection mode with the Bragg-Brentano geometry. The X-ray source was a copper anode equipped with two nickel filter foils, generating Cu Kα radiation with a wavelength of 1.5418 Å. Diffractograms were collected within a 2θ range of 5-35 with a step size of 1 °. min^{-1}.

6.3.2.6. Thermogravimetry (TG)

Samples between 5-10 mg were analyzed using Mettler Toledo TGA/DSC 3+ equipment under N_2 atmosphere at a flow rate of 50 $mL.min^{-1}$ from 30 to 600°C with a heating rate of $10°C.min^{-1}$.

6.3.2.7. Zeta Potential

Suspensions were prepared at a concentration of 0.4% in water/acetic acid from pH 4 to 10 with a conductivity varying between 2~5 mS/cm. Zeta potential measurements were performed using a Zetasizer Pro instrument equipped with DTS1070 cell. Measurements were conducted at room temperature. Each sample was measured 3 times.

6.3.2.8. Contact Angle (CA)

Contact angles were measured with a DataPhysics OCA20 instrument under ambient conditions (20 °C and 20% relative humidity) using powder pressed from the samples in a Graseby Specac laboratory press (10 ton during 1 min). To prevent cross-contamination, a dedicated testing syringe was used for each test liquid: water, 1-bromonaphthalene, propane-1,2,3-triol, and diiodomethane. A 6 µL droplet of each liquid was dispensed from the syringe tip onto the sample surface and the contact angle was measured 3 frames after the drop hits the material. The SCA20 software then calculated the contact angle for each measurement. The reported values represent the average of 3-5 repeated measurements (Kozbial et al., 2014; Zdziennicka et al., 2017).

The surface energy was calculated using two different models, Owens-Wendt-Rabel & Kaelble (OWRK) and Fowkes, only for comparison. The OWRK model combines Good and Young`s equations (Owens; Wendt, 1969; Selvakumar; Barshilia; Rajam, 2010) in Equation 2:

$$\frac{\gamma_l(cos(\theta)+1)}{2\sqrt{\gamma_l^d}} = \sqrt{\gamma_s^p}\frac{\sqrt{\gamma_l^p}}{\sqrt{\gamma_l^d}} + \sqrt{\gamma_s^d}y \quad (2)$$

Since the polar (γ_l^p) and dispersive (γ_l^d) components of the liquid surface energy are known, equation 2 can be simplified by plotting the left side against the square root of the ratio (γ_l^p / γ_l^d). This results in a linear relationship represented by data points. Performing linear regression on this data allows to determine the components of the solid's surface energy. The square of the slope corresponds to the solid's polar component (γ_s^p), and the square of the y-intercept represents the solid's dispersive component (γ_s^d).

The Fowkes model combines Young and Young-Dupree equations and dissociate the surface energy components, resulting in Equation 3:

$$\frac{\gamma_l(cos(\theta)+1)}{2} = \sqrt{\gamma_s^p}\sqrt{\gamma_l^p} + \sqrt{\gamma_s^d}\sqrt{\gamma_l^d} \quad (3)$$

First, diiodomethane (polar component = 0) was tested and the dispersive component of the solid surface energy, γ_s^d, was computed. Second, water or glycerol (polar component ≠ 0) was tested, and using γ_s^d and equation 3, the polar component of the solid surface energy, γ_s^p, was computed. Fowkes theory assumes that the total surface energy is the sum of the dispersive and polar components, so $\gamma_s = \gamma_s^p + \gamma_s^d$ (Fowkes, 1964a).

6.3.2.9. Elemental Analysis

The contents of carbon (C), hydrogen (H), nitrogen (N), and oxygen (O) in samples of pure and modified chitosan were obtained using a Thermofisher Flash Smart instrument with a Chromosorb packed column for gas chromatography. The degree of substitution (DS) was calculated using Equation 4 (Ma et al., 2010):

$$DS = \frac{(\frac{C_1}{N_1} - \frac{C_2}{N_2})}{n} \quad (4)$$

The C_1/N_1 ratio is the experimentally determined ratio obtained from Elemental Analysis, C_2/N_2 is calculated based on the formula of unmodified chitosan and n is the number of carbons introduced on the chitosan derivative.

6.3.2.10. Solid-State Nuclear Magnetic Resonance (NMR)

Solid-state carbon-13 (^{13}C) and nitrogen-15 (^{15}N) nuclear magnetic resonance (NMR) spectra were acquired using an Avance III 400 MHz spectrometer equipped with a CP-MAS probe. All experiments were conducted at a temperature of 298 K (room temperature), with a rotation speed of 12 kHz, using contact time of 2 ms.

For ^{13}C NMR, an acquisition time of 34 ms was used, a sweep width of 39.7 kHz, recycle delay of 2 seconds, and 3800 scans accumulation for each spectrum. Chemical shifts were referenced externally by setting the carbonyl resonance peak of glycine to 176.03 ppm.

For ^{15}N NMR, an acquisition time of 12 ms was used, a sweep width of 16.2 kHz, and a recycle delay of 1 second. Chemical shifts were referenced externally to the NH_4^+ peak of enriched ammonium nitrate.

The degree of deacetylation (DD) of chitosan was also determined using the cited technique following Equation 5:

$$DD = 1 - \frac{A_{CH_3}}{\frac{\sum_{i=1}^{6} A_{C_i}}{6}} \quad (5)$$

A is equal to the area calculated by the integration of the peak of the respective chemical shift.

The degree of substitution (DS) of modified chitosan was determined using a similar approach to that employed for the degree of deacetylation (DD). However, the analysis relied on the newly introduced chemical shifts non-overlapping observed in the NMR spectrum and follows Equation 6 (David et al., 2019):

$$DS = \frac{\sum_{i=1}^{n} A_{\delta_i}}{n * A_{C_1}} \quad (6)$$

A is equal to the area calculated by the integration of the peak of the respective chemical shift, n is the number of new chemical shifts, i is the number of the new carbons added, and C_1 that exhibits a chemical shift of 102 ppm and an integration of 1.

6.4. RESULTS AND DISCUSSION

6.4.1. Reactional mechanism

The reaction between DEEM and chitosan occurs through a conjugate addition-elimination mechanism (Molander; Singaram; Brown, 1984) where the amine group (H_2N-R) from chitosan acts as a nucleophile due to the presence of a lone pair of electrons on the nitrogen atom. This lone pair makes the amine electron-rich and susceptible to attack electron-deficient regions on the trisubstituted vinyl ether used (DEEM). The carbon atom directly bonded to the oxygen atom (2(R')-C=**C**-O-R") is slightly electrophilic (electron-deficient) due to the difference in electronegativity between carbon and oxygen, which pulls the electron density towards oxygen, creating a partial positive charge on the carbon. The lone electrons of the amine are attracted to the partially positive carbon atom of the ethoxymethylene group, forming a carbanion intermediate. This initiates a nucleophilic attack, where the nitrogen atom donates its lone pair to form a new covalent bond with the carbon atom and at the same time there is a release of an ethanol molecule (CH_3CH_2OH) as a byproduct (see Figure 1) (McMurry, 2015). The final product is an enamine (R'-C=C-N-R"), a molecule containing a C=C double bond and an amine group attached to the same carbon atom.

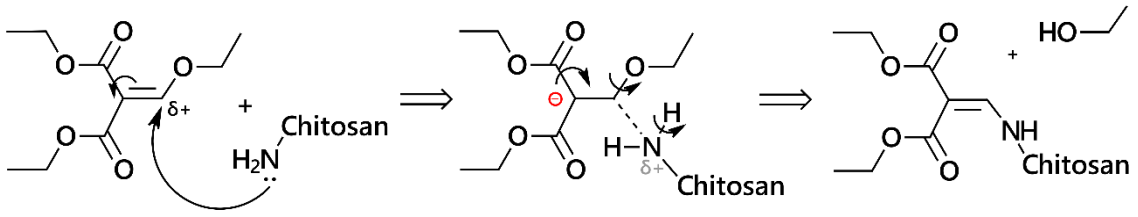

Figure 1 – Conjugate addition-elimination mechanism reaction between DEEM and chitosan.

6.4.2. FTIR

The resulting molecule presented in Figure 1 can be corroborated by the FTIR analysis shown in Figure 2, a positive sign of the success of the previously expected modification. The key peaks of the chitosan backbone, namely those associated to the

glycosidic bond and the C-N bond, at 890 cm^{-1} and 1155 cm^{-1}, respectively, remained unchanged, indicating that the core structure is intact. However, new peaks appeared, proving the introduction of DEEM. The peaks observed at 1255 cm^{-1} and 1022 cm^{-1} attributed to C-O bond stretching and C-O-C symmetrical axial deformation, respectively, are present in both chitosan and DEEM, but the intensity of these peaks significantly increases after the reaction, corroborating the introduction of C-O-C bonds from the DEEM reagent into the final product. The observed increase in the intensity of the CH_3 peaks at 2980 and 2940 cm^{-1} further supports the success of the reaction. This observation is in line with the fact that the starting chitosan possesses a high degree of deacetylation (~80%), implying the presence of a single methyl group per glucosamine unit (Drabczyk et al., 2020). The reaction scheme (Figure 1) shows the introduction of two additional methyl groups per glucosamine unit, corroborating the increase in intensity. The band observed at 1660 cm^{-1}, attributed to the vinylic C-O-C deformation vibration (regarding C=C), appears broader in the spectrum after the reaction. This broadening might be due to the potential overlap, caused by the similarity of the functional groups, with the C=O stretching vibration of the grafted group, which is typically observed around 1710 cm^{-1}. The peak at 805 cm^{-1} (C=C bond), although not directly indicative of a new functional group, supports the presence of DEEM in the structure of modified chitosan (Silverstein et al., 2014).

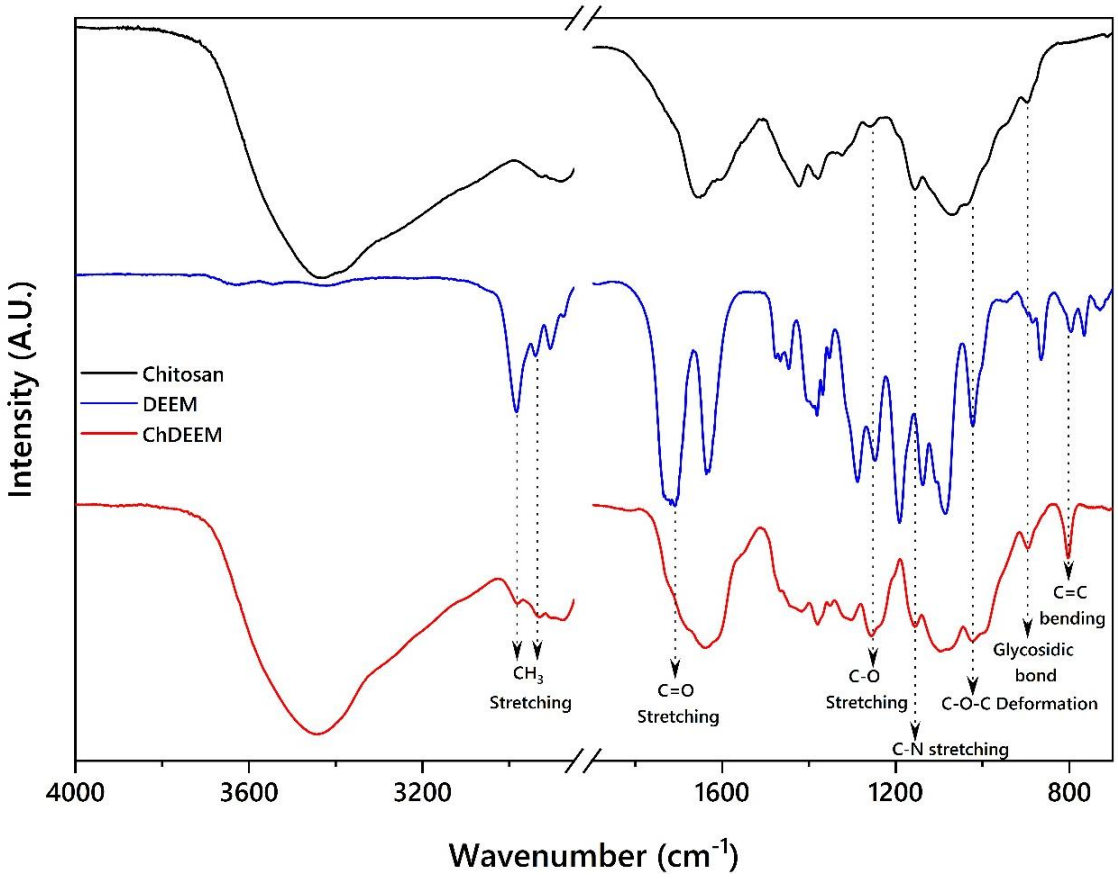

Figure 2 – FTIR spectra of chitosan and modified chitosan (ChDEEM)

The degree of deacetylation (DD) of the chitosan sample was calculated as 82.02% using the acquired spectra and Equation 1. This value is consistent with the DD labeled on the reactant flask (80%), indicating good agreement between the calculated and theoretical values.

6.4.3. NMR

Figure 3 shows the chemical shifts observed by Solid-State ^{13}C NMR. The spectra exhibit the well-known chitosan peaks at 171 ppm for the carbonyl groups of chitin, 102 ppm (C1), 80 ppm (C4), 72 ppm (C5/C3), 58 ppm (C6), 54 ppm (C2) for the carbons of the D-glucosamine molecule and 20 ppm for the methyl groups of chitin (Heux et al., 2000). After modification, the ChDEEM spectrum shows additional carbon signals with peaks at 166 ppm for ester carbons (-O-**C**=O), 158 ppm for the DEEM carbon that is bonded to the amine group (N-**C**=C), 88 ppm for sp^2 hybridized carbons that are linked to two vinylic carbons (C=**C**(C)-C), 11 ppm for DEEM methyl carbons and an increase in signal intensity at 58 ppm with the additional C-O of DEEM (Castillo; Patiny; Wist, 2011).

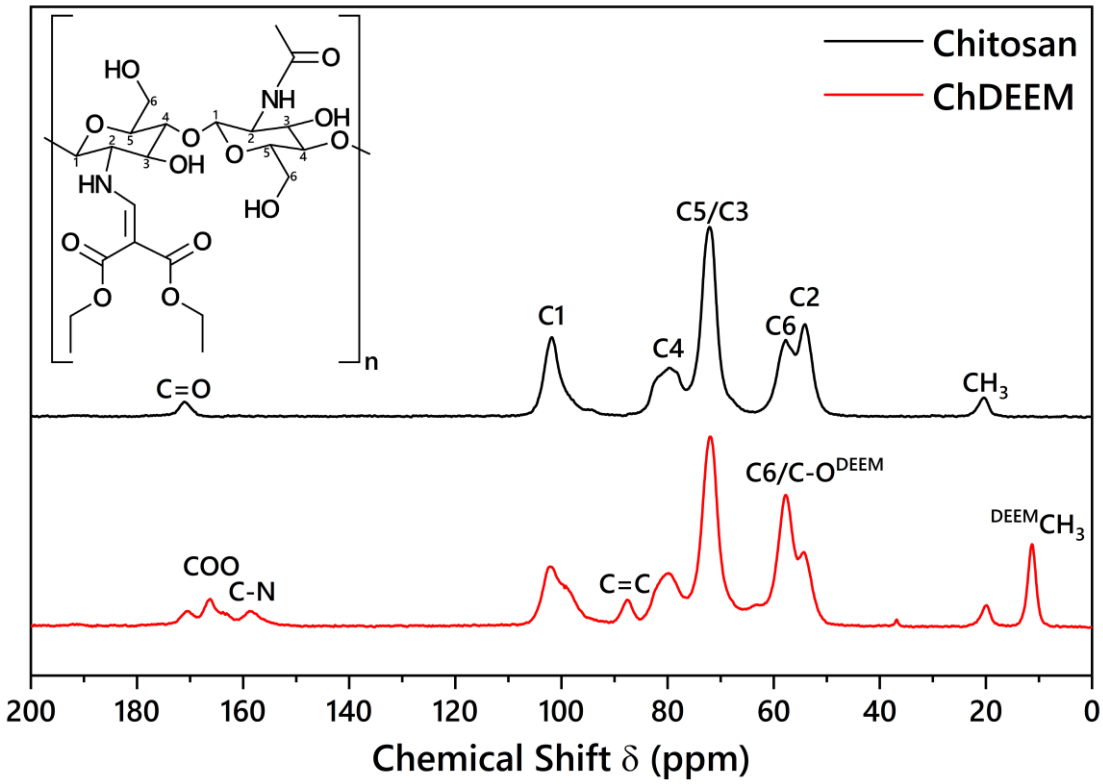

Figure 3 – ^{13}C NMR Spectra for chitosan and modified chitosan with inset molecule of ChDEEM.

The DD of the chitosan sample was calculated to be 85.3% using the acquired spectra and Equation 5. This value is consistent with the DD labeled and with de DD calculated from FTIR analysis.

Equation 6 was employed to calculate the degree of substitution (DS) of the modified chitosan samples, resulting in a value of 0.225. This equation, along with the data used in the calculation, is presented below in Equation 7.

$$DS = \frac{\frac{A_{\delta_{11}}}{2}}{A_{\delta_{102}}} \rightarrow \frac{0.225}{1} \rightarrow 0.225 \qquad (7)$$

The solid-state ^{15}N NMR spectra presented in Figure 4 show the chemical shift of the amine groups near 22 ppm for both chitosan and modified chitosan. After modification, a new peak appears around 117 ppm. This new peak is consistent with the proposed mechanism involving enamine formation (R_1-C=C-**N**-R_2), as this functional group typically exhibits chemical shifts in this range (Mooney; Winson, 1969).

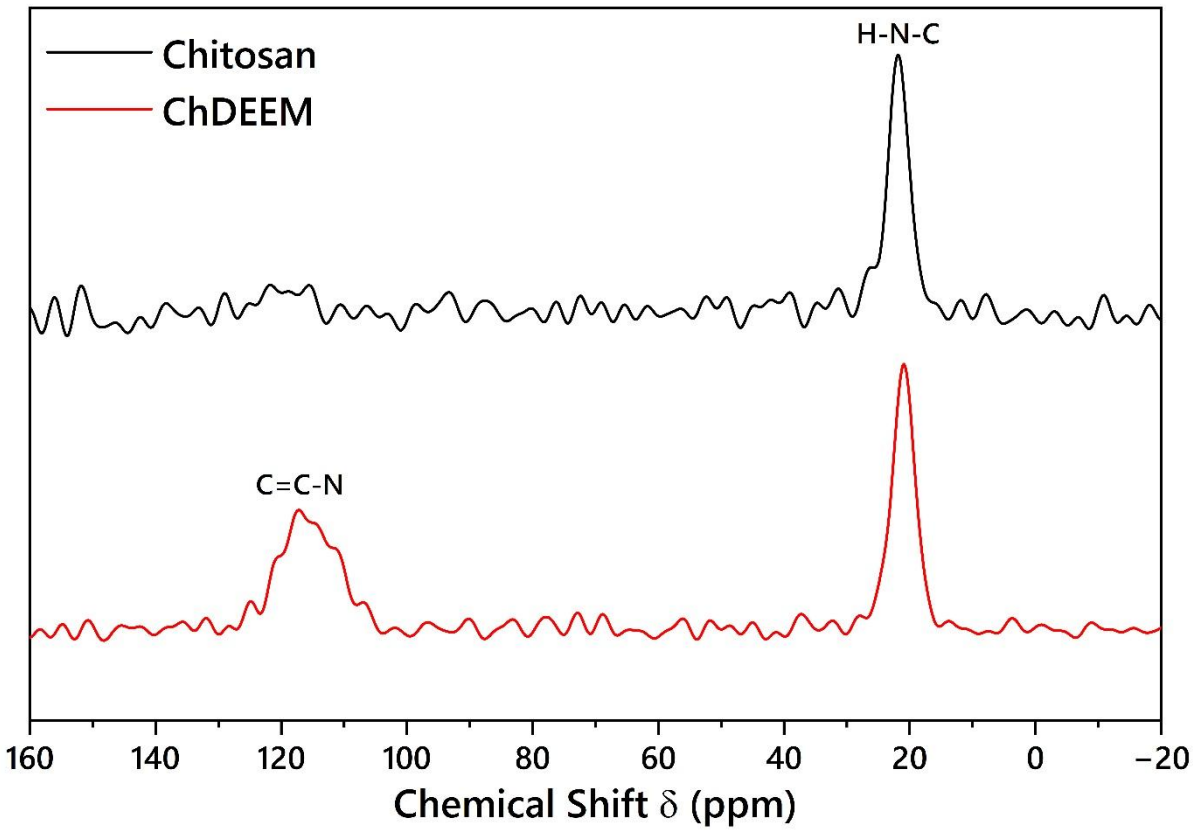

Figure 4 – ^{15}N NMR Spectra for chitosan and modified chitosan.

6.4.4. DoE and ANOVA

Once the experiments had been completed, Table 1 was updated with mass gain data, resulting in Table 2.

Table 2 – Mass gain data after experiments.

Run	Temperature (°C)	Time (h)	Molar ratio [1]:[X]	Mass gain (%)
#1	60 (-1)	1 (-1)	1.75 (0)	13.30
#2	80 (+1)	1 (-1)	1.75 (0)	16.12
#3	60 (-1)	3 (+1)	1.75 (0)	14.16
#4	80 (+1)	3 (+1)	1.75 (0)	25.57
#5	60 (-1)	2 (0)	1.5 (-1)	11.87
#6	80 (+1)	2 (0)	1.5 (-1)	11.87
#7	60 (-1)	2 (0)	2.0 (+1)	12.99
#8	80 (+1)	2 (0)	2.0 (+1)	21.93
#9	70 (0)	1 (-1)	1.5 (-1)	10.78
#10	70 (0)	3 (+1)	1.5 (-1)	10.44
#11	70 (0)	1 (-1)	2.0 (+1)	17.28
#12	70 (0)	3 (+1)	2.0 (+1)	14.67
#13	70 (0)	2 (0)	1.75 (0)	14.52

Table 3 reports the statistical dispersion F-value and significance testing P-value applied to mass gain in analysis of variance (ANOVA). However, it is important to note that the number of center point experiments in the DoE may have limited the precision of the statistical model. The P-value for temperature and molar ratio are close to the common significance threshold of 0.05, suggesting that they may have some influence on the response. However, their value is not low enough to conclusively claim that they have a statistically significant effect. Time has a p-value well above the usual threshold, indicating that there is no strong evidence for its impact. None of the squared terms (temperature^2, time^2, and molar ratio^2) showed a significant effect (p-value above 0.05 and low F-value), indicating that the observed effects of these factors are probably linear within the tested range. Temperature-time interaction showed no statistically significant effect, suggesting that the combined influence of temperature and time is probably not a major contributor in the observed response. Temperature-molar ratio and time-molar ratio interactions also lack statistical significance, indicating that their combined effects are unlikely to be major drivers in the response (Benjamin et al., 2017).

Table 3 - Analysis of variance for the mass gain.

Source	Mass gain	
	P-value	F-value
Linear		
Temperature	0.067	7.89
Time	0.438	0.80
Molar ratio	0.077	7.06
Square		
Temperature^2	0.362	1.15
Time^2	0.742	0.13
Molar ratio^2	0.392	1.00
2-Way Interaction		
*Temperature*Time*	0.237	2.17
*Temperature*Molar ratio*	0.223	2.35
*Time*Molar ratio*	0.723	0.15

A regression equation was generated to describe the relationship between the response variable (mass gain) and all the independent variables (temperature, time, and molar ratio) along with their squared terms and two-way interactions. The equation follows the general form of the following quadratic (second-order) polynomial model for three explanatory variables (Eq. 8):

$$y = a_0 + a_1x_1 + a_2x_2 + a_3x_3 + a_{11}{x_1}^2 + a_{22}{x_2}^2 + a_{33}{x_3}^2 + a_{12}x_1x_2 + a_{13}x_1x_3 + a_{23}x_2x_3 + \varepsilon \quad (8)$$

Where y is the response variable, a_0 the constant, a_n the coefficient, x_n the value of the independent variables and ε the associated error. The following equation (9) represents the actual system.

$$\begin{aligned} Massgain = {} & 115 - 4.6 * Temp - 12.9 * Time + 61 * MolRatio \\ & + 0.0207 * Temp^2 + 0.70 * Time^2 - 30.8 * MolRatio^2 \\ & + 0.215 * Temp * Time + 0.894 * Temp * MolRatio \\ & - 2.27 * Time * MolRatio \end{aligned} \quad (9)$$

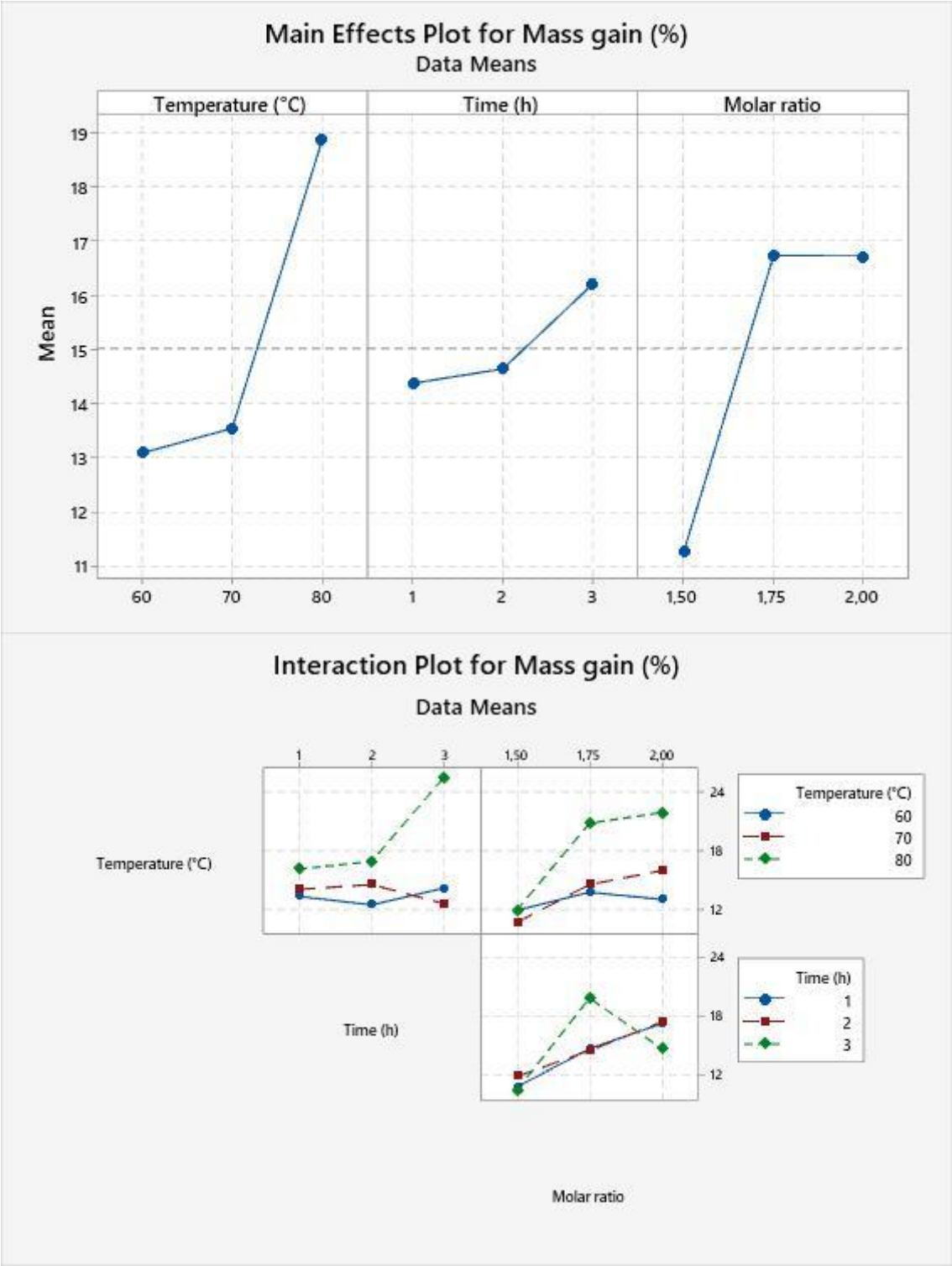

Figure 5 - Response results for mass gain: main effects and interaction plots.

The main effect plots (Figure 5) reveal that higher temperatures and longer times are associated with greater mass gain. However, the influence of temperature is more pronounced than that of time, but this effect depends on molar ratio. This dependence is further explored in the interaction plots, which show that longer times and higher molar

ratios do not necessarily lead to greater mass gain. Notably, a reaction with a molar ratio of 1.75 appears to be more favorable. Based on these results, the optimal parameters for maximizing mass gain are likely to be higher temperature (80 °C), longer time (3 h), and a molar ratio of 1.75, as shown by the surface and contour plots (Figure 6).

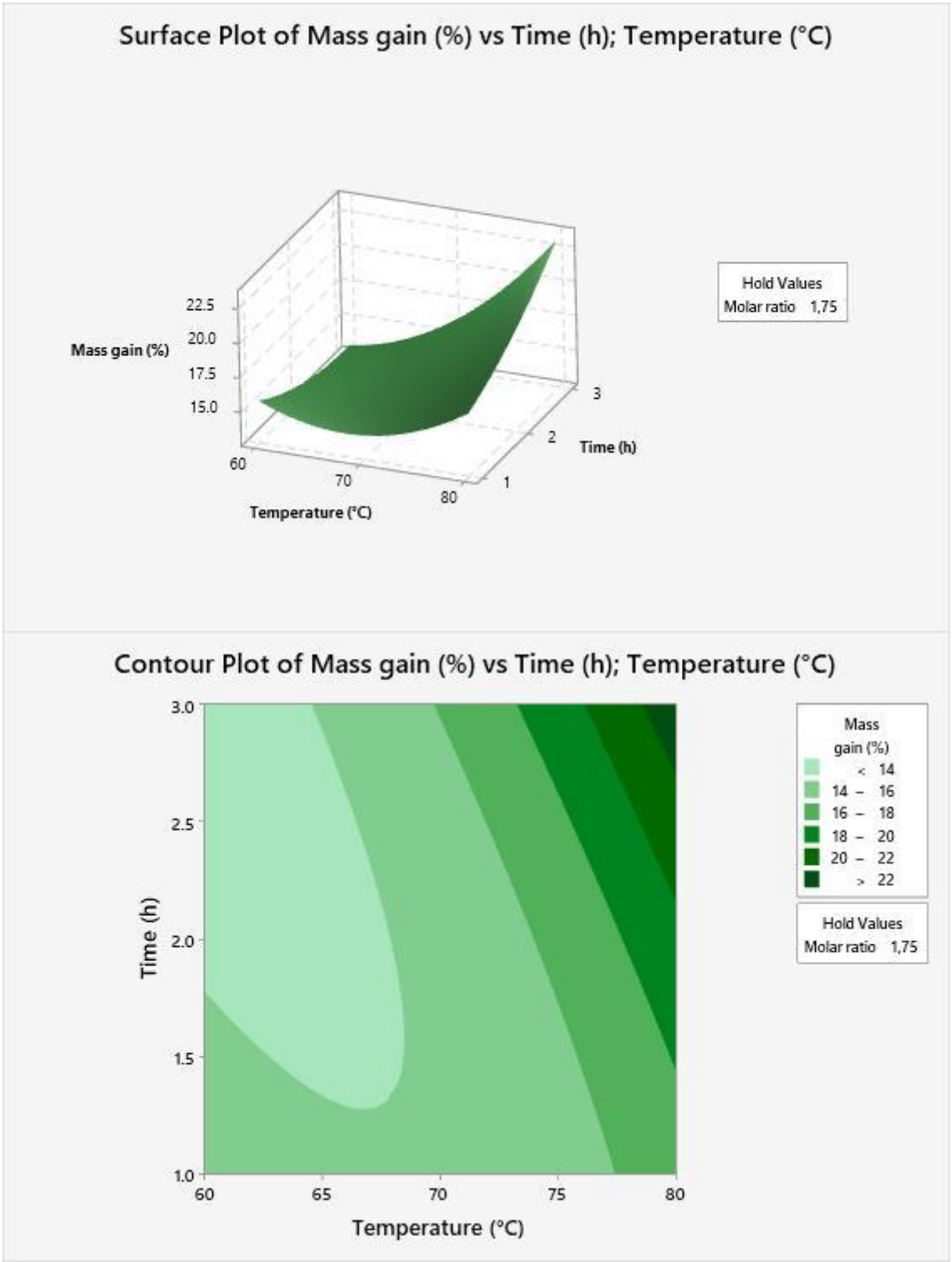

Figure 6 – Surface and contour plot of mass gain with molar ratio fixed at 1.75, at varying times and temperatures.

Furthermore, increasing the amount of reagent from 1.5 to 1.75 mol (0.25 mol increase) resulted in a 6.4% increase in mass gain. However, a further 0.25 mol increase (from 1.75 to 2 mol) yielded only a 2.6% increase, indicating a decrease in mass gain with increasing reagent quantity beyond 1.75 mol (Figure 7). This observation suggests that a molar ratio of 1.75 is more beneficial than a molar ratio of 2 for maximizing mass gain.

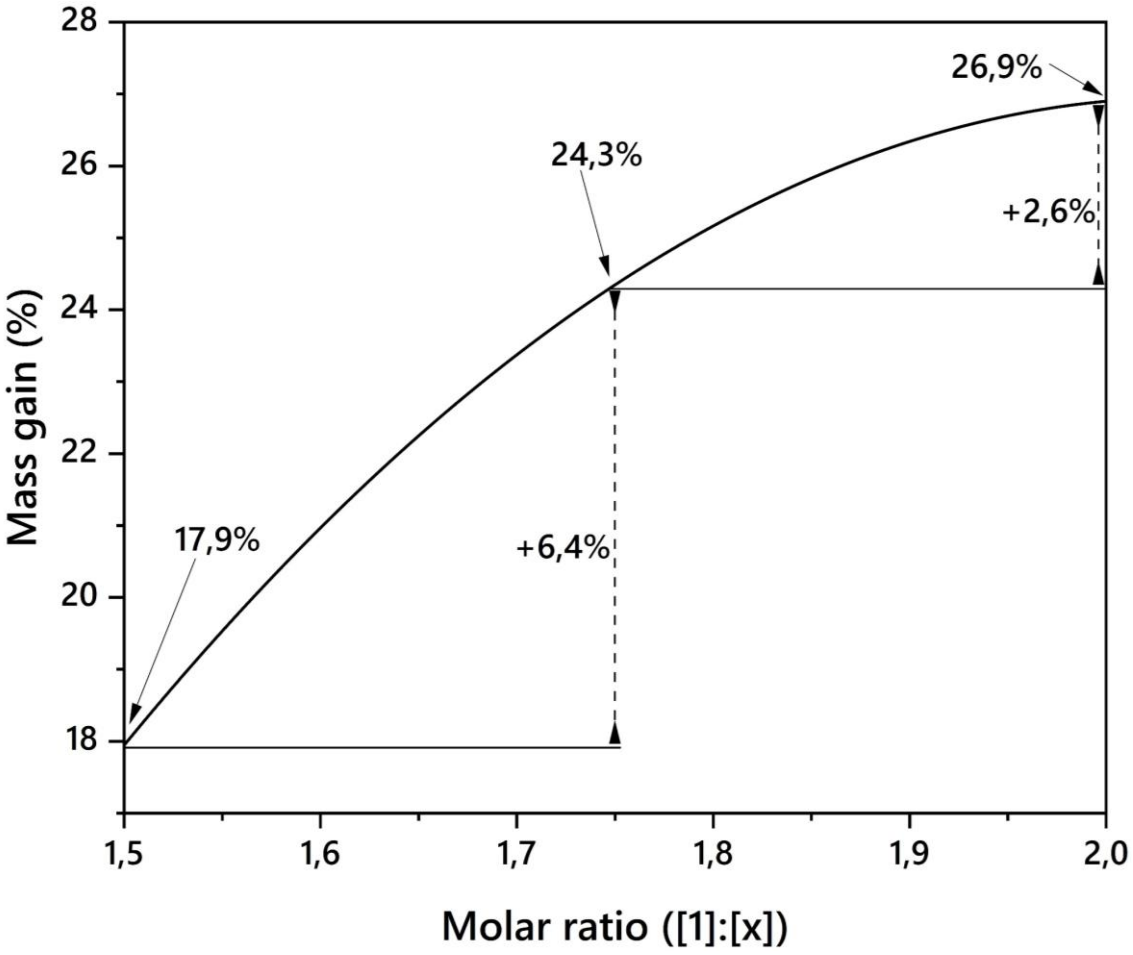

Figure 7 – Theoretical mass gain (%) determined from equation 9, at fixed temperature of 80 °C and for a time of 3 h.

Building on the preceding discussion, all the subsequent graphs and figures will focus on the sample exhibiting the greatest mass increase. This sample was prepared under the following conditions: 80°C, 3 hours, and a molar ratio of 1.75. For brevity, this sample will hereafter be referred to as ChDEEM.

6.4.5. Elemental Analysis

Table 4 shows the percentual content of C, H, N, O and the relation C/N of chitosan and ChDEEM.

Table 4 - Elemental analysis results

Sample	%C	%H	%N	%O	C/N ratio
Chitosan	40.64 ± 0.23	6.81 ± 0.21	7.47 ± 0.21	45.09 ± 0.37	5.44 ± 0.003
ChDEEM	43.73 ± 0.25	6.58 ± 0.24	5.63 ± 0.23	44.06 ± 0.41	7.77 ± 0.003

Equation 4 was employed to estimate the degree of substitution (DS) of the modified chitosan sample, resulting in a value of 0.291 ± 0.005. This equation, along with the data used in the calculation, is presented below in Equation 10.

$$\frac{7.77 - 5.44}{8} \rightarrow DS = 0.291 \pm 0.005 \quad (10)$$

6.4.6. FESEM

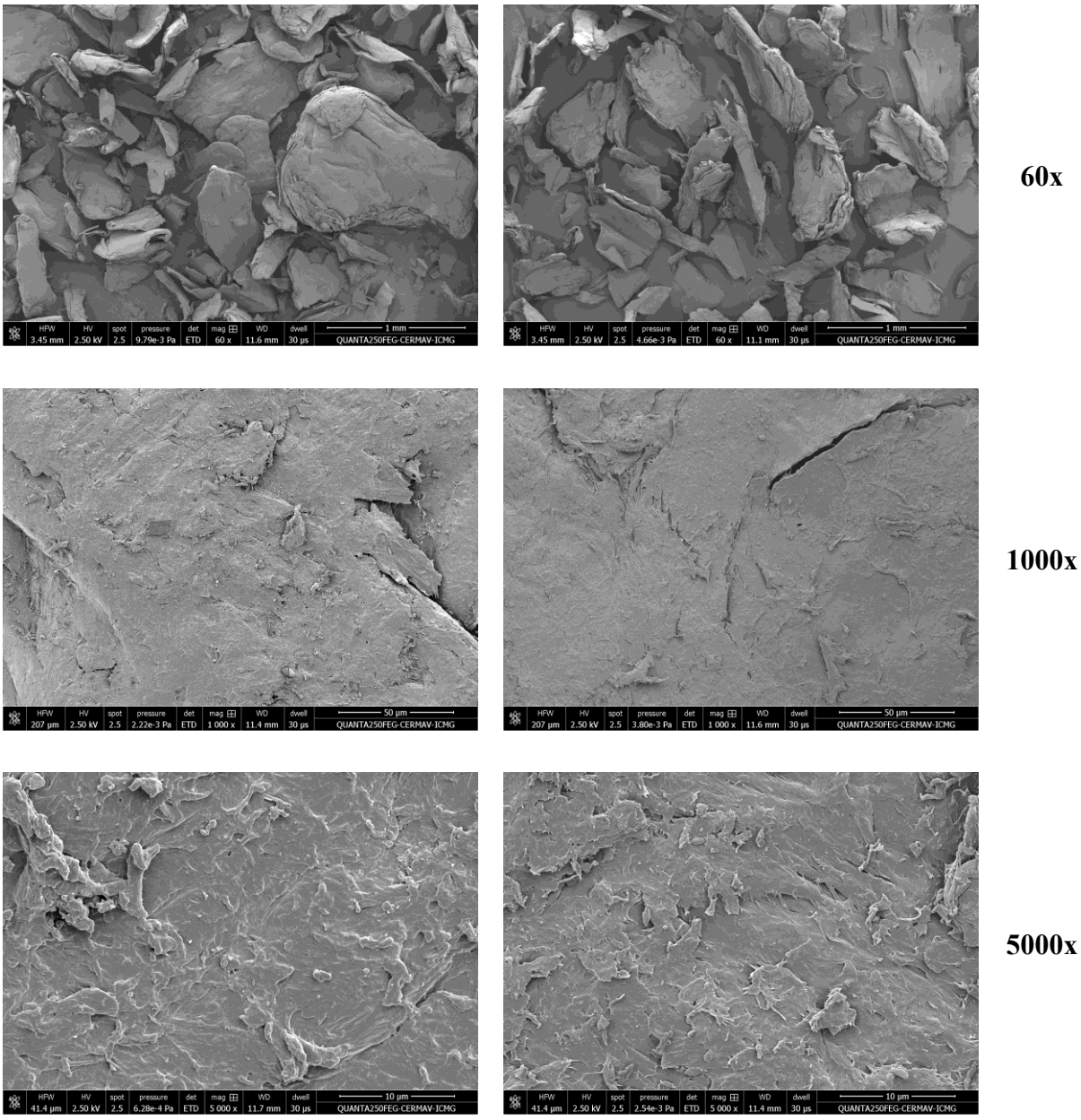

Figure 8 – FESEM micrographs of chitosan and modified chitosan (ChDEEM) at different magnifications

FESEM analysis (Figure 8) revealed no significant changes in surface morphology at lower magnifications (60x). However, at higher magnifications (1000x and 5000x), while the overall structure remained unaltered, fibrillation of chitosan appeared less pronounced. This suggests an increased entanglement of chitosan chains

(smoother surface) but with reduced organization at the finer scale (as discussed in the XRD section).

6.4.7. XRD

XRD analysis (Figure 9) can reveal potential changes in the crystallinity of chitosan after modification with DEEM. Chitosan exhibits two wide peaks around 10° (020) and 20.1° (110), indicating crystalline phase. However, a valley around 15° suggests the presence of an amorphous halo, signifying a non-crystalline portion. The peak height method estimated a crystallinity index (CI) of 79% for chitosan. In contrast, ChDEEM displays a single broader peak around 20.5° and a more prominent amorphous halo compared to chitosan. This signifies a significant decrease in crystallinity, with the peak height method estimating a CI of only 38%.

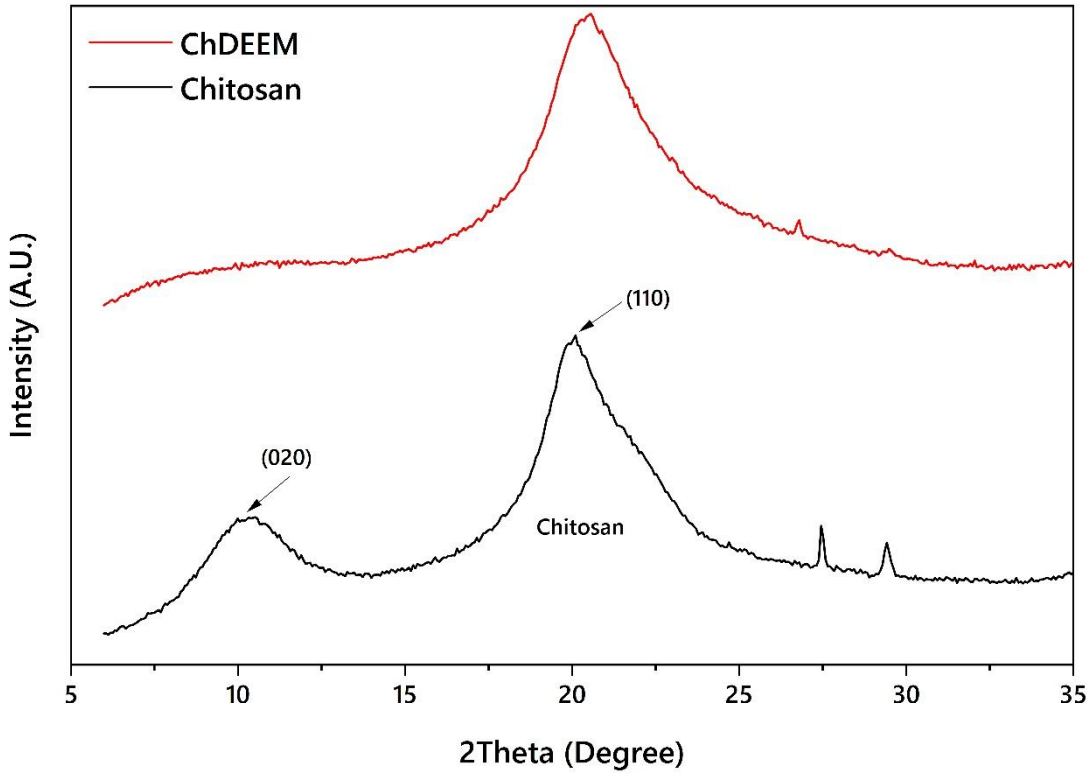

Figure 9 – X-Ray diffractograms for chitosan and modified chitosan (ChDEEM)

These observations suggest that the chemical modification process with DEEM has significantly impacted the crystallinity of chitosan. The introduction of DEEM molecules likely disrupted the arrangement of chitosan chains within the crystalline regions, leading to a more amorphous structure. This phenomenon can be explained by the bulky nature of DEEM moieties hindering the formation and organization of the

ordered crystalline structure observed for unmodified chitosan. In simpler terms, the addition of DEEM appears to have broken down the ordered arrangement of chitosan molecules, reducing its overall crystallinity (Wang et al., 2020).

6.4.8. Zeta Potential

The zeta potential measurement performed for chitosan and ChDEEM (Figure 10) shows that due to the absence of strongly ionizable groups like primary amines ($R\text{-}NH_2$), DEEM itself is expected to have minimal contribution to positive charge in the pH range investigated (pH 4-10). This further explains why the modified chitosan exhibits lower zeta potential compared to unmodified chitosan, especially at lower pH values where the amino groups of unmodified chitosan contribute significantly to the positive charge. In essence, the combination of reduced positive charge in DEEM compared to amine groups of chitosan and limited overall charge contribution of DEEM due to its structure lead to a weaker positive charge for modified chitosan, particularly at lower pH values. This results in a decrease in zeta potential and shift in the isoelectric point towards lower pH values compared to unmodified chitosan (Pereira et al., 2023; Sirviö et al., 2021).

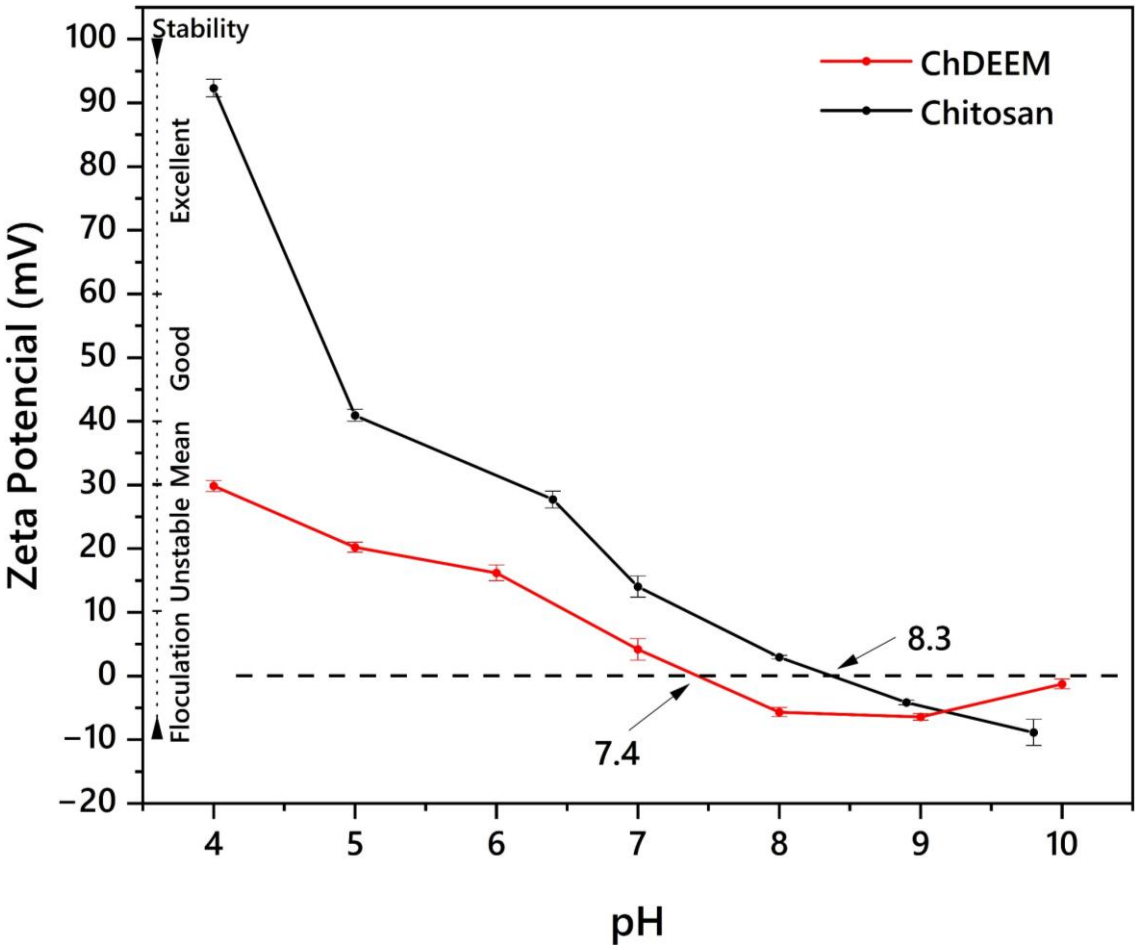

Figure 10 – Zeta potential as a function of pH for chitosan and modified chitosan with scale of stability and isoelectric point.

The modified chitosan demonstrated a marked increase in flocculation compared to its unmodified counterpart at lower pH values. This enhancement can be ascribed to the substitution of amine groups with DEEM groups, resulting in a decrease in intra- and intermolecular hydrogen bonding (Athavale et al., 2022). While the increased free volume and enhanced solvent diffusion would generally promote solubility, the introduction of a voluminous organic group significantly augments hydrophobicity, as corroborated by contact angle analysis. Solubility tests were conducted using DMSO, acetone, water, acetic acid solution, and ethanol, and the modified chitosan was found to be always flocculated in all tested solvents.

6.4.9. Contact Angle

The chemical modification process seems to have made the ChDEEM surface less attractive to polar liquids in general and also showed a slight decrease in its affinity for non-polar liquids (Table 5).

Table 5 – Contact angle data of Chitosan and ChDEEM for different liquid media.

	Chitosan	**ChDEEM**
Water	53.71 ± 0.06	68.85 ± 0.66
Propane-1,2,3-triol	65.28 ± 0.38	78.69 ± 0.85
Diiodomethane	32.03 ± 0.29	37.11 ± 0.65
1-bromonaphthalene	18.97 ± 0.54	28.18 ± 0.57

The higher the CA value, the less the affinity of the liquid for the solid surface. CA for water and glycerol (polar liquids) increases for ChDEEM compared to chitosan, suggesting an increased hydrophobicity after modification. The same trend is observed for diiodomethane and 1-bromonaphthalene (non-polar liquids). However, the increase is smaller compared to water and glycerol, mainly because of the lower initial value. This suggests ChDEEM might have become slightly less receptive to non-polar interactions, but the overall change is less significant.

As mentioned in the Experimental Section, the surface energy of chitosan and ChDEEM was calculated following the Fowkes approach by substitution and OWRK method by linearization (Table 6).

Table 6 - Surface Energy determined by Fowkes and Owens-Wendt-Rabel & Kaelble models.

	Fowkes Model			**Owens-Wendt-Rabel & Kaelble**		
$mJ.m^{-2}$	γ_s	γ_s^p	γ_s^d	γ_s	γ_s^p	γ_s^d
Chitosan	**55.19 ± 0.83**	12.49 ± 0.40	42.69 ± 0.73	**53.25 ± 0.55**	13.42 ± 0.39	39.84 ± 0.38
ChDEEM	**45.89 ± 0.94**	5.96 ± 0.37	39.93 ± 0.87	**41.12 ± 0.97**	3.01 ± 0.94	38.11 ± 0.23

Both approaches (Fowkes and OWRK methods), presented in Table 6, have a similar trend, indicating that ChDEEM has a slightly lower surface energy compared to

regular chitosan, suggesting a potential change in surface characteristics after the modification process. The surface energy values we obtained for chitosan (for both methods) falls within the range reported by Gandini (Cunha et al., 2008) for different degrees of deacetylation, viz. 31 to 62 $mJ.m^{-2}$, providing some validation for the measured values. The lower surface energy for ChDEEM can be attributed to a more hydrophobic surface after grafting of diethyl methylenemalonate and, as reported in the discussion of FESEM results, an increase in the surface`s smoothness (Li et al., 2021b).

6.4.10. Thermogravimetry

TG analysis was employed to investigate the thermal stability of chitosan and ChDEEM. The thermal events occurring across the temperature range were scrutinized, and the corresponding data are presented in Table 7. These data were extracted from the analysis of TG curves.

Table 7 – TG data for Chitosan and ChDEEM.

Event/Sample	Chitosan	ChDEEM
Evaporation of residual water		
T_{onset} (°C)	49.8	40.3
T_{max} (°C)	76.3	72.2
Mass Loss (%)	2.9	2.6
Desorption of remaining solvent		
T_{onset} (°C)	-	91.0
T_{max} (°C)	-	116.8
Mass Loss (%)	-	2.6
Main degradation stage		
T_{onset} (°C)	180.7	131.0
T_{max} (°C)	300.8	311.0
Mass Loss (%)	22.8	30.0

Figure 11 reveals two distinct multi-stage degradation events for ChDEEM and two major events for chitosan across the analyzed temperature range. The initial mass loss stage is likely attributed to the evaporation of water and low-molecular-weight compounds present within the samples. For ChDEEM, the observed decrease in thermal stability compared to chitosan in this stage might be associated to the presence of trace

residual acetone from the washing step. The nested event observed solely for ChDEEM could be related to the desorption of any remaining solvent molecules, potentially including trace amounts of DMSO adsorbed during the modification process. The second event, observed at higher temperature, is primarily associated with the main decomposition of chitosan, likely involving the breakdown of its polymer chains. The observed decrease in thermal stability, compared to unmodified chitosan, can be attributed to the presence of DEEM, which likely contributed to a decrease in crystallinity (as observed in XRD) and a reduction in intra- and intermolecular hydrogen bonding (as evidenced by zeta potential measurements). This ultimately resulted in increased interchain distances and decreased thermal stability, consistent with Delezuk (2014) (Delezuk; Pavinatto; Campana Filho, 2014).

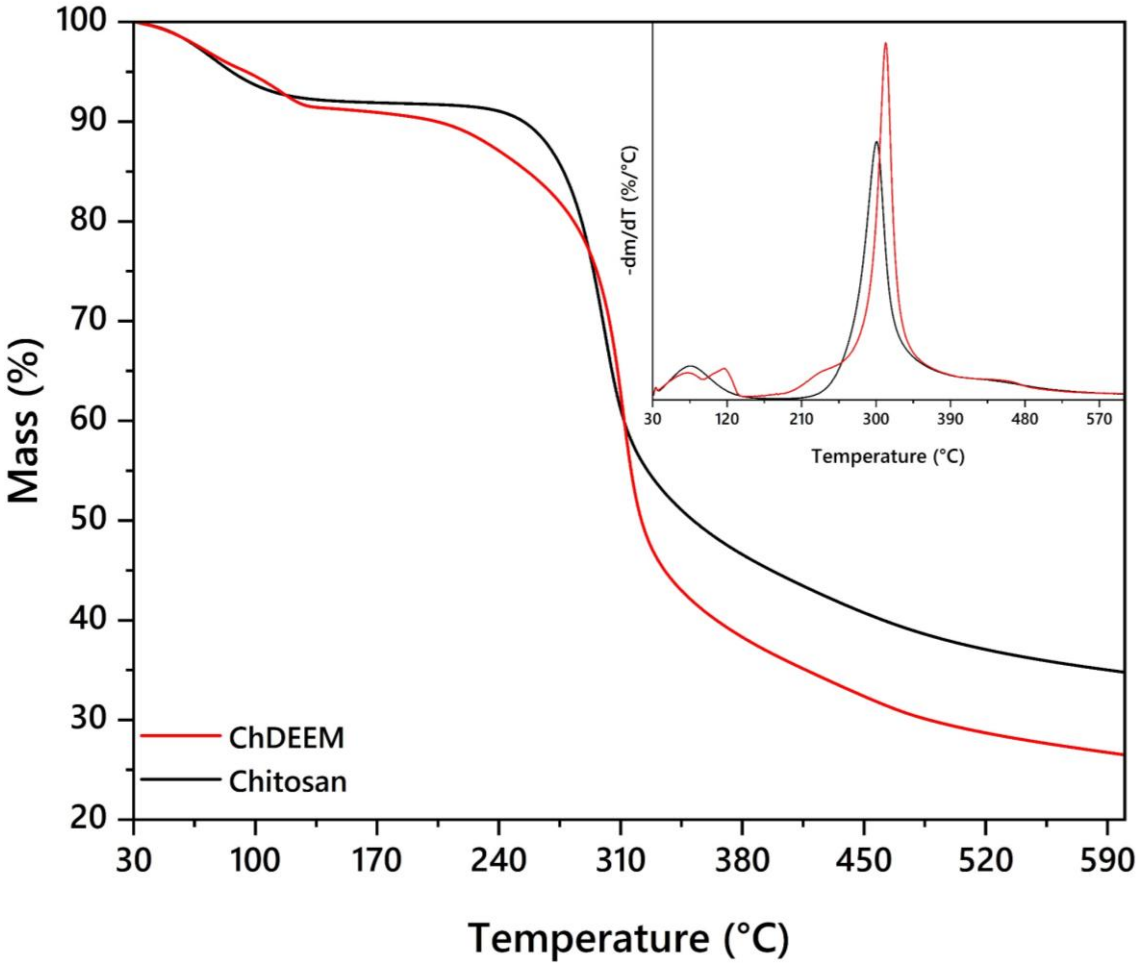

Figure 11 –TG curves comparing chitosan and modified chitosan (ChDEEM) with dTG curves as inset.

6.5. CONCLUSION

Conjugate addition-elimination of chitosan with DEEM was successfully carried out being corroborated by the C=C strong absorption band in the FTIR spectrum and new chemical shifts in the NMR spectrum. The reaction conditions for the highest mass gain (1:1.75 molar ratio, 80 °C, and 3 hours) were optimized. ChDEEM displayed a morphology and thermal behavior similar to chitosan. However, XRD revealed a decrease in crystallinity due to the incorporation of methylenemalonate groups into the chitosan polymer chain. Furthermore, zeta potential analysis indicated a decrease in the isoelectric point compared to unmodified chitosan, as expected from the introduction of these groups. Additionally, contact angle measurement showed an increase in hydrophobicity after chemical modification, as well as a decrease in surface energy and thermal stability. These findings support our hypothesis that DEEM modification enhances chitosan's properties for environmental applications.

In conclusion, the synthesis of ChDEEM through a conjugate addition-elimination reaction with diethylethoxymethylenemalonate (DEEM) presents a promising approach for developing novel chitosan derivatives with tailored properties. The insolubility of ChDEEM in water makes it a promising candidate for environmental applications, particularly in the removal of dyes, organic molecules, and heavy metals. Additionally, the presence of the double bond within the chitosan derivative opens up possibilities for further functionalization and composite formation, potentially expanding ChDEEM's utility in material science for applications such as packaging with enhanced properties or drug delivery systems with controlled release mechanisms. Future studies will focus on evaluating the adsorption capacity and selectivity of ChDEEM for specific pollutants, as well as exploring its potential for other applications such as catalysis or biomedicine.

6.6. ACKNOWLEDGEMENT

We gratefully acknowledge the financing by the Coordenação de Aperfeiçoamento de Pessoal de Nível Superior – Brasil (CAPES) – Finance Code 001 - for the doctoral scholarship and PDSE (Programa de Doutorado-sanduíche no Exterior); the LGP^2 /PAGORA staff from Grenoble INP for the support in developing part of this work; to Isabelle Jeacomine from the Institute de Chimie Moleculaire de Grenoble (CNRS/CERMAV) for the ^{13}C and ^{15}N NMR analysis; to Sandrine Adach from the SynBioN (Universitè de Lorraine/CNRS) for the elemental analysis performed; LGP^2 is part of the LabEx Tec 21 (Investissements d'Avenir - grant agreement n◦ANR-11-LABX-

0030) and of the PolyNat Carnot Institut (Investissements d'Avenir - grant agreement nº ANR-11- CARN-030-01).

7. OPTIMIZED ONE-POT REACTION AND CHARACTERIZATION OF A CYANOETHOXYETHYLATED CHITOSAN

7.1. ABSTRACT

Chitosan offers a wide range of applications due to its reactive amino groups, which enable various modifications. This study presents the synthesis of a chitosan derivative (ChECEA) using ethyl 2-cyano-3-ethoxyacrylate (ECEA). The reaction was conducted under various conditions to optimize the mass gain of the ChECEA. Stoichiometry (1.5 and 2M), temperature (60 to 95 °C), and reaction time (1 to 3.5 h) were varied. The ChECEA was characterized using a variety of techniques, including Fourier Transform Infrared Spectroscopy (FTIR), Nuclear Magnetic Resonance (NMR), Thermogravimetry (TG), Scanning Electron Microscopy (SEM), X-Ray Diffraction (XRD), Zeta Potential, Contact Angle (CA), and Elemental Analysis (EA). FTIR confirmed the successful modification, evidenced by a sharp peak at 2220 cm^{-1} corresponding to the CN bond stretching. NMR analysis revealed new chemical shifts (166, 158, 115, and 11 ppm), and in combination with EA, was used to estimate the degree of substitution (DS) as 0.640 and 0.725, respectively. TG indicated a decrease in thermal stability and Zeta Potential suggested reduced suspension stability. Conversely, contact angle measurements showed increased hydrophobicity and decreased surface energy. Finally, XRD analysis revealed a decrease in the crystallinity index (from 79% to 55%), likely due to the incorporation of cyanoethoxyacrylate groups.

7.2. INTRODUCTION

Chitosan, also known as soluble chitin, is composed of monomeric units of β-(1-4)-2-amino-2-deoxy-D-glucose and is the only cationic polysaccharide in nature (Yu; Kecen; Xiaosai, 2018). It is obtained by alkaline or enzymatic deacetylation of chitin, which can be extracted from various sources, including invertebrates such as insect cuticles (Vilar Junior et al., 2016; Zainol Abidin et al., 2020) and crustacean shells (Yeul; Rayalu, 2013), green algae (Blank; Hinman, 2016), and certain microorganisms like yeast (Chatterjee et al., 2005) and fungi (Huq et al., 2022).

The potential for chitosan in various applications stems from its renewable sources, such as fisheries waste, and its valuable characteristics, including non-toxicity, biocompatibility, biodegradability, and non-carcinogenicity. Therefore, chitosan has potential utilities in various fields like biomedicine (Zhao et al., 2018a), wastewater

treatment (Hameed et al., 2022; Salehi et al., 2022; Zhao et al., 2018b), food packaging (Song et al., 2018; Xu et al., 2022), functional membranes (Salehi; Daraei; Arabi Shamsabadi, 2016; Yang et al., 2019), anticancer (Adhikari et al., 2022; Adhikari; Garai; Yadav, 2023), among several other features (Cañas; Delgado; Gartner, 2016; Rafique et al., 2016).

Chitosan's versatility is attributed to its reactive amino groups, which enable a diverse array of chemical modifications, such as acylation (Nanda et al., 2019; Niemczyk et al., 2019; Piegat et al., 2020), carboxylation (Chen et al., 2004; Na et al., 2010), alkylation (Sun et al., 2021; Zhang et al., 2019a), quaternization (Luan et al., 2018; Zhang et al., 2018), sulfonation (Huang et al., 2019; Kazachenko et al., 2021), phosphorylation (Han et al., 2020), thiolation (Prabahar; Udhumansha; Qushawy, 2020), graft copolymerization (Li et al., 2021a), and Schiff base formation (Cao et al., 2021; Haj; Mohammed; Mohammood, 2020), as well as alkoxymethylation (Pereira et al., 2023) and other related reactions.

Chitosan, a versatile polymer with a broad range of applications, requires further modifications to optimize its performance for specific purposes. This study hypothesizes that the introduction of alkoxymethylene groups to chitosan through a reaction with ethyl 2-cyano-3-ethoxyacrylate (ECEA) will yield a novel chitosan derivative with significantly reduced aqueous stability. This modification is expected to enhance the material's suitability for the efficient adsorption of dyes, organic molecules, and heavy metals. Moreover, the introduction of a cyanoacrylate functional group could potentially improve the drug delivery (Jafernik et al., 2023; Li et al., 2018) and tissue adhesive (Wang et al., 2024) properties already associated with chitosan.

7.3. EXPERIMENTAL

7.3.1. Materials

Chitosan (Ch) with average molecular weight (80% deacetylation degree (DD) ~ AGU molar mass of 169.57 g.mol^{-1}), ethyl 2-cyano-3-ethoxyacrylate (99%) (ECEA) were purchased from Merck Chemicals, dimethyl sulfoxide (DMSO) (99.5%) and acetone (99.8%) were purchased from Roth. All solvents and reagents were used without further purification.

7.3.2. Methods

7.3.2.1. Chitosan's modification

The chitosan modification was made changing the temperature, how long the reactants mixed and the molar ratio between them. It was taken 0.5 grams of chitosan and dissolved it in DMSO at different temperatures. Then, it was added a specific amount of reactant (ECEA) and mixed them for various lengths of time. This created materials with different ratios of chitosan to ECEA. Once the mixing time was complete, Soxhlet extraction with acetone, during 4 hours, was used to remove any leftover starting materials. Finally, the cleaned product was dried and stored. The chemical equation for the reaction is presented in Figure 1 (Mathias et al., 2025a; Molander; Singaram; Brown, 1984; Pereira et al., 2023).

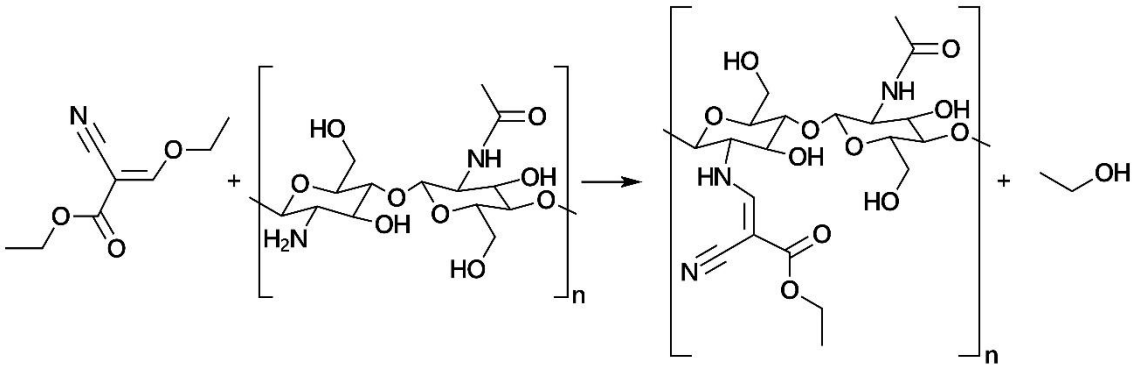

Figure 1: Visualization of the molecules in the reaction between ECEA and chitosan.

7.3.2.2. DoE and ANOVA

To optimize the synthesis of ChECEA, a two-stage Design of Experiments (DoE) approach was employed.

Stage 1: Exploring Different Options (Full Factorial Design)

Three key factors influencing the synthesis were investigated: reaction time (1 and 3 hours), temperature (60 and 80 °C), and molar ratio of chitosan to ECEA (1.5 and 2). A full factorial design of 2^3 (eight) experiments was chosen for this initial stage, as can be seen on Table 1. This approach allows for the evaluation of the main effects of each factor and their potential interactions on the response variable (desired property of ChECEA).

Table 1: Full factorial design

Run	Temperature (°C)	Time (h)	Molar ratio [1]:[X]
1	80	1	2.0
2	80	1	1.5
3	80	3	2.0
4	60	3	2.0
5	80	3	1.5
6	60	3	1.5
7	60	1	2.0
8	60	1	1.5

Stage 2: Fine-Tuning the Best Conditions (Central Composite Design)

Based on the insights gained from the full factorial design, a central composite design (CCD) was employed in the second stage. The CCD focused on the same three factors (reaction time, temperature, and molar ratio) but with more precise levels. Time was varied from 2.5 to 3.5 hours in 0.5-hour increments, temperature ranged from 75 to 95 °C in 10 °C increments, and the molar ratio was fixed at 2. CCD offers a more efficient exploration of the factor space around the optimal region identified in Stage 1. It allows for the estimation of both linear and non-linear effects of the factors on the response variable, leading to a more robust optimization process, the design can be seen on Table 2.

Table 2: Central composite design

Run	Temperature (°C)	Time (h)
1	75	2.5
2	85	2.5
3	75	3.5
4	85	3.5
5	75	3.0
6	85	3.0
7	95	2.5
8	95	3.5
9	95	3.0

The collected response data from the DoE experiments were analyzed using statistical software such as Minitab®. To understand the relationship between the investigated factors (reaction time, temperature, and molar ratio) and the desired outcome of ChECEA synthesis, a second-order polynomial model was employed. This model incorporates both linear and quadratic terms for each factor, allowing for the exploration of potential interactions between them.

The adequacy of the fitted model was rigorously assessed through residual analysis and various diagnostic checks. This ensures the model accurately captures the underlying trends in the data and provides reliable predictions. To identify statistically significant factors and their interactions that influence the ChECEA synthesis process, an analysis of variance (ANOVA) was performed (Onjia, 2016).

7.3.2.3. Fourier-transform infrared spectroscopy (FTIR)

For analysis by Fourier Transform Infrared Spectroscopy (FTIR), the samples were prepared as KBr discs. The ratio of sample to KBr was kept at 1:99 to ensure sufficient sample concentration for analysis. The prepared KBr discs were then analyzed using a Perkin Elmer Spectrum 65 instrument. The instrument scanned the samples across a broad range of infrared wavelengths, specifically from 4000 cm^{-1} to 600 cm^{-1}. The scan resolution was set to 4 cm^{-1}, ensuring a detailed picture of the infrared absorption profile. To improve the signal-to-noise ratio and enhance data quality, 16 scans were accumulated

for each sample. The degree of deacetylation (DD) of chitosan was determined using the cited technique following the adapted Equation 1, originally presented by (Brugnerotto et al., 2001).

$$DD = 100 - \frac{\frac{A_{1320}}{A_{1420}} - 0.3822}{0.03133} \quad (1)$$

Where A_{1320}/A_{1420} is the absorbance ratio at 1320 and 1420 cm^{-1}.

7.3.2.4. Field Emission Scanning Electron Microscopy (FESEM)

To investigate the morphological changes induced by the modification process on the surface of the samples, Field Emission Scanning Electron Microscopy (FESEM) analysis was employed. This high-resolution imaging technique provides detailed information about the surface topography and features at various magnifications.

The samples were analyzed using a FEI QUANTA-FEG 250 microscope. Images, also known as micrographs, were captured at three different magnifications: 60x, 1000x, and 5000x. This range allows for a comprehensive examination of the surface, from capturing the overall structure at lower magnification to visualizing finer details and potential modifications at higher magnifications.

7.3.2.5. X-ray Diffraction (XRD)

X-ray diffraction (XRD) analysis was performed to investigate the crystalline structure of the powder samples. The analysis employed a PANalytical X'Pert Pro MPD diffractometer operated in reflection mode with the Bragg-Brentano geometry.

The diffractometer utilized a copper (Cu) anode X-ray source equipped with two nickel (Ni) filter foils. These filters selectively remove unwanted radiation from the X-ray source, ensuring a monochromatic beam of CuKα radiation with a wavelength of 1.5418 Å.

The samples were scanned through a range of 2θ angles, from 5° to 40°. The scan step size was set at $1°.min^{-1}$ ensuring a sufficient number of data points to capture detailed information about the crystal structure.

7.3.2.6. Thermogravimetry (TG)

To understand the thermal decomposition behavior of the dry samples, a Mettler Toledo TGA/DSC 3+ instrument was employed. The analysis was conducted under a

controlled nitrogen (N_2) atmosphere with a constant flow rate of 50 $mL.min^{-1}$. This inert atmosphere minimizes undesired reactions with oxygen that could occur during heating.

The samples were subjected to a temperature program that started at 30 °C and ramped up to 600 °C at a heating rate of 10 $°C.min^{-1}$. This heating profile allows for controlled thermal decomposition and provides data on the weight changes and heat flow associated with various temperature transitions experienced by the samples.

7.3.2.7. Zeta Potential

Suspensions were prepared at a concentration of 0.4% by weight in a mixture of water and acetic acid. The pH of this mixture was varied with addition of sodium hydroxide (NaOH) and hydrochloric acid (HCl) to create a range of values from 4 to 10. The zeta potential measurements were carried out using a Zetasizer Pro instrument equipped with a DTS1070 cell with 2 $mS.cm^{-1}$ as the minimum of samples' conductivity. All measurements were conducted at room temperature to ensure consistent conditions. To improve the reliability of the data, each sample was measured three times, and the average value was reported.

7.3.2.8. Contact Angle (CA)

To assess the surface properties and wettability of the samples, contact angle measurements were employed. The measurements were performed using a DataPhysics OCA20 instrument under controlled ambient conditions: a temperature of 20 °C and a relative humidity of 20%. To prevent any contamination between different liquids, a dedicated testing syringe was used for each test liquid. Four specific liquids were chosen for the analysis: water, 1-bromonaphthalene, propane-1,2,3-triol (glycerol), and diiodomethane. A small droplet of 6 µL from each liquid was carefully dispensed onto the sample surface using the designated syringe, and the fourth frame after the drop fall over the surface was used as the choose value.

The SCA20 software, which controls the instrument, then automatically calculated the contact angle for each measurement. The reported contact angle values in the study represent the average of 3 repeated measurements on each sample. Additionally, Table 3 provides information about the surface energy components of the test liquids used according to (Kozbial et al., 2014; Zdziennicka et al., 2017)). Knowing these values allows to calculate the surface energy components of the samples using established mathematical models based on the measured contact angles.

Table 3 - Polar and Dispersive Surface Energy Components of the Test Liquids

	γ_l (mJ.m^{-2})	γ_l^p (mJ.m^{-2})	γ_l^d (mJ.m^{-2})
Water	72.8	45.6	27.2
Propane-1,2,3-triol	64.0	27.7	36.3
Diiodomethane	50.8	0.0	50.8
1-bromonaphthalene	44.4	0.9	43.5

To obtain a more comprehensive picture of the surface energy of the samples, calculations were performed using two established models: the Owens-Wendt-Rabel & Kaelble (OWRK) model and the Fowkes model. The OWRK model offers a more detailed approach by combining the concepts from Good's equation and Young's equation. Good's equation relates the surface tension of a liquid to its polar and dispersive components, while Young's equation describes the relationship between the contact angle, surface tension of the liquid, and surface energy of the solid. By incorporating both these equations, the OWRK model (Equation 2) allows for the calculation of both the polar and dispersive components of the solid's surface energy based on the measured contact angles of different test liquids with known surface energy components (Owens; Wendt, 1969; Selvakumar; Barshilia; Rajam, 2010):

$$\frac{\gamma_l(cos(\theta)+1)}{2\sqrt{\gamma_l^d}} = \sqrt{\gamma_s^p}\frac{\sqrt{\gamma_l^p}}{\sqrt{\gamma_l^d}} + \sqrt{\gamma_s^d}y \qquad (2)$$

Since the polar (γ_l^p) and dispersive (γ_l^d) components of the liquid surface energy are known, equation 2 can be simplified by plotting the left side against the square root of the ratio (γ_l^p / γ_l^d). This result in a linear relationship represented by data points. Performing linear regression on this data allows to determine the components of the solid's surface energy. The square of the slope corresponds to the solid's polar component (γ_s^p), and the square of the y-intercept represents the solid's dispersive component (γ_s^d).

The Fowkes model combines Young and Young-Dupree equations and dissociate the surface energy components (Fowkes, 1964b), resulting in Equation 3:

$$\frac{\gamma_l(cos(\theta)+1)}{2} = \sqrt{\gamma_s^p}\sqrt{\gamma_l^p} + \sqrt{\gamma_s^d}\sqrt{\gamma_l^d} \quad (3)$$

First, diiodomethane (polar component = 0) was tested and the dispersive component of the solid surface energy, γ_s^d, was computed. Second, water or glycerol (polar component ≠ 0) was tested, and using γ_s^d and Equation 3, the polar component of the solid surface energy, γ_s^p, was computed. Fowkes theory assumes that the total surface energy is the sum of the dispersive and polar components, so $\gamma_s = \gamma_s^p + \gamma_s^d$.

7.3.2.9. Solid-State Nuclear Magnetic Resonance (NMR)

Solid-state carbon-13 (^{13}C) NMR spectra were obtained using an Avance III 400 MHz spectrometer equipped with a CP-MAS probe. The experiments were performed under the following conditions: temperature 298 K (room temperature), rotation speed 12 kHz, contact time 2 ms, acquisition time 34 ms, sweep width 39.7 kHz, recycle delay 2 seconds, and 3800 scans. Chemical shifts were referenced externally to the carbonyl resonance peak of glycine (176.03 ppm).

The degree of deacetylation (DD) of chitosan was calculated using the same NMR technique and parameters described above, following Equation 4 (Czechowska-Biskup et al., 2011).

$$DD = 1 - \frac{A_{CH_3}}{\frac{\sum_{i=1}^{6} A_{C_i}}{6}} \quad (4)$$

A is equal to the area calculated by the integration of the peak of the respective chemical shift.

The degree of substitution (DS) of modified chitosan was determined using a similar approach to that employed for the degree of deacetylation (DD). However, the analysis relied on the newly introduced chemical shifts non-overlapping observed in the NMR spectrum and follows Equation 5 (David et al., 2019):

$$DS = \frac{\sum_{i=1}^{n} A_{\delta_i}}{n * A_{C_1}} \quad (5)$$

A is equal to the area calculated by the integration of the peak of the respective chemical shift, n is the number of new chemical shifts, i is the number of the new carbons added, and C_1 is the chemical shift of 102 ppm that is always 1.

7.3.2.10. Elemental Analysis

The contents of carbon (C), hydrogen (H), nitrogen (N), and oxygen (O) in samples of pure and modified chitosan were obtained using a Thermofisher Flash Smart instrument. The samples were combusted at a high temperature (950°C) in the presence of copper oxide under a stream of oxygen for a brief period (15 seconds). This decomposition process yielded CO_2, H_2O, SO_2, and NO_X, with the nitrogen oxides being reduced to N_2 (nitrogen) by copper. A stream of helium swept the entire system, and the combustion gases were subsequently measured by gas chromatography using a Chromosorb packed column and a catharometer detector under manufacturer-specified conditions. The pyrolysis of the compound took place in the presence of a nickel catalyst under a helium stream. The resulting CO gas was measured by gas chromatography using a molecular sieve-filled column and a catharometer detector. The results were recorded and analyzed using Eager smart software. The degree of substitution (DS) was calculated using Equation 6 according (Pereira et al., 2023):

$$\frac{C_1}{N_1}(1 - DS) + \frac{C_2}{N_2}(DS) = \frac{C_3}{N_3}0.853 \quad (6)$$

The C_1/N_1 ratio is calculated based on the formula of unmodified chitosan, while C_2/N_2 represents the ratio of the ECEA group introduced into chitosan. C_3/N_3 is the experimentally determined ratio obtained from Elemental Analysis, and 0.853 it's the deacetylation degree measured by NMR.

7.4. RESULTS AND DISCUSSION

7.4.1. FTIR

The chitosan backbone's preservation after the process is confirmed by the FTIR spectrum (Figure 2). The existence of two crucial bands serves as proof of this: The β-(1-4) glycosidic bond, which is the crucial connection between the d-glucosamine and N-acetyl-d-glucosamine units within the chitosan structure, is represented by 890 cm^{-1}, and the amine (C-N) stretching vibration, another distinctive feature of the chitosan molecule, is represented by 1155 cm^{-1}. The bands that appears at 1023 cm^{-1}, 2980 cm^{-1} and 2935 cm^{-1}, respectively corresponding to C-O-C deformation (already present on glucose ring) and CH_3 stretching (already present on N-Acetylglucosamine), has in its intensity

augment an indicative of successful modification. The FTIR spectrum further verifies the existence of an inheritance from the ECEA molecule. This is corroborated by three other bands: 2220 cm^{-1}, which corresponds to the stretching vibration of the nitrile group (CN), 1618 cm^{-1}, which represents the C=C stretching vibration and 1684 cm^{-1}, which corresponds to the C=O stretching vibration (Silverstein et al., 2014).

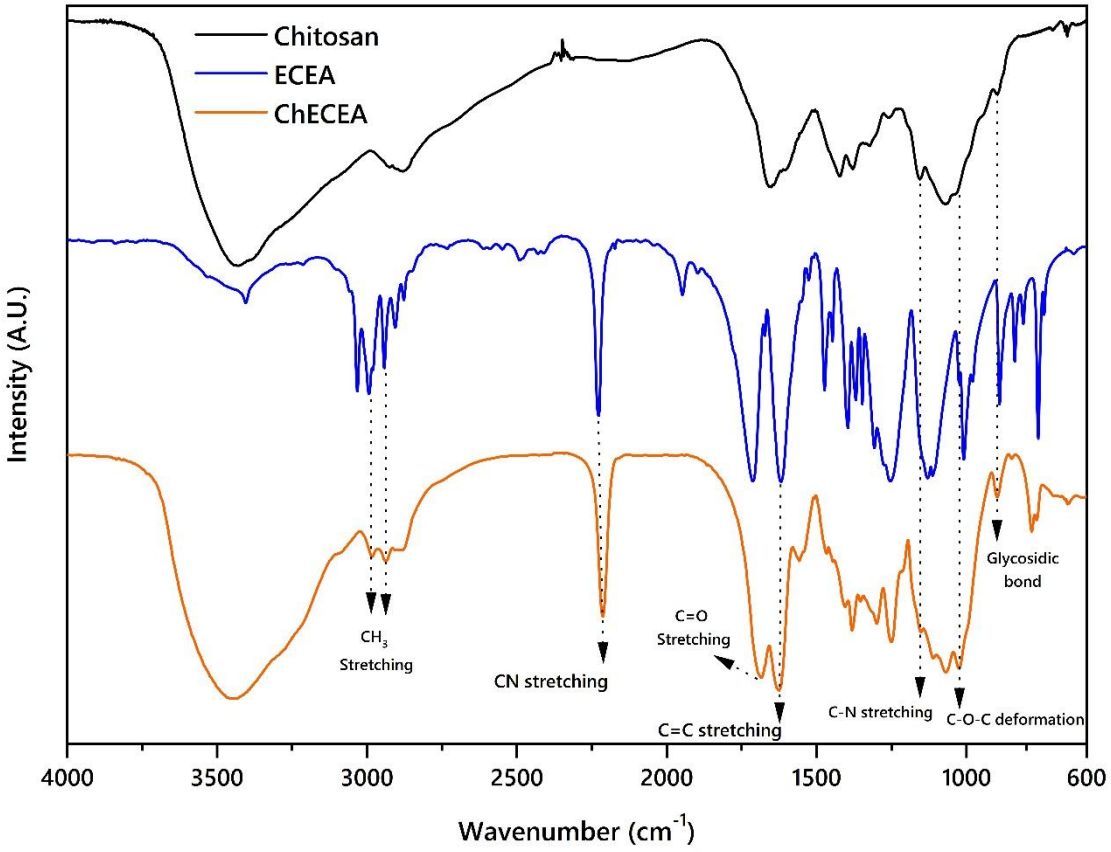

Figure 2 – FTIR spectra of chitosan and chitosan modified (ChECEA) with the backbone bands and new ones.

The degree of deacetylation (DD) of the chitosan sample was calculated as 82.02% using the acquired spectra and Equation 1. This value is consistent with the DD labeled on the reactant flask, indicating good agreement between the calculated and theoretical values.

7.4.2. Nuclear Magnetic Resonance

Figure 3 presents the solid-state ^{13}C NMR chemical shifts. The spectrum exhibits the characteristic chitosan peaks at 171 ppm (chitin carbonyl groups), 102 ppm (C1), 80 ppm (C4), 72 ppm (C5/C3), 58 ppm (C6), and 54 ppm (C2), corresponding to the D-

glucosamine carbons. Additionally, a peak at 20 ppm is observed for the methyl groups of chitins (Heux et al., 2000). Following modification, the ChECEA spectrum reveals new carbon signals: 166 ppm for ester carbons (-O-**C**=O), 158 ppm for the ECEA carbon bonded to the amine group (N-**C**=C), 115 ppm for the nitrile group (**C**N), and 11 ppm for ECEA methyl carbons. Moreover, an increase in signal intensity at 58 ppm is evident, attributed to the additional **C**-O bond introduced by ECEA (Gatial et al., 1996; Milata et al., 1995).

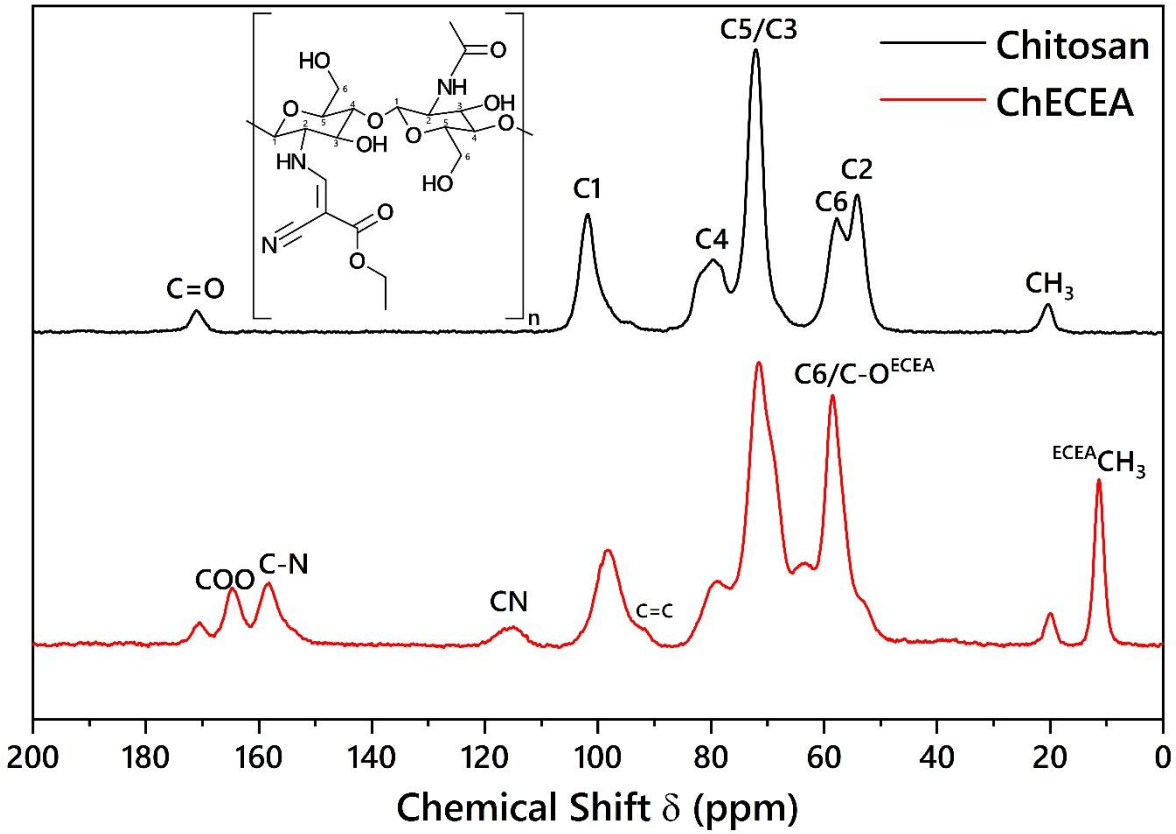

Figure 3 – ^{13}C NMR Spectra for chitosan and modified chitosan with inset molecule of ChECEA.

The DD of the chitosan sample was calculated to be 85.3% using the acquired spectra and Equation 4. This value is consistent with the DD labeled and with de DD calculated from FTIR analysis.

Equation 5 was used to mathematically estimate the degree of substitution (DS) of the modified chitosan sample. By considering only the integrated area of the new methyl group from ECEA, a DS value of 0.64 was obtained. This equation, along with the data used in the calculation, is presented below in Equation 7.

$$DS = \frac{A_{\delta_{11}}}{A_{\delta_{102}}} \rightarrow 0.64 \quad (7)$$

7.4.3. DoE and ANOVA

After all the experiments from the full factorial design were completed, Table 1 was updated to a new table, Table 4.

Table 4 – Mass gain data after experiments.

Run	Temperature (°C)	Time (h)	Molar ratio [1]:[X]	Mass gain (%)
1	80 (+1)	1 (-1)	2.0 (+1)	31.62
2	80 (+1)	1 (-1)	1.5 (-1)	37.57
3	80 (+1)	3 (+1)	2.0 (+1)	59.39
4	60 (-1)	3 (+1)	2.0 (+1)	32.99
5	80 (+1)	3 (+1)	1.5 (-1)	39.87
6	60 (-1)	3 (+1)	1.5 (-1)	40.87
7	60 (-1)	1 (-1)	2.0 (+1)	24.56
8	60 (-1)	1 (-1)	1.5 (-1)	25.63

While the data collected (presented in Table 4 wasn't sufficient for a complete factorial regression analysis with ANOVA (analysis of variance), it still provided valuable insights. By analyzing the main effects plot and interaction plot (Figure 4) generated from this data, we were able to identify potential areas for improvement in the reaction process.

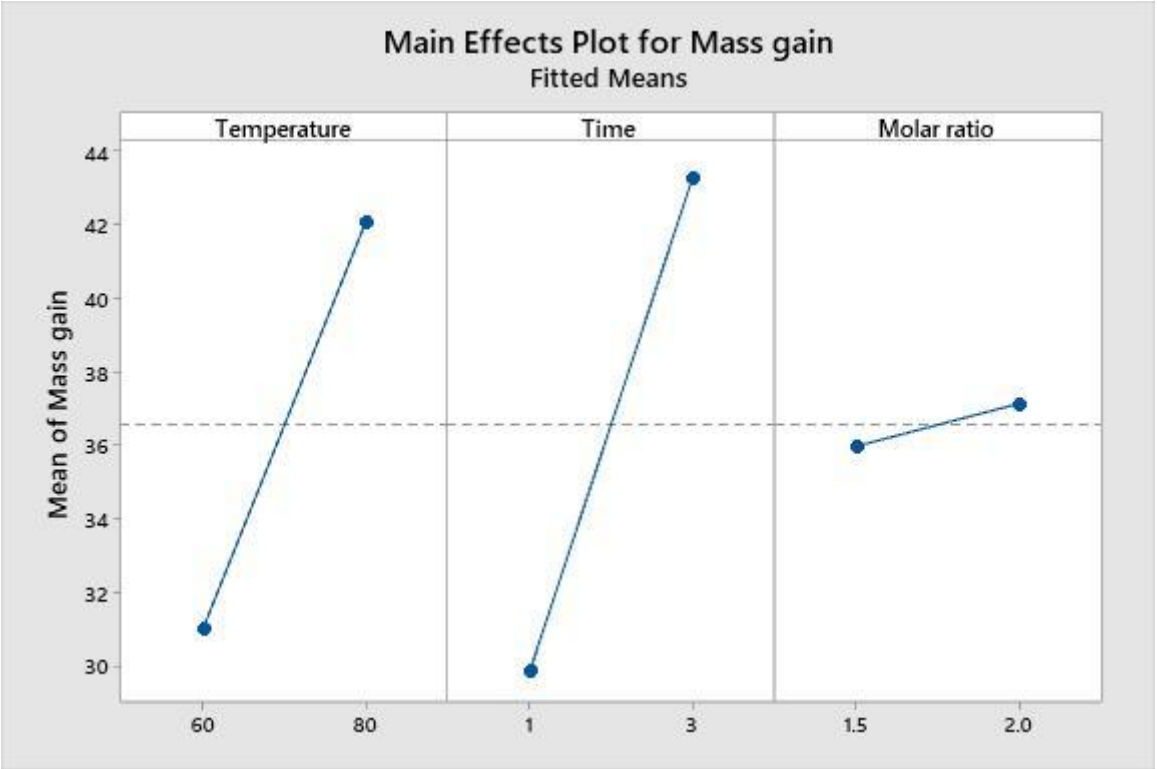

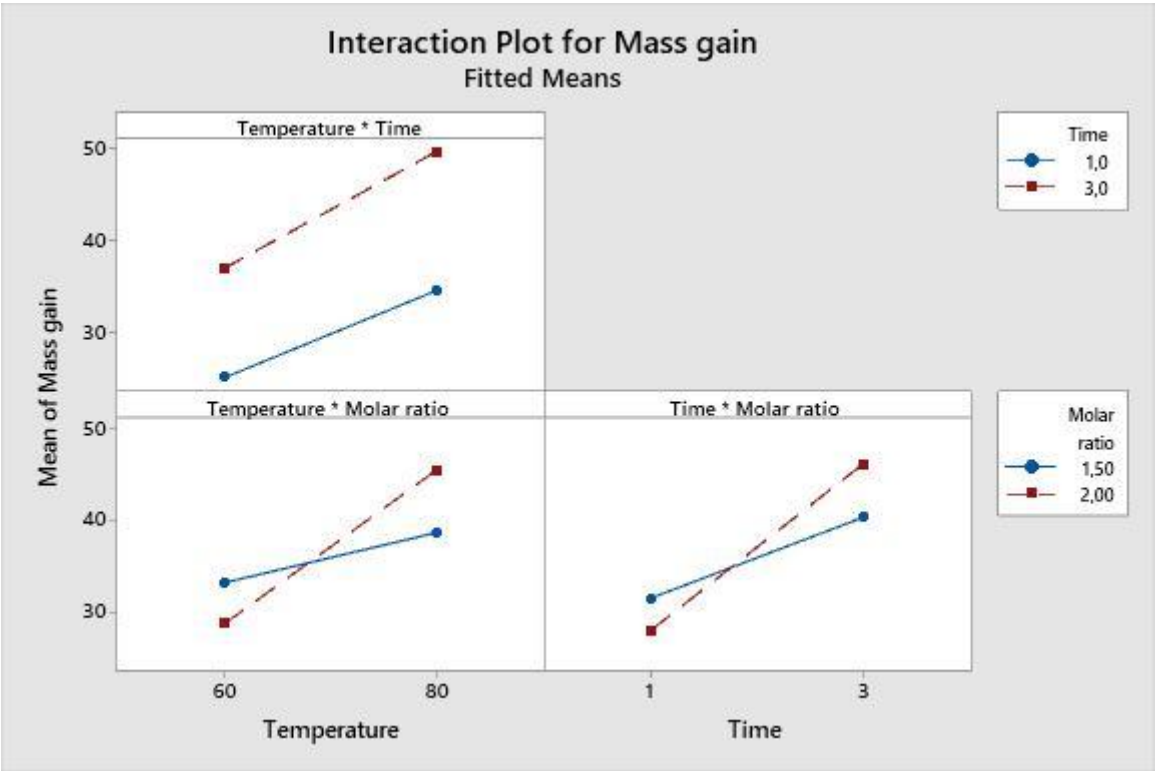

Figure 4: Response results for mass gain on full factorial: main effects and interaction plots.

Figure 4 illustrates the influence of reaction parameters on the observed mass gain. The data reveals that increasing both reaction time and temperature lead to a higher mass

gain. This suggests that extending the reaction duration and operating at a higher temperature promote the desired reaction and product formation, which likely contributes to the observed increase in mass. However, the trend for the molar ratio appears to be different. The data shows a weak correlation between the molar ratio of reactants and the resulting mass gain. This implies that within the range of molar ratios investigated, this specific parameter might not significantly impact product formation or overall mass change, conversely, for other ethoxylates, a significantly stronger correlation between the molar ratio of reactants and the resulting mass gain is observed, elucidating the unique specificity of each reagent/system (Mathias et al., 2025a).

Refined DoE Focuses on Time and Temperature (Central Composite Design)

Based on this observation, a new Design of Experiments (DoE) was conducted to further optimize the reaction conditions. This new DoE focused solely on varying time and temperature while keeping the molar ratio constant at 1:2. The rationale behind this approach was to refine the optimal reaction conditions within the identified range of time and temperature, where the molar ratio seemed to have less influence on the mass gain. The data obtained from this Central Composite Design (CCD) focusing on time and temperature variations is presented in Table 5.

Table 5: Mass gain data of the central composite design

Run	Temperature (°C)	Time (h)	Mass gain (%)
1	75 (-1)	2.5 (-1)	54.40
2	85 (0)	2.5 (-1)	49.51
3	75 (-1)	3.5 (+1)	53.16
4	85 (0)	3.5 (+1)	53.21
5	75 (-1)	3.0 (0)	57.23
6	85 (0)	3.0 (0)	55.21
7	95 (+1)	2.5 (-1)	60.13
8	95 (+1)	3.5 (+1)	58.91
9	95 (+1)	3.0 (0)	59.42

An Analysis of Variance (ANOVA) was performed to statistically evaluate the influence of reaction parameters (temperature, time) and their quadratic terms (temperature^2, time^2) on the observed mass gain (refer to 5 for the complete data).

Table 6 - Analysis of variance for the mass gain.

Source	Mass gain	
	P-value	F-value
Linear		
Temperature	0.291	1.63
Time	0.858	0.04
Square		
Temperature^2	0.060	8.68
Time^2	0.219	2.40

In Table 6 can be found the F-values and p-values of the ANOVA test. Based on the F-values and p-values obtained, the linear effects of both temperature and reaction time appear to be less significant in influencing mass gain within the investigated range. This suggests that simply increasing temperature or extending the reaction duration might not lead to substantial changes in the observed outcome. Nonetheless the squared term of temperature has a considerably higher F-value and a much lower p-value, suggesting a statistically significant effect, implying a curvature in the relationship between temperature and mass gain. There might be an optimal temperature range for maximizing mass gain. So, increasing temperature might not always be beneficial, but there is a region in the parabola where temperature leads to the highest mass gain, and exceeding that point might have negative consequences, as can be seen in the Figure 5, that represents the interaction plot and the surface plot for mass gain.

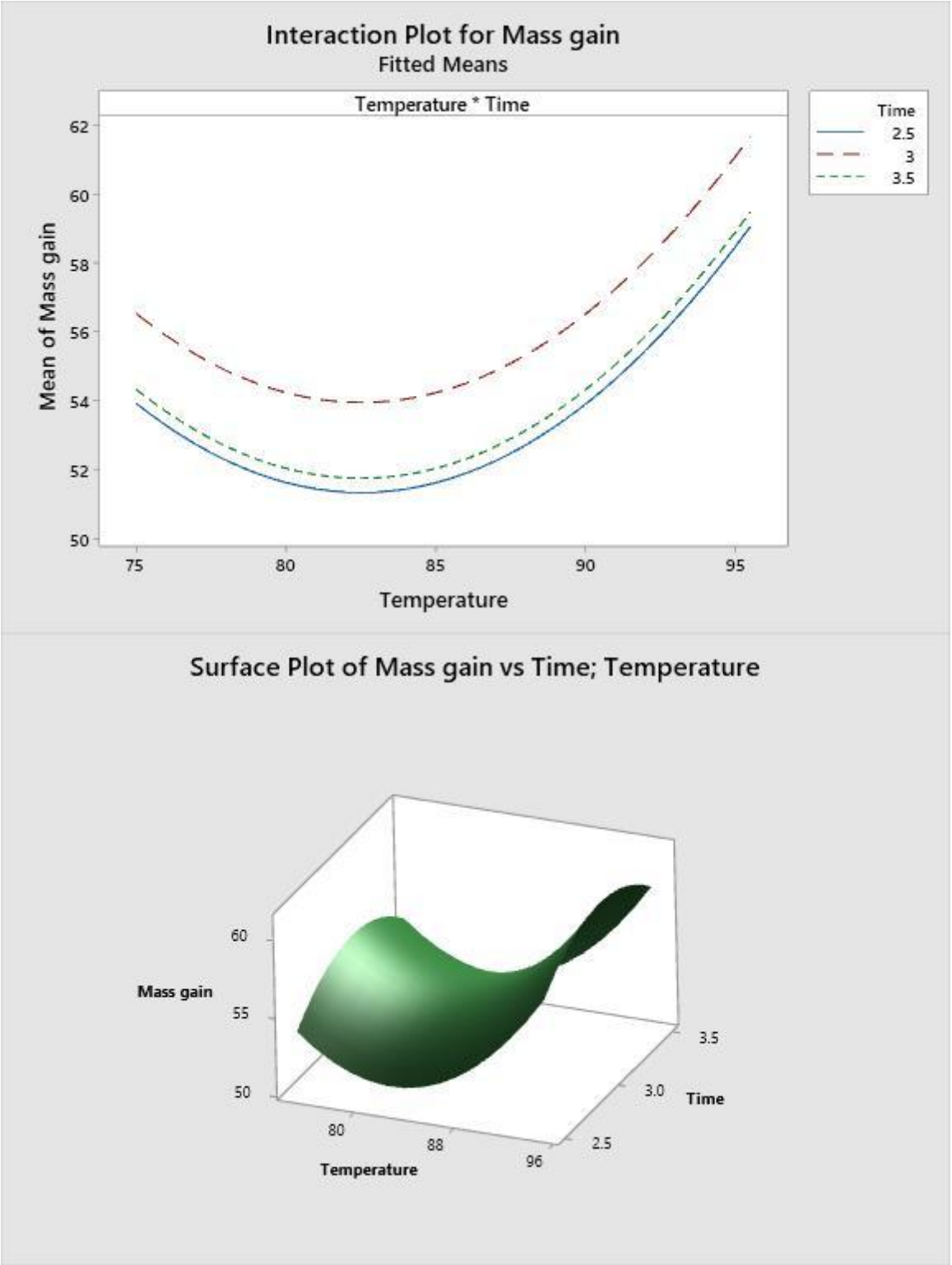

Figure 5 – Interaction and surface plot of mass gain, at varying times and temperatures.

The analysis of the interaction plot of the squared terms provides valuable insights into how temperature and time interact to affect mass gain. Interestingly, the plot reveals

that higher temperatures consistently lead to greater mass gain, regardless of the reaction time used. However, the influence of time seems to be less impactful compared to temperature. While there is still an effect of time, it's not as strong as the temperature effect. Therefore, prioritizing higher temperatures (around 95 °C) along with a moderate reaction time (around 3 hours) is likely the most efficient approach to maximize mass gain for a molar ratio of 2.0, as evident in the surface plots.

Building upon the preceding discussion, all future graphs and figures will concentrate on the sample that showed the greatest increase in mass. This particular sample was prepared under specific conditions: a temperature of 95°C, a reaction time of 3 hours, and a molar ratio of 2.0. For the sake of convenience, we will refer to this sample as "ChECEA" from here on out.

7.4.4. Elemental Analysis

Table 7 shows the percentual content of C, H, N, O and the relation C/N of chitosan and ChECEA.

Table 7 - Elemental analysis results

Sample	%C	%H	%N	%O	C/N ratio
Chitosan	40.09 ± 0.20	6.63 ± 0.25	13.04 ± 0.15	40.24 ± 0.22	3.07 ± 0.065
ChECEA	44.44 ± 0.28	5.57 ± 0.24	8.29 ± 0.20	33.88 ± 0.58	5.36 ± 0.069

Equation 6 was employed to estimate the degree of substitution (DS) of the modified chitosan sample, resulting in a value of 0.725 ± 0.095. This equation, along with the data used in the calculation, is presented below in Equation 8.

$$3.07(1 - DS) + 5.14(DS) = 5.36 * 0.853 \rightarrow DS = 0.725 \pm 0.095 \quad (8)$$

7.4.5. FESEM

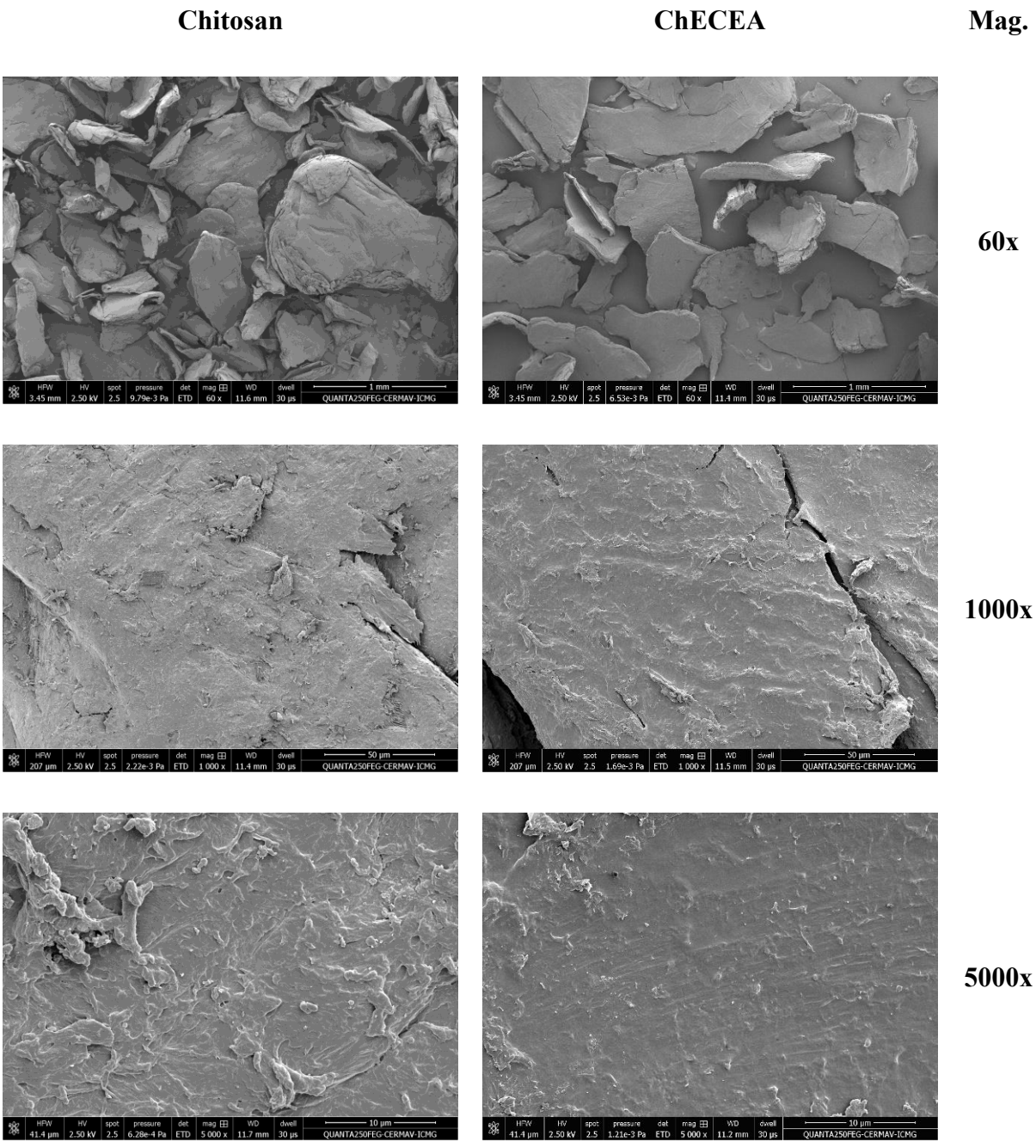

Figure 6 – FESEM micrographs of chitosan and chitosan modified (ChECEA).

The analysis didn't reveal any major alterations in the surface morphology (Figure 6). However, at higher magnifications (1000x and 5000x), some interesting changes became apparent. While the overall structure remained similar, the characteristic fiber-like structures of chitosan appeared less pronounced. The surface also appeared smoother and more cohesive. These observations suggest a potential increase in entanglement

between the chitosan chains. However, this entanglement come at the cost of reduced organization at the finer scale, as discoursed on XRD section (Li et al., 2021b).

7.4.6. XRD

As can be seen in Figure 7, the unmodified chitosan exhibits two broad peaks around 10° (corresponding to the (020) crystal plane) and 20.1° ((110) crystal plane), indicating the presence of crystalline phases. However, a valley around 15° suggests an amorphous phase, signifying a non-crystalline portion within the chitosan structure. Using the peak height method (Segal et al., 1959), the crystallinity index (CI) of chitosan was estimated to be 79%. In contrast, the XRD pattern of ChECEA displays a single, broader peak around 20.5° and a more prominent amorphous halo compared to chitosan. This signifies a significant decrease in crystallinity upon modification. The estimated CI of ChECEA, using the peak height method, is 55%.

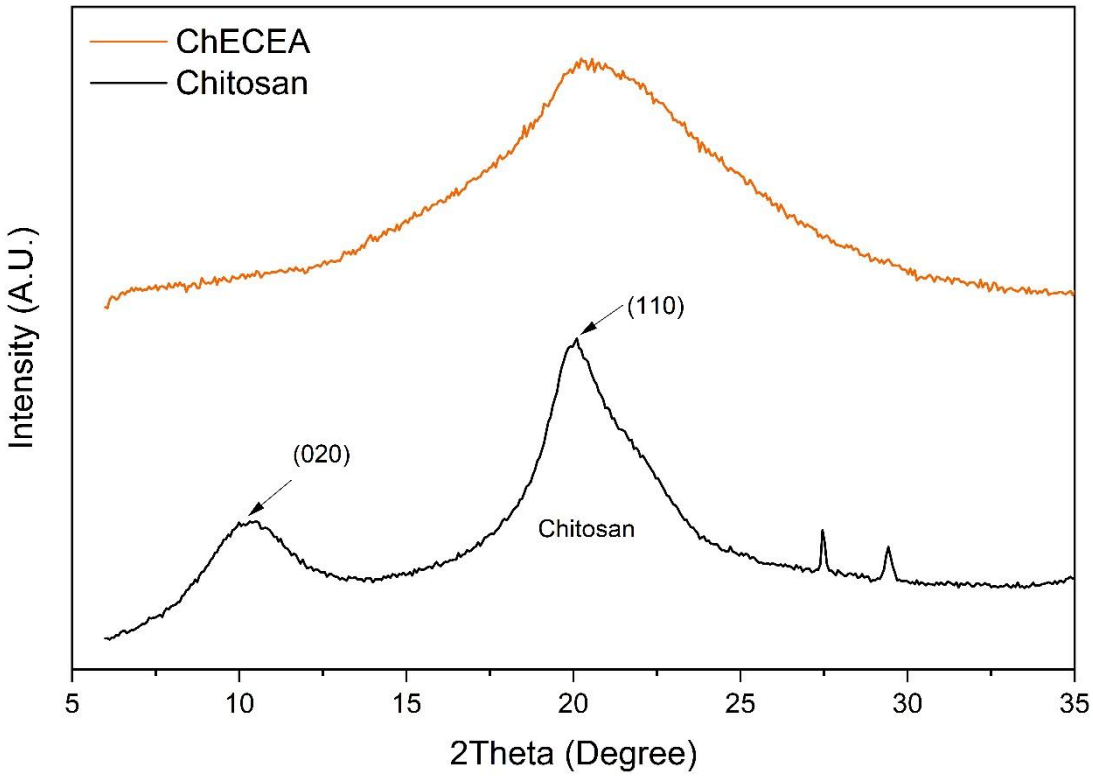

Figure 7 – X-ray diffractograms of chitosan and chitosan modified (ChECEA)

The degree of crystallinity changes observed show that there is a very big effect on chitosan from ECEA modification. Grafting ECEA disrupts arrangement orderliness among chitosan chains in areas that are crystalline. This causes disarray leading to an amorphous and less organized structure. It could be the fault of the large size of ECEA.

Their sizes and quantities may impede creation as well as alignment processes necessary for normal crystal formation in non-altered chitosan.

7.4.7. Zeta Potential

The Figure 8 showed that, at acidic pH, there is a predominant protonation of chitosan's amino groups ($R\text{-}NH_2 + H^+ \rightarrow R\text{-}NH_3^+$) granting to the molecule a polycationic character. After the grafting there is a reduction in the number of positively charged amine groups, leading to a decrease in the overall cationic surface charge and a lower ζ-potential at pH 4.

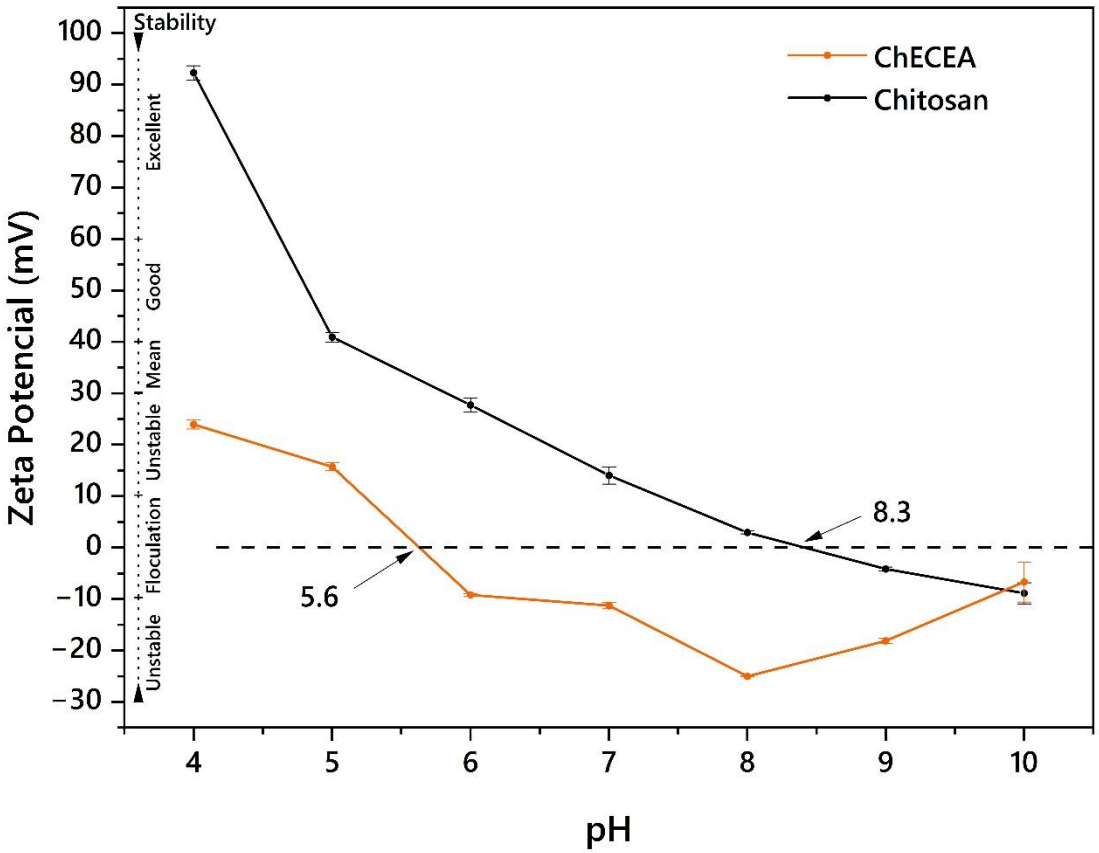

Figure 8 – Zeta potencial comparing chitosan and chitosan modified with scale of stabilization and isoelectric point (IEP).

The theoretical isoelectric point (IEP) of chitosan, based on its typical value of pKa (~6.5) (Fraser-Reid; Tatsuka; Thiem, 2008), is expected to be between pH 6 and 7. However, the observed IEP in Figure 8 was 8.3. This discrepancy can be explained by the degree of deacetylation (DD) of chitosan, as reported in works by Maciel (2017) and Sirviö (2021). Since our chitosan has a high deacetylation degree of approximately 80% (meaning 20% acetylation), the IEP can be shifted to higher pH values.

The ζ-potential for chitosan drops until the pH 10 aligning with the ongoing deprotonation of the amine groups at higher pH values, and for ChECEA drops until the pH 8 and go back up until pH 10, this can be attributed to a steric hindrance and conformational changes in the chitosan chains in solution could be caused by the grafted acrylate groups. Higher pH values may cause electrostatic repulsion, which would cause the polymer chains to lengthen and stiffen due to the increased negative charge density on both the unmodified chitosan chains and ChECEA chains. This chain extension may lessen the total surface area that affects the measurement of the zeta potential, which could result in a higher value of ζ-potential (Maciel et al., 2017; Sirviö et al., 2021).

7.4.8. Contact Angle

It can be seen by analyzing the Table 8 that after the modification of the surface of the material became less attracted to liquids with high polar components been corroborated by the increase in the contact angle for water. There is also an increase in the contact angle for the liquids with high non-polar components as diiodomethane and 1-bromonaphthalene, showing that the attraction is lessen as well. The decrease in the contact angle for glycerol, can be due to the three hydroxyl groups that can interact strongly with the hydroxyl and amine groups from the chitosan's molecule, by hydrogen bonding, allied to the, stronger than with water, dipole-dipole bonding with the grafted nitrile groups, leading to a lower contact angle compared to water, another possible reason it's the acrylate group introduced by ChECEA might introduce some steric hindrance as discussed on the ζ-potential, this could influence how the chitosan chains pack on the surface, potentially creating micro- or nano-scale topographical features trapping glycerol molecules and further contributing to a lower contact angle.

Table 8 – Contact angle data on Chitosan and ChECEA.

	Chitosan	**ChECEA**
Water	53.71 ± 0.06	59.90 ± 0.59
Propane-1,2,3-triol	65.28 ± 0.38	58.10 ± 0.37
Diiodomethane	32.03 ± 0.29	38.10 ± 0.58
1-bromonaphthalene	18.97 ± 0.54	27.70 ± 0.57

As described in the experimental section, the surface energies of chitosan and ChECEA were calculated by two methods: the Fowkes method, which involved

substitution, and the Owens-Wendt-Rabel and Kaelble (OWRK) method, which involved linearization.

Table 9 - Surface Energy determined by Fowkes and Owens-Wendt-Rabel & Kaelble models.

	Fowkes Model			**Owens-Wendt-Rabel & Kaelble**		
$mJ.m^{-2}$	γ_s	γ_s^p	γ_s^d	γ_s	γ_s^p	γ_s^d
Chitosan	**55.19 ± 0.83**	12.49 ± 0.40	42.69 ± 0.73	**53.25 ± 0.55**	13.42 ± 0.39	39.84 ± 0.38
ChECEA	**50.30 ± 0.67**	10.30 ± 0.30	40.01 ± 0.60	**43.01 ± 0.51**	8.69 ± 0.48	34.32 ± 0.17

The calculated surface energy presented in Table 9 showed the same tendency for both models, a decrease in the polar and dispersive component, after the modification. This reduction is related to the graftization process where it was substituted an amine group (possible interactions by dipole-dipole and hydrogen bonding) for an ethyl-2-cyano-3-(**R**)-acrylate, where **R** is the glucosamine's nitrogen from chitosan (possible interactions by dipole-dipole with cyano group and london dispersion forces with ethyl group) (Li et al., 2021b; Shibata; Kuntzleman, 2009).

7.4.9. TG

Figure 9 shows two distinct weight loss events for both ChECEA and chitosan across the studied temperature range. The initial weight loss at lower temperatures is likely attributed to the evaporation of water and other low-molecular-weight compounds present within the samples.

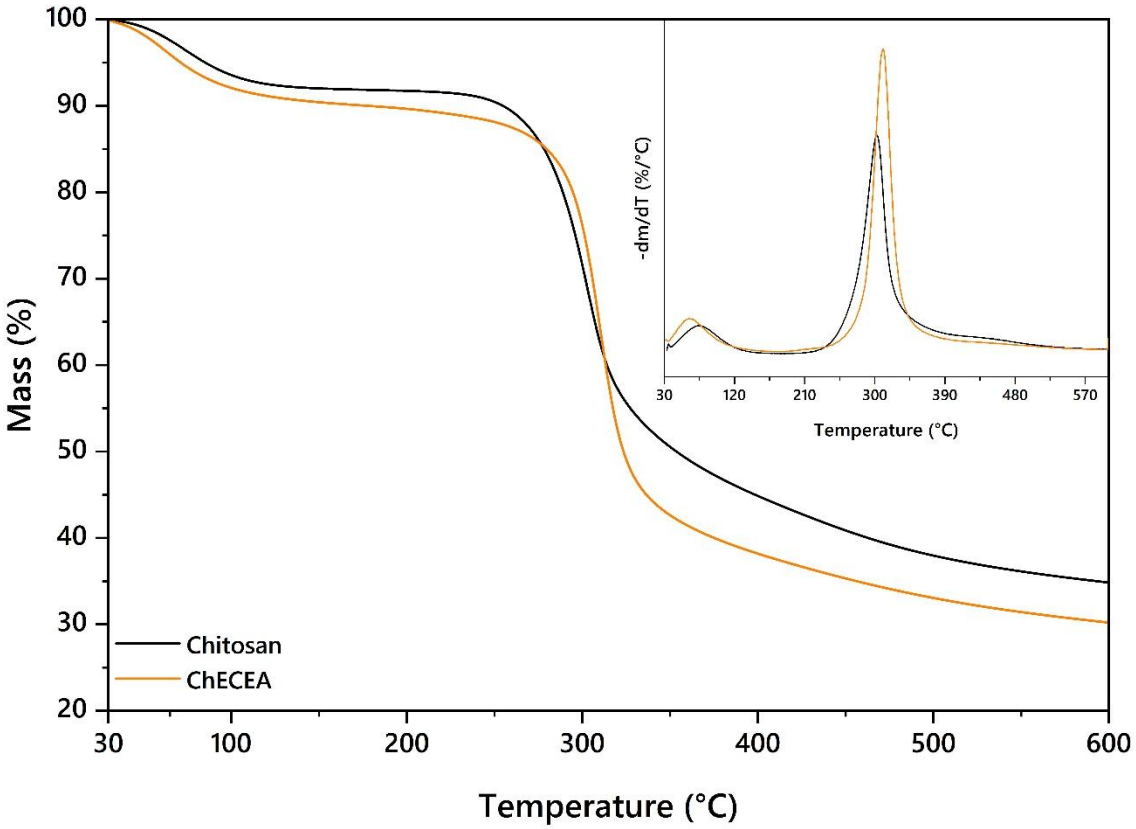

Figure 9 –TGA thermogram comparing chitosan and modified chitosan (ChECEA) with dTG curves as inset.

The second, more significant weight loss event observed at higher temperatures is primarily associated with the main decomposition of chitosan. This likely involves the breakdown of its polymer chains through the breakage of glycosidic bonds. Compared to unmodified chitosan, the presence of ECEA contributes to a decrease in thermal stability, as shown in Table 10. This decrease might be linked to the increased amorphous phase observed in the XRD analysis (Figure 7). An amorphous region, with less ordered chitosan chains, can lead to lower thermal stability (Alamri et al., 2025).

Table 10 – TGA data for Chitosan and ChECEA.

Event/Sample	Chitosan	ChECEA
Evaporation of residual water		
T_{onset} (°C)	38.9	34.9
T_{max} (°C)	76.3	61.6
Mass Loss (%)	7.9	9.7
Main decomposition stage		
T_{onset} (°C)	201.5	184.6
T_{max} (°C)	300.8	310.7
Mass Loss (%)	53.8	56.7

7.5. CONCLUSION

The successful modification of chitosan with ECEA was confirmed by the FTIR spectrum and the appearance of new chemical shifts in the NMR spectrum. The reaction conditions were optimized to achieve the highest mass gain. ChECEA exhibited a morphology and thermal behavior similar to chitosan. However, X-ray diffraction (XRD) analysis revealed a decrease in crystallinity due to the incorporation of cyanoethoxyacrylate groups into the chitosan polymer chain. Moreover, zeta potential measurements indicated a decrease in the isoelectric point compared to unmodified chitosan, as expected from the introduction of these groups. Additionally, contact angle measurements demonstrated an increase in hydrophobicity and a decrease in surface energy following chemical modification.

In conclusion, the synthesis of ChECEA represents a promising approach for developing novel chitosan derivatives with tailored properties. The enhanced hydrophobicity and reduced crystallinity of ChECEA make it a suitable candidate for environmental applications, particularly in the removal of dyes, organic molecules, and heavy metals. Moreover, the presence of the double bond within the chitosan derivative offers opportunities for further functionalization and composite formation, potentially expanding ChECEA's utility in material science for applications such as packaging with enhanced properties, with the incorporation of nitrile groups it may also contribute to enhanced drug delivery systems with controlled release mechanisms and tissue adhesives.

7.6. ACKNOWLEDGEMENT

We gratefully acknowledge the financing by the Coordenação de Aperfeiçoamento de Pessoal de Nível Superior – Brasil (CAPES) – Finance Code 001 - for the doctoral scholarship and PDSE (Programa de Doutorado-sanduíche no Exterior); the LGP^2/PAGORA staff from Grenoble INP for the support in developing part of this work; to Isabelle Jeacomine from the Institute de Chimie Moleculaire de Grenoble (CNRS/CERMAV) for the ^{13}C NMR analysis; to Sandrine Adach from the SynBioN (Université de Lorraine/CNRS) for the elemental analysis performed; LGP^2 is part of the LabEx Tec 21 (Investissements d'Avenir - grant agreement n◦ANR-11-LABX-0030) and of the PolyNat Carnot Institut (Investissements d'Avenir - grant agreement n◦ANR-11-CARN-030-01).

8. ELECTRON-WITHDRAWING SUBSTITUENTS IN ENAMINIC CHITOSAN DERIVATIVES: EFFECTS ON ADSORPTION BEHAVIOR TOWARD CRYSTAL VIOLET

8.1. ABSTRACT

Controlling adsorption mechanisms through systematic functionalization remains a central challenge in advanced materials development. Herein, chitosan derivatives bearing conjugated enaminic linkages with substituent having electronic character, viz. diester (DEEM), mononitrile (ECEA), and dinitrile (EMM) functionalities, and progressively increasing the degree of substitution (DS = 0.29-0.91) were investigated to elucidate how the combined effects of substituent electronic character and substitution density influence electronic redistribution within the polymer matrix and, consequently, adsorption behavior toward Crystal Violet (CV). Zeta potential measurements revealed systematic modulation of protonation equilibria across pH, with increasing electron-withdrawing strength and the degree substitution altering surface charge transitions. Nonlinear Sips modeling, statistically superior to Langmuir and Freundlich models, demonstrated substantial enhancement of adsorption capacity, reaching 382.81 $mg.g^{-1}$ at neutral pH for the dinitrile derivative. Progressive deviation from ideal Langmuir behavior with functionalization indicates adsorption processes that deviate from energetically uniform and independent site models. The enhanced adsorption behavior cannot be attributed solely to electrostatic interactions; rather, the combined influence of substituent electronic character and degree of substitution modifies the interfacial energetic distribution through bulk electronic redistribution. These results highlight the role of enaminic functionalization in modulating adsorption energetics in polysaccharide-based materials.

8.2. INTRODUCTION

The continuous discharge of synthetic dyes into aquatic environments remains a technically relevant challenge due to their high structural stability, aromatic complexity, and resistance to natural degradation processes (Berradi et al., 2019). Among various treatment technologies, adsorption has emerged as a versatile and molecularly adaptable strategy, capable of addressing structurally diverse organic contaminants without generating harmful by-products (Imgharn et al., 2021). The performance of adsorption systems, however, is fundamentally governed by the chemical nature of the adsorbent and

its ability to establish controlled interfacial interactions with target molecules (Amjlef et al., 2021).

Biopolymers have attracted considerable attention as sustainable adsorbent platforms owing to their intrinsic functional group density and chemical tunability. Among them, chitosan is particularly attractive due to the presence of primary amine groups along its backbone, which provide reactive sites for chemical modification and enable modulation of acid-base and coordination behavior (Desbrières; Guibal, 2018). Native chitosan exhibits pH-dependent charge properties and can interact with anionic or cationic species depending on protonation state. Nevertheless, its adsorption capacity and selectivity are often limited by restricted surface area, partial solubility under acidic conditions, and relatively homogeneous energetic distribution of active sites (Kim; Park; Cho, 2012).

To overcome these limitations, numerous chemical modification strategies have been explored, including crosslinking (Hemmati; Karimi; Mowla, 2025; Wang et al., 2026b), graft polymerization (Zhang et al., 2025), surface impregnation (Manzo-Valencia et al., 2024), and formation of composite systems with inorganic fillers (Li et al., 2026b; Liu et al., 2026). Such modifications generally aim to enhance structural stability (Liu; Guo; Yang, 2025), increase surface accessibility (Pal et al., 2025), or introduce additional functional groups capable of improving adsorption performance (Qasemi; Anbia; Rezaie, 2025). While chemically modified chitosan systems frequently exhibit improved adsorption capacities, systematic analyses linking substituent electronic effects and substitution density to adsorption energy heterogeneity and kinetic regime transitions remain limited.

In particular, the role of substituent electronic character and degree of substitution along the polymer backbone remains insufficiently explored. Functional groups with different electron-withdrawing strengths can alter the electronic distribution within the chitosan matrix (Ebrahimzadeh, 2025), modify protonation equilibria, and potentially reshape the interfacial energetic landscape. However, most reported studies treat chemical modification as a structural or morphological enhancement rather than as a controlled electronic perturbation of the polymer backbone. Consequently, the relationship between bulk electronic modification and adsorption heterogeneity is rarely examined in a systematic manner.

Crystal Violet (CV), a cationic triphenylmethane dye widely employed as a model organic contaminant (Belpaire et al., 2015; Xiao et al., 2020), provides a useful probe molecule for investigating adsorption behavior in amine-containing polymers. Its aromatic structure and positive charge allow electrostatic interaction with negatively polarized domains while also enabling potential intermolecular interactions at higher surface coverage. Therefore, CV adsorption offers a convenient framework for evaluating how electronic redistribution within modified chitosan derivatives influences adsorption capacity, heterogeneity, and kinetic regime.

In this context, the present study investigates a series of previously synthesized enaminic chitosan derivatives bearing substituents with distinct electron-withdrawing character, diester, mononitrile, and dinitrile functionalities, combined with progressively increasing degree of substitution (Mathias et al., 2025a, 2025b; Pereira et al., 2023). Rather than introducing inorganic fillers or high-surface-area supports, the approach relies on controlled bulk functionalization of the polymer backbone through conjugated enaminic linkages. This strategy enables systematic modulation of electronic density within the matrix while preserving the biopolymeric framework.

The central hypothesis is that increasing substituent electron-withdrawing strength and degree of substitution induce progressive electronic redistribution along the chitosan backbone, thereby influencing protonation equilibria, interfacial charge behavior, and adsorption energetics. To test this hypothesis, adsorption of CV was evaluated at controlled pH conditions, and equilibrium data were analyzed using nonlinear Langmuir, Freundlich, and Sips models. Particular emphasis was placed on identifying deviations from homogeneous Langmuir-type behavior and correlating heterogeneity parameters with structural modification. Kinetic modeling was further employed to examine potential shifts in adsorption regime associated with electronic functionalization.

By integrating zeta potential analysis, nonlinear isotherm modeling, and kinetic evaluation, this work seeks to establish a structure-property-performance relationship linking substituent electronic character, degree of substitution, and adsorption energetics in chitosan-based materials. Through this approach, the study aims to offer theoretical explanations for how controlled enaminic functionalization can modulate adsorption behavior beyond simple electrostatic considerations.

8.3. EXPERIMENTAL

8.3.1. Materials

Chitosan with average molecular weight (190~310 kDa - 80 % deacetylation degree (DD) - AGU molar mass of 169.57 $g.mol^{-1}$, Merck) was used as the biopolymeric precursor. The enaminic derivatives previously synthesized, diester (DEEM) (Mathias et al., 2025a), mononitrile (ECEA) (Mathias et al., 2025b), and dinitrile (EMM) (Pereira et al., 2023), were employed as adsorbent materials. A schematic representation of the molecular structures of chitosan and its corresponding derivatives is presented in Figure 1. Crystal Violet (>96%, Merck) was used as the model adsorbate without further purification.

All aqueous solutions were prepared using deionized water. Orthophosphate buffer solutions were prepared following the methodology described by Christian & Purdy (1962), ensuring controlled ionic strength across all pH values investigated (pH 5, 7 and 9).

8.3.2. Methods

8.3.2.1. Zeta Potential Measurements

The measurements were performed using an Anton Paar Litesizer DLS 500 equipped with an Omega cuvette, employing the electrophoretic light scattering (ELS) method. Dispersions were prepared at a concentration of 1 $g.L^{-1}$ in orthophosphate buffer solution, consistent with the adsorption experiments. The pH of the dispersions (5, 6, 7, 8, and 9) was adjusted using the corresponding buffer solutions. Measurements were conducted at 23 °C following a stabilization period of 60 s prior to data acquisition.

For each sample, two replicate measurements were performed on the same dispersion, each consisting of 100 runs. Reported values correspond to the average of these measurements. Electrophoretic mobility value was converted to zeta potential using the Smoluchowski approximation.

8.3.2.2. Batch Adsorption Experiments

Batch adsorption experiments were conducted using 25 mg of adsorbent dispersed in 25 mL of Crystal Violet solution (adsorbent dosage: 1 $g.L^{-1}$). All suspensions were agitated in Erlenmeyer flasks using an orbital shaker at the lowest available speed setting (rotation speed not specified) at 23 °C for 24 h to ensure equilibrium.

For isotherm studies, ten initial dye concentrations were investigated for each chitosan derivative and pH condition. The concentration range was selected to adequately capture both low-coverage and near-saturation regimes (4–500 $mg.L^{-1}$). The pH was adjusted to 5, 7, or 9 using orthophosphate buffer solutions with constant ionic strength of 0.2 M, and was agitated during 24h.

All experiments were performed in triplicate, and average values were used for modeling. The adsorption capacity at equilibrium (q_e, $mg.g^{-1}$) was calculated using Equation 1:

$$q_e = \frac{(C_0 - C_e)V}{m} \quad (1)$$

where C_0 and C_e ($mg.L^{-1}$) are the initial and equilibrium concentrations, respectively, V (L) is the solution volume, and m (g) is the mass of adsorbent.

The percentual removal was calculated using Equation 2:

$$\%Removal = \frac{(C_0 - C_e)}{C_0} * 100 \quad (2)$$

Kinetic adsorption experiments were performed for all materials at pH 5, 7, and 9 using a fixed initial dye concentration. Aliquots were collected at predetermined time intervals (from 1 to 30 min, followed by extended intervals up to equilibrium). The total monitoring time ranged from approximately 40 to 250 min, depending on the chitosan derivative and pH, until no significant variation in residual concentration was observed.

Experimental kinetic data were fitted using nonlinear least squares regression to pseudo-first-order (PFO), pseudo-second-order (PSO), Elovich, and Weber–Morris models. For PFO and PSO models, both rate constants and theoretical equilibrium adsorption capacities were obtained. Model adequacy was evaluated using adjusted R^2 values.

For both equilibrium and kinetic experiments, residual dye concentrations were determined using a Shimadzu UV-3600 spectrophotometer at the maximum absorption wavelength of Crystal Violet (589 nm). Calibration curves were constructed using standard solutions prepared under identical ionic strength and pH conditions. Prior to UV-Vis analysis, all samples were appropriately diluted to ensure absorbance values within the linear detection range (0.1–1.0). This procedure minimizes deviations from Beer-

Lambert behavior and reduces potential aggregation effects of CV at higher concentrations.

8.3.2.3. Isotherm and Kinetic Modeling

Equilibrium adsorption data were analyzed using nonlinear least squares regression without linearization of the governing equations. The Langmuir, Freundlich, and Sips models were employed to describe adsorption isotherms.

The Langmuir model (Langmuir, 1918) assumes monolayer adsorption onto energetically homogeneous sites and is expressed as equation 3:

$$q_e = \frac{q_{max} K_L C_e}{1 + K_L C_e} \tag{3}$$

where q_e ($mg.g^{-1}$) is the equilibrium adsorption capacity, q_{max} ($mg.g^{-1}$) is the maximum adsorption capacity, K_L ($L.mg^{-1}$) is the Langmuir constant, and C_e ($mg.L^{-1}$) is the equilibrium concentration.

The Freundlich model (Freundlich; Heller, 1939), which accounts for heterogeneous surface adsorption, is given by equation 4:

$$q_e = K_F \sqrt[n]{C_e} \tag{4}$$

where K_F $(mg.g^{-1})(L.mg^{-1})^{1/n}$ is the Freundlich constant and *n* is the heterogeneity parameter.

The Sips model (Sips, 1948) (also known as Langmuir-Freundlich), which combines features of Langmuir and Freundlich behavior and accounts for surface heterogeneity at low concentrations while predicting saturation at high concentrations, is expressed as equation 5:

$$q_e = \frac{q_{max} (k_S C_e)^n}{1 + (k_S C_e)^n} \tag{5}$$

where K_S is the Sips equilibrium constant and *n* represents the heterogeneity factor.

Kinetic data were fitted using pseudo-first-order (PFO), pseudo-second-order (PSO), Elovich, and Weber-Morris intraparticle diffusion models.

The nonlinear form of the PFO model (Corbett, 1972) is represented as equation 6:

$$q_t = q_e(1 - e^{-k_1 t}) \quad (6)$$

where q_t ($mg.g^{-1}$) is the adsorption capacity at time t, q_e ($mg.g^{-1}$) is the equilibrium adsorption capacity, and k_1 (min^{-1}) is the rate constant.

The PSO model (Blanchard; Maunaye; Martin, 1984) is expressed as equation 7:

$$q_t = \frac{q_e^2 k_2 t}{1 + q_e k_2 t} \quad (7)$$

where k_2 ($g.mg^{-1}min^{-1}$) is the PSO rate constant.

The Elovich model (Aharoni; Tompkins, 1970) is described by equation 8:

$$q_t = \frac{1}{\beta} \ln (1 + \alpha\beta t) \quad (8)$$

where α ($mg.g^{-1}.min^{-1}$) is the initial adsorption rate and β ($g.mg^{-1}$) is related to surface coverage and activation energy.

The Weber-Morris (Weber; Morris, 1963) intraparticle diffusion model is expressed as equation 9:

$$q_t = k_{diff} \sqrt[2]{t} + C \quad (9)$$

where k_{diff} ($mg.g^{-1}.min^{-1/2}$) is the intraparticle diffusion rate constant and C reflects boundary layer thickness.

8.4. RESULTS AND DISCUSSION

8.4.1. Surface charge redistribution induced by enaminic functionalization.

A schematic representation of the investigated materials is shown in Figure 1. The progressive structural modification from pristine chitosan to the diester, mononitrile, and dinitrile derivatives introduces systematic variations in both substituent electronic character and degree of substitution along the biopolymer backbone. While all derivatives share the formation of conjugated enaminic linkages at the primary amine sites, the nature of the terminal functional groups differs significantly. The enaminic linkage establishes

a π-conjugated pathway between the nitrogen atom and the attached electron-withdrawing substituents, enabling intramolecular electronic communication along the modified segment. In particular, ester groups exert a moderate electron-withdrawing inductive effect, whereas nitrile functionalities display a stronger withdrawing character. This progressive increase in electronic strength promotes resonance-assisted intramolecular charge redistribution within the conjugated enaminic framework, consistent with a resonance-assisted intramolecular charge transfer (RAICT) effect (Misra; Bhattacharyya, 2018). As the degree of substitution increases, both the extent of electronically perturbed domains and the cumulative polarization of the polymer backbone intensify. This bulk electronic redistribution alters the local electron density of the matrix and ultimately manifests in modified interfacial behavior at the solid-liquid interface.

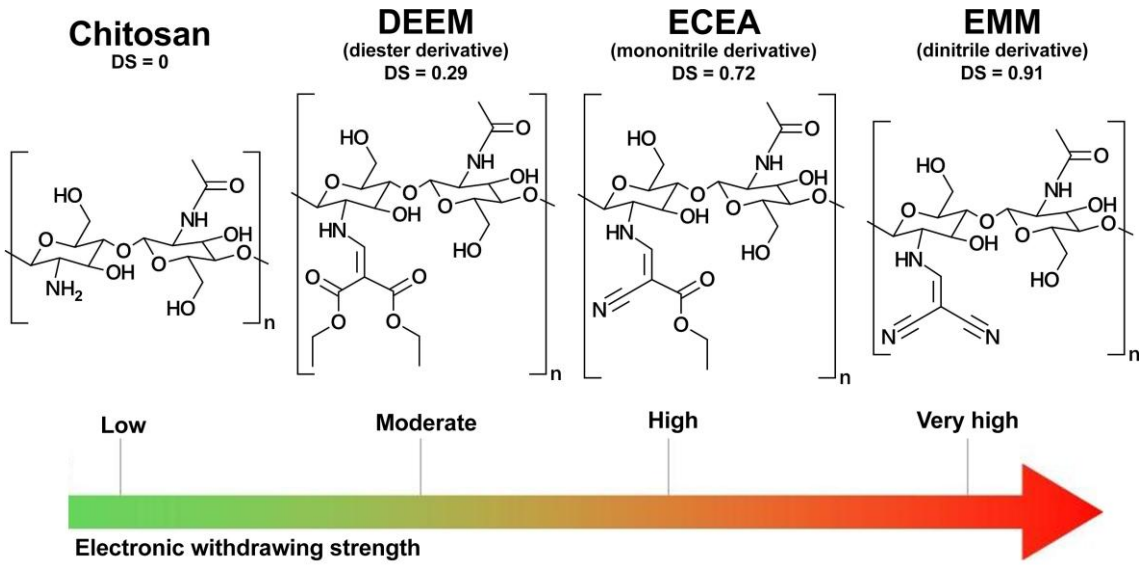

Figure 1 - Schematic representation of chitosan and its derivatives with increasing electronic withdrawing character.

From an electronic standpoint, ester functionalities exert a moderate electron-withdrawing inductive effect (Marqvorsen; Brinkø; Jensen, 2020), whereas nitrile groups display a stronger inductive character. The presence of two nitrile moieties in the dinitrile derivative amplifies this effect (Mei et al., 2017; Monika et al., 2020; Zhang et al., 2019b), resulting in a more pronounced redistribution of electron density along the enaminic conjugated system. As the degree of substitution increases from the diester to the dinitrile material, both the density of electronically modified sites and the cumulative withdrawing effect intensify, providing a structural basis for the modulation of surface charge behavior discussed below.

The evolution of zeta potential as a function of pH for all materials is presented in Figure 2. Pristine chitosan exhibits the expected pH-dependent behavior, with positive surface charge under mildly acidic conditions (ζ = +5.27 mV at pH 5) and a gradual transition to negative values as pH increases, reflecting progressive deprotonation of primary amine groups.

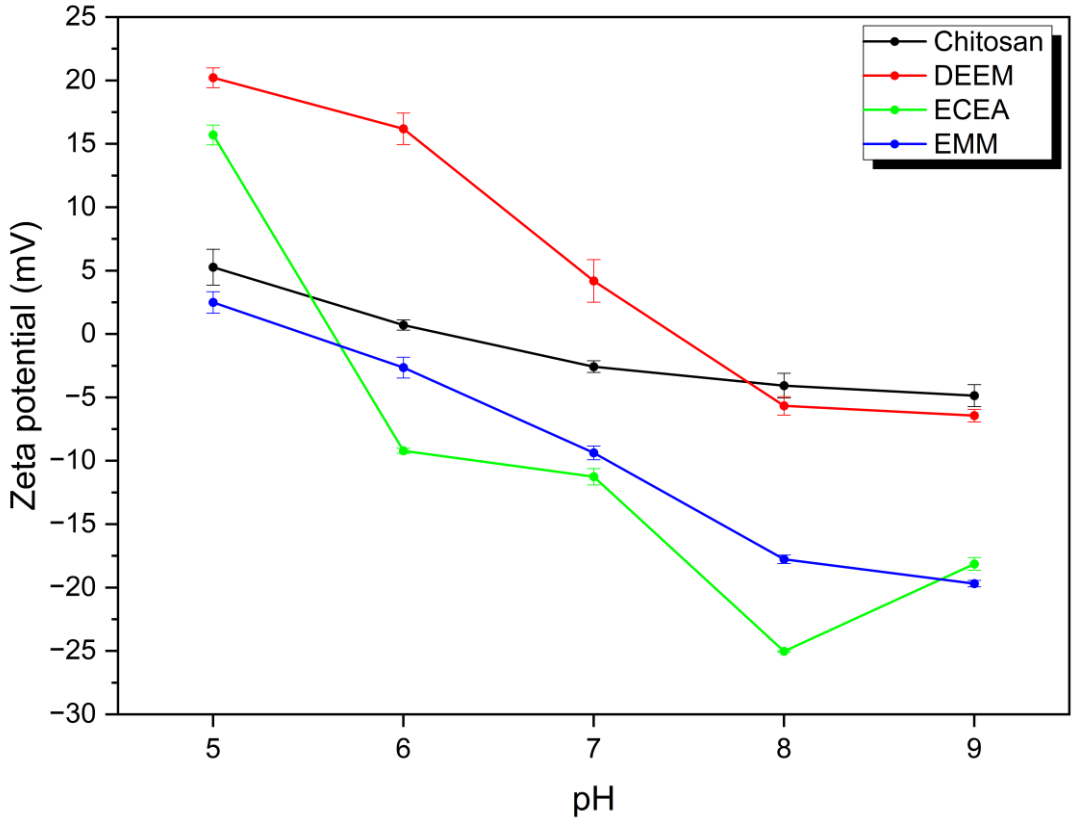

Figure 2 - Zeta potential for pristine chitosan, diester, mononitrile and dinitrile in ortophosphate buffer.

In contrast, functionalization through enaminic conjugation progressively alters this equilibrium. The diester derivative (DS = 0.29) displays significantly enhanced positive surface charge under acidic conditions (ζ = +20.2 mV at pH 5), suggesting stabilization of protonated nitrogen species. However, its surface charge decreases near neutrality and becomes negative above pH 8, indicating modified protonation behavior relative to pristine chitosan.

The effect becomes more pronounced with increasing degree of substitution and stronger electron-withdrawing character. The mononitrile derivative (DS = 0.72) undergoes a marked charge inversion between pH 5 and 6, transitioning from positive (+15.7 mV) to negative values (-9.2 mV), evidencing suppression of protonation

associated with the nitrile functionality. The dinitrile material (DS = 0.91) exhibits the most suppressed protonation behavior, with near-neutral charge at pH 5 and progressively increasing negative surface potential toward alkaline conditions (-19.7 mV at pH 9).

These results indicate that the combined influence of substituent electronic character and substitution density strongly governs the acid-base equilibrium at the polymer-solution interface. For higher degrees of substitution, a substantial fraction of primary amine groups is replaced by conjugated enaminic linkages, reducing the density of protonable sites while simultaneously altering local electronic polarization. The progressive modulation of surface charge with functionalization highlights the central role of electronic surface redistribution in defining interfacial behavior.

8.4.2. Adsorption isotherms and substitution-degree-dependent energy heterogeneity

Equilibrium adsorption data were fitted using nonlinear least squares regression to Langmuir, Freundlich, and Sips models, with model adequacy evaluated through adjusted R^2 values. Across all derivatives, the Sips model consistently provided superior statistical fitting compared to the classical isotherms, indicating adsorption behavior consistent with surface heterogeneity and deviation from ideal monolayer assumptions. Representative adsorption isotherms with nonlinear Sips fitting at pH 7 are shown in Figure 3.

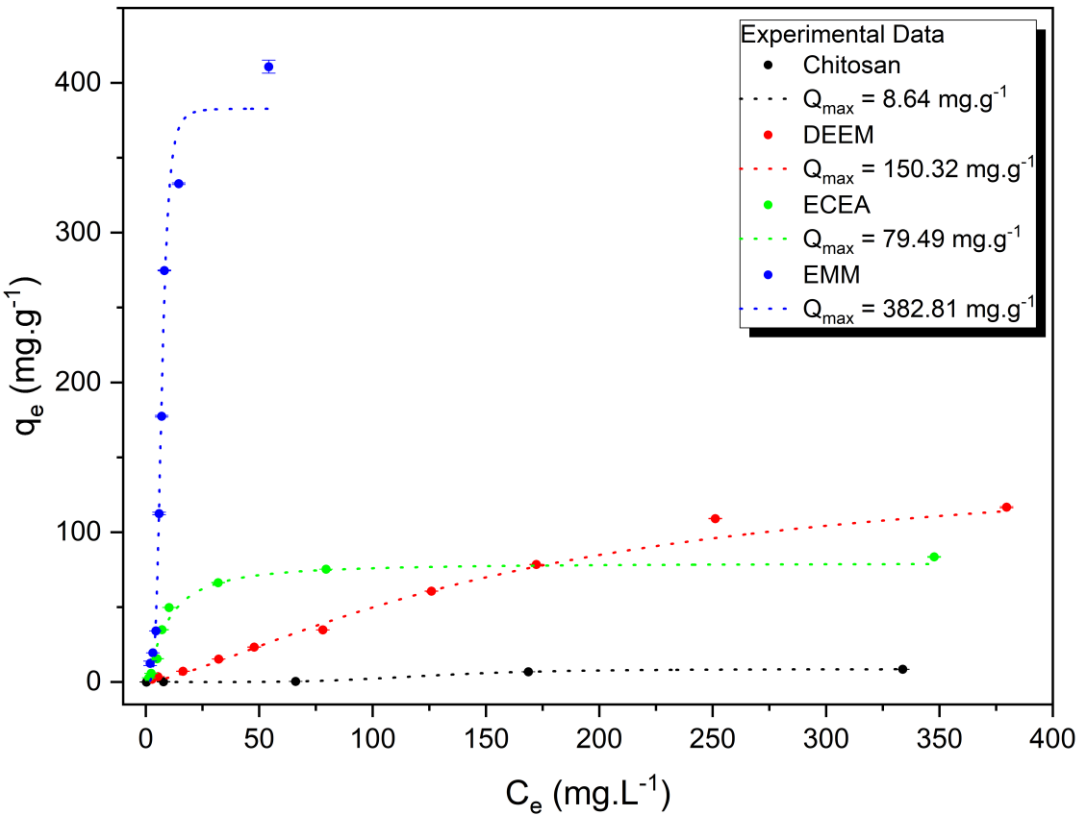

Figure 3 - Adsorption isotherms of crystal violet at pH 7 with nonlinear Sips fitting for chitosan and its derivatives.

Pristine chitosan exhibited limited adsorption capacity with pronounced pH dependence, consistent with its protonation-controlled surface chemistry. While Langmuir fitting was acceptable under limited conditions, near-neutral pH behavior was more accurately captured by the Sips model, suggesting intrinsic energetic heterogeneity even in the unmodified polymer. This behavior is consistent with the incomplete deacetylation of chitosan, which results in a non-uniform distribution of amine and acetamide units along the backbone, thereby generating energetically differentiated adsorption domains.

The diester-functionalized material (DS = 0.29) showed enhanced capacity relative to pristine chitosan, particularly at neutral pH. Under acidic conditions, adsorption remained partially compatible with Langmuir behavior, indicating that electrostatic interactions dominated when protonated sites were abundant.

Increasing electronic withdrawing strength and the degree of substitution progressively intensified deviations from Langmuir-type adsorption. The mononitrile derivative (DS = 0.72) displayed higher adsorption capacities and more pronounced heterogeneity, reflected in improved Sips fitting relative to both Langmuir and Freundlich

models. Table 1 presents the fitting results of the equilibrium data for the isotherm models.

Table 1 - Equilibrium parameters for crystal violet adsorption for chitosan and its derivatives at pH 5, 7 and 9.

Material	pH	Langmuir Equation			Freundlich Equation			Sips Equation			
		q_{max}	K_L	R^2	*n*	K_F	R^2	q_{max}	*n*	K_S	R^2
		$mg.g^{-1}$	$L.mg^{-1}$	-	-	$mg^{1-1/n}.L^{1/n}.g^{-1}$	-	$mg.g^{-1}$	-	$(L.mg^{-1})^{1/n}$	-
Chitosan	5	51.86	0.01	0.913	1.64	0.97	0.859	36.90	3.31	0.0058	0.978
	7	29.46	0.00	0.880	1.13	0.05	0.866	8.64	4.55	0.0080	0.999
	9	14.16	0.02	0.988	2.36	1.31	0.899	15.66	0.88	0.0160	0.990
DEEM	5	19.60	0.04	0.997	1.84	1.29	0.995	24.21	0.84	0.0197	0.997
	7	447.33	0.00	0.971	1.13	0.79	0.970	150.32	1.38	0.0060	0.980
	9	17.32	0.04	0.851	2.12	1.35	0.925	32.37	0.62	0.0048	0.963
ECEA	5	66.13	0.02	0.967	3.07	8.16	0.965	86.30	0.62	0.0081	0.967
	7	87.26	0.09	0.966	2.43	12.40	0.874	79.49	1.29	0.1080	0.980
	9	94.41	0.01	0.966	1.80	2.79	0.929	67.21	2.74	0.0149	0.986
EMM	5	285.17	0.03	0.752	1.77	16.26	0.540	213.99	1.29	0.0593	0.971
	7	577.44	0.06	0.800	0.65	3.48	0.800	382.81	4.56	0.1434	0.974
	9	197851.17	0.00	0.880	0.87	0.83	0.891	290.11	12.21	0.0094	0.995

The most significant transformation was observed for the dinitrile derivative (DS = 0.91). For this material, Langmuir fitting yielded physically inconsistent parameters under certain pH conditions, while Freundlich failed to adequately describe high-concentration behavior. In contrast, the Sips model maintained high adjusted R^2 values across all pH levels, confirming the emergence of highly heterogeneous adsorption energetics. The marked deviation observed from Langmuir behavior indicates that adsorption cannot be described solely as a homogeneous monolayer process with energetically independent sites. Instead, the superior fitting of the Sips model suggests a distribution of adsorption energies and possible energetic coupling between adsorbed molecules.

Notably, the Sips heterogeneity parameter (*n*) increased markedly with electronic strength and the degree of substitution, particularly under neutral and alkaline conditions ($n = 4.56$ at pH 7; $n = 12.21$ at pH 9 for the highest substituted derivative). Such elevated *n* values indicate strong deviation from independent site adsorption and are consistent with increasingly heterogeneous energetic domains (Foo; Hameed, 2010; Murphy et al.,

2023). The dependence of q_{max} and heterogeneity parameter n on functionalization is summarized in Figure 4.

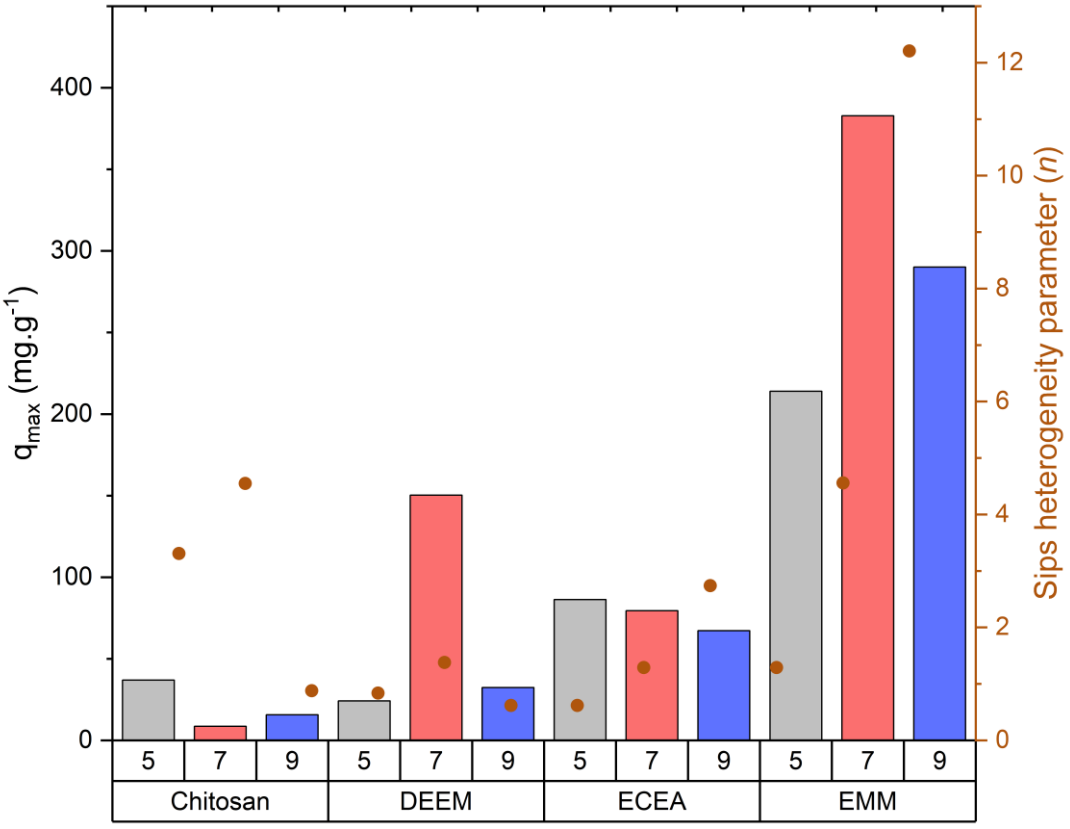

Figure 4 - Substitution-dependent evolution of adsorption capacity and surface energy heterogeneity at pH 5, 7 and 9.

Adsorption enhancement scales not only with surface charge magnitude but with the extent of electronic redistribution imposed by conjugated enaminic functionalization. While increased negative surface charge under neutral conditions promotes electrostatic attraction toward the cationic dye, the substantial increase in adsorption capacity for the highly substituted derivative exceeds what would be expected from electrostatics alone. At alkaline pH, although the polymer surface becomes more negatively charged, the decrease in adsorption capacity suggests that additional factors, such as ionic strength effects, double-layer compression, and possible changes in dye speciation, modulate the contribution of electrostatic interactions.

The consistent superiority of the Sips (Langmuir-Freundlich) model over the Langmuir model indicates deviation from energetically uniform and independent adsorption sites. Since the Sips model explicitly accounts for a distribution of adsorption energies across heterogeneous binding domains, elevated heterogeneity parameters are widely interpreted as reflecting broadened energetic distributions rather than identical

surface sites (Mabuza; Mahlobo, 2025). The present results suggest that electronic modulation of the polymer matrix reshapes the interfacial energetic landscape, promoting heterogeneous adsorption behavior consistent with non-uniform site occupation and potentially more complex surface or lateral interactions (adsorbate-adsorbate) at higher coverage.

In addition to the increase in adsorption capacity, removal efficiency trends further highlight the impact of enaminic functionalization. Across all investigated pH values (5, 7, and 9), removal efficiency increases systematically from pristine chitosan to the dinitrile derivative. At neutral pH, for instance, the dinitrile material achieved removal efficiencies up to 97.1%, compared to 83.2% for the mononitrile derivative, 42.0% for the diester derivative, and 22.0% for chitosan. This consistent progression across pH conditions underscores the combined influence of substituent electronic character and the degree of substitution on adsorption performance. The pH-dependent removal efficiencies are summarized in Figure 5.

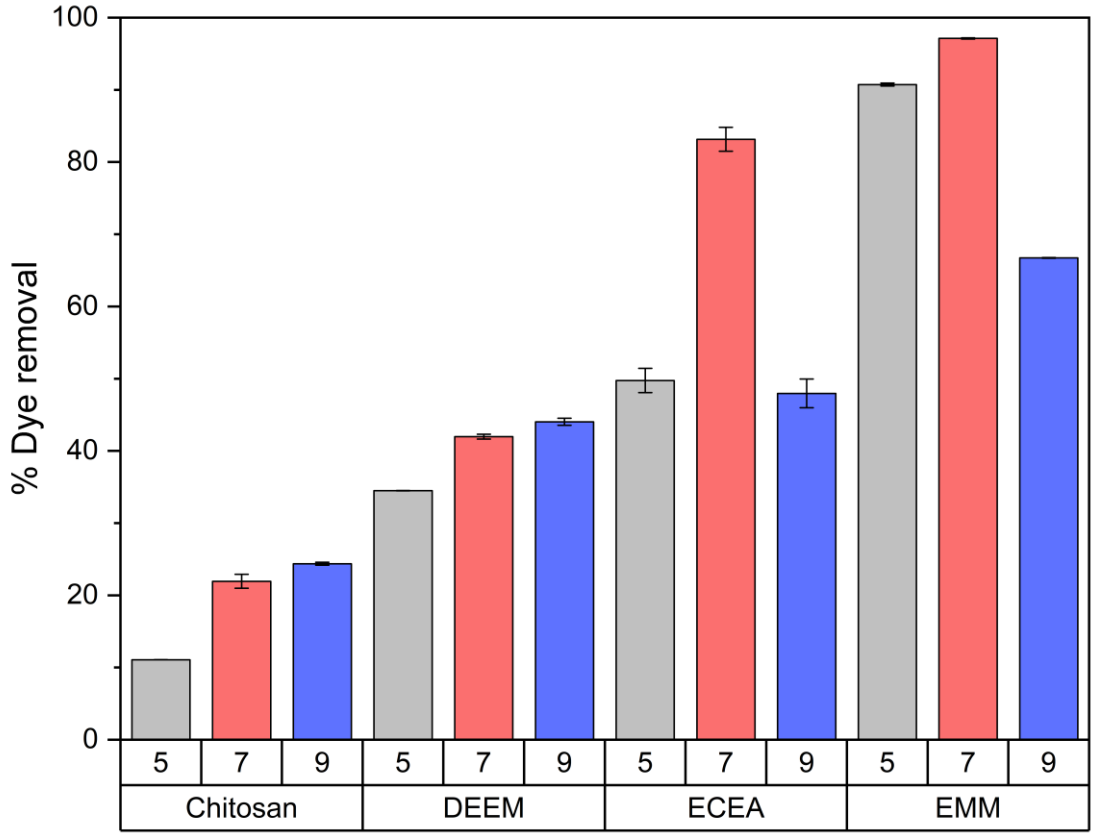

Figure 5 - Removal efficiency of Crystal Violet at different pH values (5, 7, and 9) for chitosan and its derivatives

8.4.3. Kinetic modeling and mechanistic transition

Adsorption kinetics were evaluated using pseudo-first-order (PFO), pseudo-second-order (PSO), Elovich, and Weber-Morris intraparticle diffusion models. Model adequacy was assessed using adjusted R^2 values. Complete nonlinear fitting parameters for PFO, PSO, and Elovich models are summarized in Table 2. Representative kinetic profiles at neutral pH are shown in Figure 6.

Pristine chitosan exhibited pronounced pH-dependent kinetic behavior. Under acidic conditions, PSO provided slightly improved statistical fitting relative to PFO, whereas near-neutral pH PFO fitting became more dominant. This shift suggests a change in the relative contribution of adsorption rate processes as protonation decreases.

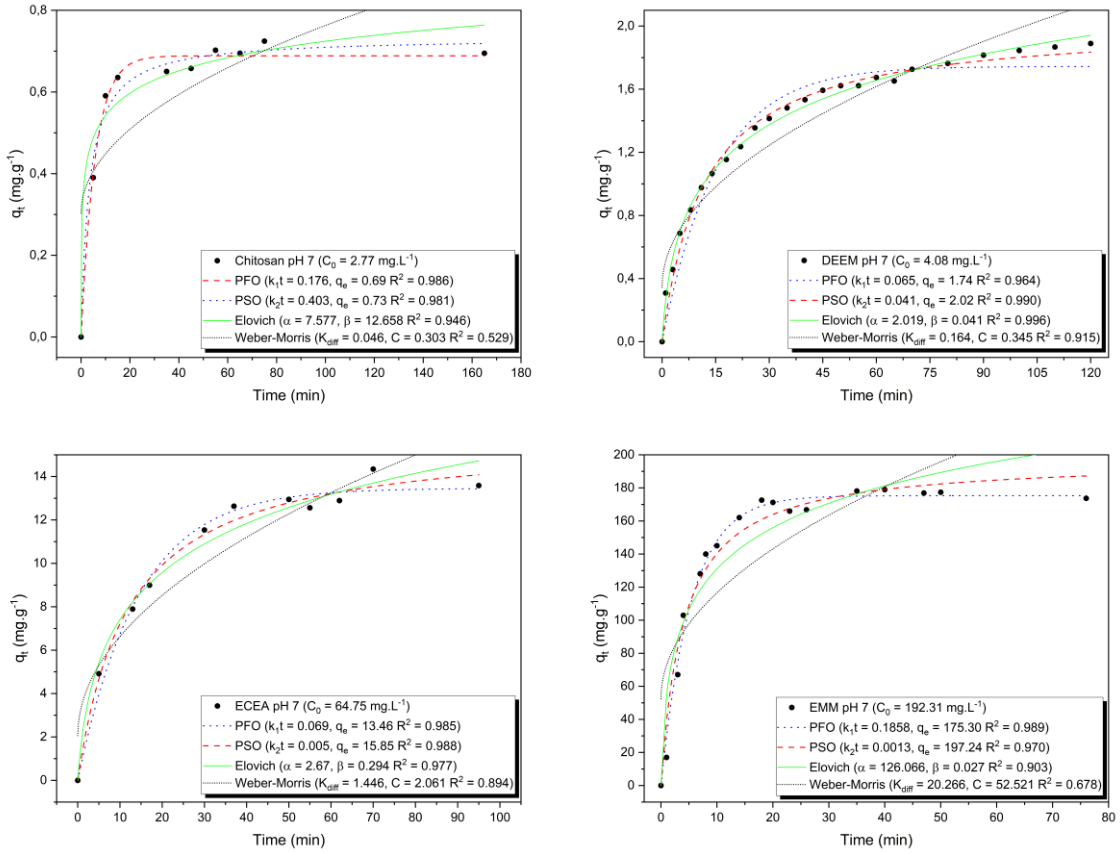

Figure 6 - Representative adsorption kinetic profiles at pH 7 with nonlinear model fitting.

Enaminic functionalization systematically altered kinetic profiles. The diester derivative (DS = 0.29) displayed predominant PSO fitting across most pH values, indicating adsorption behavior better described by second-order kinetics relative to pristine chitosan. The mononitrile derivative (DS = 0.72) showed mixed behavior, with PSO dominance under alkaline conditions and PFO under mildly acidic conditions, suggesting a transitional regime influenced by both degree of substitution and substituent electronic character.

The Weber-Morris model did not yield linear profiles passing through the origin for any derivative, indicating that intraparticle diffusion is not the sole rate-limiting step (Singh et al., 2016). Instead, adsorption appears to involve multiple contributing processes, whose relative significance varies with the withdrawing group inserted in chitosan.

When interpreted alongside isotherm analysis, the kinetic data reinforce that adsorption behavior is governed by the combined influence of substituent electronic character and substitution density. The diester-functionalized derivative, containing

moderately electron-withdrawing ester groups, retains kinetic features partially consistent with PSO behavior. In contrast, incorporation of nitrile functionalities, characterized by stronger electron-withdrawing effects, progressively modifies the kinetic regime, particularly at high degree of substitution.

Table 2 - Nonlinear kinetic fitting parameters for PFO, PSO, and Elovich models for chitosan and its derivatives.

Material	pH	C_0	PFO Equation			PSO Equation			Elovich Equation		
			k_1t	q_e	R^2	q_e	$_{k2}$t	R^2	alfa	*beta*	R^2
			min^{-1}	$mg.g^{-1}$	-	$mg.g^{-1}$	$g.mg^{-1}.min^{-1}$	-	$mg.g^{-1}.min^{-1}$	$g.mg^{-1}$	-
Chitosan	5	307.37	26.33	0.116	0.929	30.47	0.004	0.936	6.71	0.15	0.918
	7	2.77	0.69	0.176	0.986	0.73	0.403	0.981	7.58	12.66	0.946
	9	9.41	2.3	0.193	0.804	2.52	0.106	0.898	2.45	2.44	0.976
DEEM	5	8.77	2.25	0.036	0.985	2.74	0.014	0.994	0.154	1.471	0.98
	7	4.08	1.74	0.065	0.964	2.02	0.041	0.99	0.362	2.399	0.996
	9	4.08	2.03	0.051	0.978	2.44	0.023	0.989	0.224	1.735	0.986
ECEA	5	36.31	10.57	0.028	0.978	12.8	0.002	0.945	0.596	0.322	0.896
	7	64.75	13.46	0.069	0.985	15.85	0.005	0.988	2.67	0.294	0.977
	9	4.08	2.51	0.183	0.957	2.76	0.089	0.991	1.954	2.05	0.995
EMM	5	96.63	42.86	0.917	0.9	45.04	0.035	0.963	35702.9	0.29	0.978
	7	192.31	175.3	0.186	0.989	197.24	0.0013	0.97	126.07	0.027	0.903
	9	346.17	289.11	0.576	0.99	310.07	0.003	0.973	1741.1	0.023	0.878

The most significant kinetic shift was observed for the highly substituted dinitrile derivative (DS = 0.91). Under neutral and alkaline conditions, pseudo-first-order kinetics predominated, coinciding with elevated heterogeneity parameters derived from Sips modeling. The combined kinetic and equilibrium results indicate adsorption processes that deviate from simple independent-site models and are consistent with increasingly heterogeneous surface energetics. This transition cannot be attributed solely to the degree of substitution, but rather to the synergistic influence of substituent electronic strength and the fraction of surface sites modified through enaminic conjugation. While kinetic models do not independently establish molecular-level mechanisms, their systematic evolution with functionalization remains consistent with the progressive energetic heterogeneity indicated by isotherm analysis.

8.4.4. Structure-property-performance correlation

The adsorption behavior of the enaminic chitosan derivatives arises from a hierarchical interplay between molecular structure, surface electronic properties, and adsorption energetics. By systematically varying both the nature of the substituent (ester versus nitrile) and the degree of substitution along the biopolymer backbone, controlled modification of the surface electronic distribution was achieved.

At the structural level, enaminic functionalization progressively reduces the population of free primary amine groups while introducing conjugated domains with tunable electron-withdrawing strength. The diester derivative induces moderate electronic perturbation, whereas incorporation of one or two nitrile functionalities substantially enhances the electron-withdrawing strength of the substituent. When combined with increasing the degree of substitution, this leads to progressive redistribution of electron density across the polymer interface (Lu et al., 2022; Pereira; Gehlen, 2007; Tarai et al., 2020).

This electronic surface redistribution significantly affects protonation equilibrium and surface charge behavior, as demonstrated by zeta potential measurements. Higher substitution density and stronger electron-withdrawing groups suppress amine protonation and shift the surface toward more negative potentials under neutral and alkaline conditions. However, adsorption performance does not scale linearly with surface charge magnitude alone, indicating that electrostatic attraction represents only part of the governing mechanism.

Isotherm analysis further reveals that interfacial electronic modulation alters the interfacial energetic distribution. The superiority of the Sips model and the systematic increase of the heterogeneity parameter (n), particularly for the dinitrile derivative, demonstrate that adsorption deviates from homogeneous Langmuir-type behavior as electronic modification intensifies. Elevated n values under neutral and alkaline conditions suggests increasing energetic heterogeneity and behavior inconsistent with strictly independent site adsorption models.

Kinetic modeling supports this interpretation. The transition from regimes better described by pseudo-second-order kinetics in lower-modified systems to predominantly pseudo-first-order behavior in the highly substituted dinitrile derivative indicates a shift in adsorption dynamics. Rather than being adequately described by isolated and

energetically uniform surface sites, adsorption in the highly modified materials appears consistent with progressively heterogeneous surface domains and potential energetic coupling effects.

Taken together, these findings establish a coherent correlation:
(i) substituent electronic character defines the magnitude of electron-withdrawing perturbation;
(ii) degree of substitution determines the fraction of electronically modified surface sites; and
(iii) their combined effect governs surface charge modulation, adsorption energy heterogeneity, and kinetic regime transitions.

Thus, enaminic functionalization provides a systematic approach for modulating interfacial electronic properties and adsorption energetics in polysaccharide-based materials. This principle extends beyond the specific dye investigated here and offers a general framework for rational design of biopolymeric adsorbents with tunable adsorption behavior.

To contextualize the adsorption performance within the family of structurally related materials, Table 3 - Literature-reported adsorption capacities and isotherm models for Crystal Violet removal using chitosan-derived materials.Table 3 summarizes reported maximum adsorption capacities for CV removal using chitosan-based adsorbents under comparable conditions. Pristine chitosan beads typically exhibit limited adsorption capacity (e.g., 5.48 $mg.g^{-1}$ at pH 7), while chemically modified chitosan derivatives and composites generally report q_{max} values ranging from approximately 18 to 220 $mg.g^{-1}$ at near-neutral pH. More advanced chitosan-based magnetic or composite systems have achieved capacities up to 333–390 mg g^{-1}, predominantly described by Langmuir or Freundlich models.

Under comparable pH conditions (pH 7), the dinitrile-functionalized derivative developed in this work exhibits a maximum adsorption capacity of 382.81 $mg.g^{-1}$, ranking among the highest values reported for chitosan-based materials. This performance is achieved through bulk enaminic functionalization without incorporation of high-surface-area inorganic fillers or additional porous supports. Furthermore, the adsorption behavior is more accurately described by the Sips model, indicating pronounced energetic heterogeneity relative to many literature systems predominantly modeled using Langmuir

isotherms. The materials developed here also maintain significant adsorption performance across a broader pH range (pH 5-9), whereas most literature reports focus primarily on optimal adsorption conditions. This broader pH tolerance further highlights the robustness of the electronic modification strategy. These observations reinforce that controlled electronic modification of the chitosan can yield adsorption capacities comparable to highly modified chitosan composites while simultaneously altering adsorption energetics and mechanistic behavior.

Table 3 - Literature-reported adsorption capacities and isotherm models for Crystal Violet removal using chitosan-derived materials.

Adsorbent	pH	q_{max}	Isotherm model	References
Chitosan/Glu magnetic composite microsphere	7.0	390.0	Langmuir	(Yan et al., 2013)
Chitosan/EMM	7.0	382.81	Sips	This work
Magnetic chitosan nanocomposite	7.0	333.33	Freundlich	(Massoudinejad; Rasoulzadeh; Ghaderpoori, 2019)
Crosslinked chitosan-oxalate and modified mango seed	9.7	306.51	Freundlich	(Abdulhameed et al., 2025)
Chitosan-cysteine/bentonite	8.0	219.45	Freundlich	(Ahmad; Ejaz, 2023)
Cross-linked chitosan coated bentonite	5.0	169.49	Langmuir	(Vithalkar; Jugade, 2020)
Chitosan graft poly(acrylamide-itaconic acid)	9.0	167.3	-	(Liu et al., 2018)
Chitosan/nanodiopside	7.5	104.66	Langmuir	(Nasab et al., 2019)
Cu-chitosan nano-biocomposite	9.5	84.75	Freundlich	(Shukla et al., 2021)
Chitosan magnetic composite microsphere	7.0	82.2	Langmuir	(Yan et al., 2013)
Chitosan–graphite oxide modified polyurethane	8.0	69.94	Freundlich	(Qin et al., 2015)
Chitosan/hydrocaffeic acid	7.0	43.74	Langmuir	(Chao et al., 2004)
Chitosan/3,4-dihydroxyphenylacetic acid	7.0	41.31	Langmuir	
Chitosan/3,4-dihydroxybenzoic acid	7.0	27.53	Langmuir	
Chitosan/4-hydroxybenzoic acid	7.0	18.30	Langmuir	
Chitosan beads	7.0	5.48	Langmuir	(Pal; Pan; Saha, 2013)

8.5. CONCLUSION

This study demonstrates that adsorption behavior in enaminic chitosan derivatives is governed by the combined influence of substituent electronic character and the degree of substitution along the polymer backbone. Progressive functionalization, ranging from

diester to mono- and dinitrile derivatives, induces systematic redistribution of surface electronic density and alters protonation equilibria across pH.

Zeta potential measurements revealed controlled modulation of surface charge behavior, while nonlinear Sips analysis confirmed increasing deviation from ideal Langmuir-type adsorption as electronic perturbation intensifies. The highest substituted dinitrile derivative exhibited markedly enhanced adsorption capacity (up to 382.81 $mg.g^{-1}$ at neutral pH) together with elevated heterogeneity parameters, consistent with increasingly heterogeneous adsorption energetics under neutral and alkaline conditions.

The adsorption enhancement cannot be attributed solely to electrostatic attraction. Instead, the interplay between substituent electronic strength and the degree of substitution modifies the interfacial energetic distribution, influencing both equilibrium behavior and adsorption kinetics. The observed transition in kinetic regimes is consistent with progressive deviation from independent-site adsorption models as surface electronic modulation intensifies.

Overall, these findings establish conjugated enaminic functionalization as a systematic approach for modulating surface electronic structure and adsorption energetics in biopolymeric materials. The structure-property-performance relationships elucidated here provide a framework for rational functionalization of polysaccharide-based adsorbents with tunable energetic heterogeneity.

8.6. ACKNOWLEDGMENT

The authors acknowledge financial support from the Coordination for the Improvement of Higher Education Personnel (CAPES, Finance Code 001) through a doctorate scholarship. The authors also thank the Financiadora de Estudos e Projetos (FINEP) and the Federal University of São Carlos (UFSCar) for providing research infrastructure and laboratory facilities. Additionally, the authors acknowledge Grenoble INP – Pagora for hosting the research internship carried out through the CAPES PDSE program, which contributed to the development of this work. LGP2 is part of the LabEx Tec 21 (Investissements d'Avenir - grant agreement n°ANR-11-LABX-0030) and PolyNat Carnot Institute (Investissements d'Avenir - grant agreement n°ANR-11-CARN-030-01).

9. DICLOFENAC ADSORPTION BY CHITOSAN ALKOXYMETHYLENE DERIVATIVES: EFFECT OF ELECTRON-WITHDRAWING SUBSTITUENTS ON ADSORPTION PERFORMANCE

9.1. ABSTRACT

Chitosan is widely investigated as a bio-based adsorbent for emerging contaminants; however, its adsorption performance toward anionic pharmaceuticals at neutral pH is often limited. In this study, chitosan was chemically modified with diester (DEEM), ester-nitrile (ECEA), and dinitrile (EMM) substituents to investigate the effect of functional group density on the adsorption of sodium diclofenac. The degree of substitution (DS) increased progressively from 0.29 (DEEM) to 0.73 (ECEA) and 0.91 (EMM), enabling systematic evaluation of structure-property relationships. Adsorption isotherms were best described by the Sips model, with the maximum adsorption capacity increasing from 6.63 $mg \cdot g^{-1}$ for pristine chitosan to 219.47 $mg \cdot g^{-1}$ for EMM, while the Sips affinity constant also increased with DS. A transition from S-type to L-type isotherms was observed, indicating a shift from cooperative adsorption to higher intrinsic affinity as functionalization increased. Kinetic analysis showed that adsorption for the highly substituted derivatives followed pseudo-second-order behavior, consistent with a surface-controlled process. Zeta potential measurements at pH 7 revealed near-neutral surface charge for all materials, suggesting that classical electrostatic attraction is not the dominant mechanism. Instead, the enhanced adsorption performance is attributed to ion-dipole stabilization between the diclofenac carboxylate and dipolar electron-withdrawing substituents introduced into the chitosan backbone. These results demonstrate that functional group density plays a key role in governing adsorption capacity and affinity, which will benefit the design of chemically modified biopolymer adsorbents for pharmaceutical removal.

9.2. INTRODUCTION

Pharmaceutical compounds are increasingly recognized as emerging contaminants due to their continuous release into aquatic environments and their persistence in conventional wastewater treatment systems (Corpus et al., 2024; Daughton; Ternes, 1999). Among them, non-steroidal anti-inflammatory drugs (NSAIDs) are frequently detected in surface waters, groundwater, and wastewater effluents, raising concerns about ecological and human health risks (Aus der Beek et al., 2015; Gkika et al., 2023). Sodium diclofenac has been widely reported as one of the most prevalent

pharmaceutical residues in aquatic systems due to its high consumption and incomplete removal in treatment plants (Petrie et al., 2013; Vieno; Sillanpää, 2014).

Adsorption has emerged as an effective strategy for the removal of pharmaceutical contaminants owing to its operational simplicity, high efficiency, and versatility in material design. In this context, biopolymers have received considerable attention as sustainable adsorbent platforms (Crini; Lichtfouse, 2019; Onyekachukwu et al., 2025). Chitosan, a naturally derived polysaccharide obtained from chitin deacetylation, is especially attractive due to its abundance, biodegradability, and the presence of reactive amino groups that enable chemical modification. Nevertheless, pristine chitosan often exhibits limited adsorption capacity for anionic pharmaceuticals under neutral conditions, mainly because its surface charge becomes weakly positive or nearly neutral as the pH approaches neutrality (Ravi et al., 2024; Shehab et al., 2025; Vakili et al., 2014).

To overcome these limitations, several strategies have been explored to enhance the adsorption performance of chitosan, including crosslinking, grafting, and the introduction of functional groups capable of modifying the surface chemical environment (Benettayeb et al., 2023; Hemmati; Karimi; Mowla, 2025; Wang et al., 2026b). Chemical functionalization offers a particularly promising route because it allows the incorporation of specific moieties that can alter the polarity, electronic distribution, and interaction potential of the polymer backbone. In this regard, electron-withdrawing substituents such as ester and nitrile groups may significantly influence the adsorption behavior by modifying the local dipolar character of the surface (Misra; Bhattacharyya, 2018; Shagdarova; Zhuikova; Il'ina, 2025).

Despite the extensive literature on modified chitosan adsorbents, the relationship between functional group density and the resulting adsorption mechanism remains insufficiently understood, particularly for systems involving anionic pharmaceuticals. In many studies, adsorption performance is predominantly interpreted in terms of electrostatic interactions. However, surface charge alone does not always account for the observed behavior, especially under near-neutral conditions where electrostatic attraction is limited. Consequently, systematic investigations that directly correlate the degree of substitution with adsorption capacity, affinity, and kinetic behavior are necessary to clarify how chemical functionalization governs the interaction mechanisms in such systems (Gkika et al., 2023; Liakos et al., 2021; Shagdarova; Zhuikova; Il'ina, 2025).

In this work, chitosan was chemically modified using three electrophilic reagents to introduce diester (DEEM), ester-nitrile (ECEA), and dinitrile (EMM) substituents, generating derivatives with progressively increasing degrees of substitution. These materials were evaluated as adsorbents for sodium diclofenac in aqueous solution, with the aim of establishing a direct correlation between functional group density and adsorption performance. Equilibrium and kinetic adsorption experiments were combined with surface charge analysis to investigate how progressive functionalization influences adsorption capacity, affinity, and mechanism. The results provide insight into how the incorporation of electron-withdrawing substituents modifies the interfacial environment of chitosan and promotes enhanced adsorption of anionic pharmaceuticals.

Based on these considerations, we hypothesize that the progressive incorporation of electron-withdrawing substituents into the chitosan backbone alters the interfacial electronic environment of the polymer, increasing the density of polar interaction sites capable of stabilizing anionic pharmaceutical species. In particular, the introduction of nitrile-containing groups is expected to enhance adsorption through ion–dipole interactions with the diclofenac carboxylate, thereby increasing both adsorption capacity and affinity. To test this hypothesis, chitosan was systematically modified to generate derivatives with increasing degrees of substitution, and their adsorption performance toward sodium diclofenac was evaluated through equilibrium, kinetic, and surface charge analyses to establish a direct relationship between functional group density and adsorption mechanism.

9.3. EXPERIMENTAL

9.3.1. Materials

Chitosan with average molecular weight (190~310 kDa - 80 % deacetylation degree (DD) ~ AGU molar mass of 169.57 g.mol^{-1}, Merck) was used as the biopolymeric precursor. The enaminic derivatives previously synthesized, diester (DEEM) (Mathias et al., 2025a), mononitrile (ECEA) (Mathias et al., 2025b), and dinitrile (EMM) (Pereira et al., 2023), were employed as adsorbent materials. A schematic representation of the molecular structures of chitosan and its corresponding derivatives is presented in Figure 1. Sodium Diclofenac (> 98.5%, Merck) was used as the model adsorbate without further purification.

9.3.2. Methods

9.3.2.1. Batch Adsorption Experiments

Batch adsorption experiments were conducted using 25 mg of adsorbent dispersed in 25 mL of Sodium Diclofenac solution (adsorbent dosage: 1 $g.L^{-1}$). All suspensions were agitated in Erlenmeyer flasks using an orbital shaker at the lowest available speed setting (rotation speed not specified) at 23 °C for 24 h to ensure equilibrium

For isotherm studies, ten initial diclofenac concentrations were investigated for each chitosan derivative. The concentration range was selected to adequately capture both low-coverage and near-saturation regimes (4-500 $mg.L^{-1}$).

All experiments were performed in triplicate, and average values were used for modeling. The adsorption capacity at equilibrium (q_e, $mg.g^{-1}$) was calculated using Equation 1:

$$q_e = \frac{(C_0 - C_e)V}{m} \quad (1)$$

where C_0 and C_e ($mg.L^{-1}$) are the initial and equilibrium concentrations, respectively, V (L) is the volume of the solution, and m (g) is the mass of adsorbent.

The removal percentage was calculated using Equation 2:

$$\%Removal = \frac{(C_0 - C_e)}{C_0} * 100 \quad (2)$$

Kinetic adsorption experiments were performed for all chitosan derivative using a fixed initial concentration. Aliquots were collected at predetermined time intervals (from 1 to 30 min, followed by extended intervals up to equilibrium). The total monitoring time ranged from approximately 40 to 250 min, depending on the chitosan derivative, until no significant variation in residual concentration was observed.

Experimental kinetic data were fitted using nonlinear least squares regression to pseudo-first-order (PFO), pseudo-second-order (PSO), Elovich, and Weber–Morris models. For PFO and PSO models, both rate constants and theoretical equilibrium adsorption capacities were obtained. Model adequacy was evaluated using adjusted R^2 values.

For both equilibrium and kinetic experiments, residual dye concentrations were determined using a Shimadzu UV-3600 spectrophotometer at the maximum absorption

wavelength of Sodium Diclofenac (288 nm). Calibration curves were constructed using standard solutions prepared under identical ionic strength and pH conditions. Prior to UV-Vis analysis, all samples were appropriately diluted to ensure absorbance values within the linear detection range (0.1–1.0). This procedure minimizes deviations from Beer–Lambert behavior and reduces potential aggregation effects of Sodium Diclofenac at higher concentrations.

9.3.2.2. Isotherm and Kinetic Modeling

Equilibrium adsorption data were analyzed using nonlinear least squares regression without linearization of the governing equations. The Langmuir, Freundlich, and Sips models were employed to describe adsorption isotherms.

The Langmuir model (Langmuir, 1918) assumes monolayer adsorption onto energetically homogeneous sites and is expressed as Equation 3:

$$q_e = \frac{q_{max} K_L C_e}{1 + K_L C_e} \tag{3}$$

where q_e ($mg.g^{-1}$) is the equilibrium adsorption capacity, q_{max} ($mg.g^{-1}$) is the maximum adsorption capacity, K_L ($L.mg^{-1}$) is the Langmuir constant, and C_e ($mg.L^{-1}$) is the equilibrium concentration.

The Freundlich model (Freundlich; Heller, 1939), which accounts for heterogeneous surface adsorption, is given by Equation 4:

$$q_e = K_F \sqrt[n]{C_e} \tag{4}$$

where K_F $(mg.g^{-1})(L.mg^{-1})^{1/n}$ is the Freundlich constant and n is the heterogeneity parameter.

The Sips model (Sips, 1948) (also known as Langmuir-Freundlich), which combines features of Langmuir and Freundlich behavior and accounts for surface heterogeneity at low concentrations while predicting saturation at high concentrations, is expressed as Equation 5:

$$q_e = \frac{q_{max} (k_S C_e)^n}{1 + (k_S C_e)^n} \tag{5}$$

where K_S is the Sips equilibrium constant and *n* represents the heterogeneity factor.

Kinetic data were fitted using pseudo-first-order (PFO), pseudo-second-order (PSO), Elovich, and Weber-Morris intraparticle diffusion models.

The nonlinear form of the PFO model (Corbett, 1972) is represented as Equation 6:

$$q_t = q_e(1 - e^{-k_1 t}) \quad (6)$$

where q_t ($mg.g^{-1}$) is the adsorption capacity at time t, q_e ($mg.g^{-1}$) is the equilibrium adsorption capacity, and k_1 (min^{-1}) is the rate constant.

The PSO model (Blanchard; Maunaye; Martin, 1984) is expressed as Equation 7:

$$q_t = \frac{q_e^2 k_2 t}{1 + q_e k_2 t} \quad (7)$$

where k_2 ($g.mg^{-1}min^{-1}$) is the PSO rate constant.

The Elovich model (Aharoni; Tompkins, 1970) is described by Equation 8:

$$q_t = \frac{1}{\beta} \ln (1 + \alpha\beta t) \quad (8)$$

where α ($mg.g^{-1}.min^{-1}$) is the initial adsorption rate and β ($g.mg^{-1}$) is related to surface coverage and activation energy.

The Weber-Morris (Weber; Morris, 1963) intraparticle diffusion model is expressed as Equation 9:

$$q_t = k_{diff} \sqrt[2]{t} + C \quad (9)$$

where k_{diff} ($mg.g^{-1}.min^{-1/2}$) is the intraparticle diffusion rate constant and C reflects boundary layer thickness.

9.4. RESULTS AND DISCUSSION

9.4.1. Structural modification and functional group density

The adsorption performance of chemically modified chitosan strongly depends on the nature and density of introduced functional groups. In the present study, chitosan with

a degree of deacetylation of approximately 80% was progressively modified with diester (DEEM), ester-nitrile (ECEA), and dinitrile (EMM) substituents, presented on Figure 1. The degree of substitution (DS) increased systematically from 0.29 (DEEM) to 0.73 (ECEA) and 0.91 (EMM), indicating a nearly complete conversion of the available amine sites in the most substituted material.

Considering the initial availability of primary amine groups in chitosan, the high DS achieved for EMM suggests a substantial alteration of the chemical environment of polymer backbone. The conversion of amine groups into enamine-linked substituents bearing electron-withdrawing functionalities significantly modifies the local electronic distribution along the biopolymer chains (Misra; Bhattacharyya, 2018).

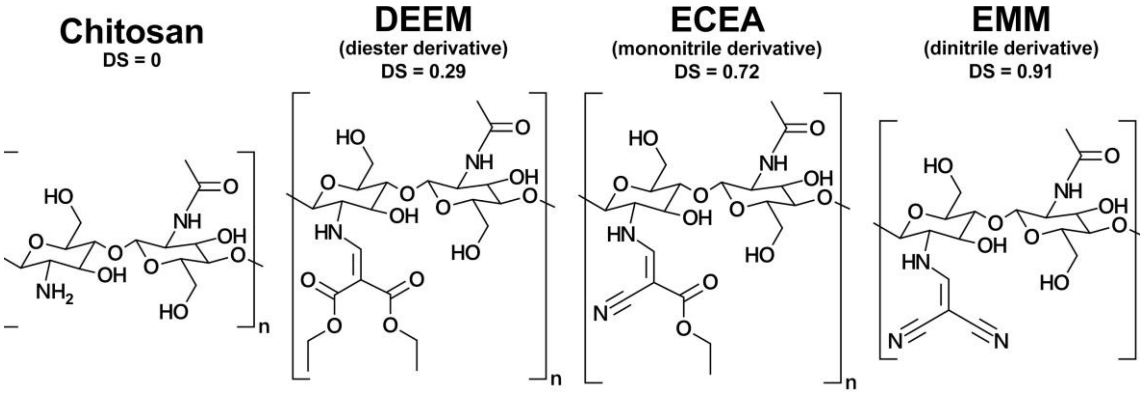

Figure 1 - Schematic representation of chitosan modification with diester (DEEM), ester–nitrile (ECEA), and dinitrile (EMM) substituents. Degree of substitution (DS) increases progressively from DEEM to EMM

The progressive incorporation of ester and nitrile moieties increases the density of polar substituents within the biopolymer matrix. While both groups exhibit electron-withdrawing character via inductive effects, nitrile functionalities possess a higher dipolar character, which may contribute more significantly to the modification of the interfacial microenvironment (Marqvorsen; Brinkø; Jensen, 2020; Mei et al., 2017; Zhang et al., 2019b). Therefore, the systematic increase in DS provides a suitable platform to evaluate the direct correlation between functional group density and adsorption performance toward anionic pharmaceuticals.

The zeta potential values of pristine and modified chitosan derivatives were measured at pH 7 to evaluate the contribution of electrostatic interactions to diclofenac adsorption. All materials exhibited near-neutral surface charge under the investigated conditions. Pristine chitosan presented a slightly positive potential (+0.37 ± 0.51 mV),

whereas DEEM and EMM showed slightly negative values (−0.07 ± 0.20 mV and −2.23 ± 0.38 mV, respectively), and ECEA remained close to neutrality (+0.15 ± 0.30 mV).

9.4.2. Adsorption isotherms and regime transition

The adsorption isotherms of sodium diclofenac onto pristine and modified chitosan materials (presented in Figure 2) revealed a pronounced dependence on functional group density. The experimental equilibrium capacity increased markedly with increasing degree of substitution (DS), following the order: Chitosan < DEEM < ECEA < EMM.

The maximum experimental adsorption capacity (q_e) reached 207.88 ± 0.09 $mg \cdot g^{-1}$ for EMM, which is in close agreement with the maximum capacity predicted by the Sips model (219.47 $mg \cdot g^{-1}$), indicating that saturation was effectively approached within the investigated concentration range (up to ~680 $mg \cdot L^{-1}$). In contrast, pristine chitosan exhibited a q_{max} of only 6.63 $mg \cdot g^{-1}$, demonstrating that chemical modification enhances adsorption performance, with the magnitude of the enhancement depending strongly on the chemical structure and electronic character of the introduced substituents.

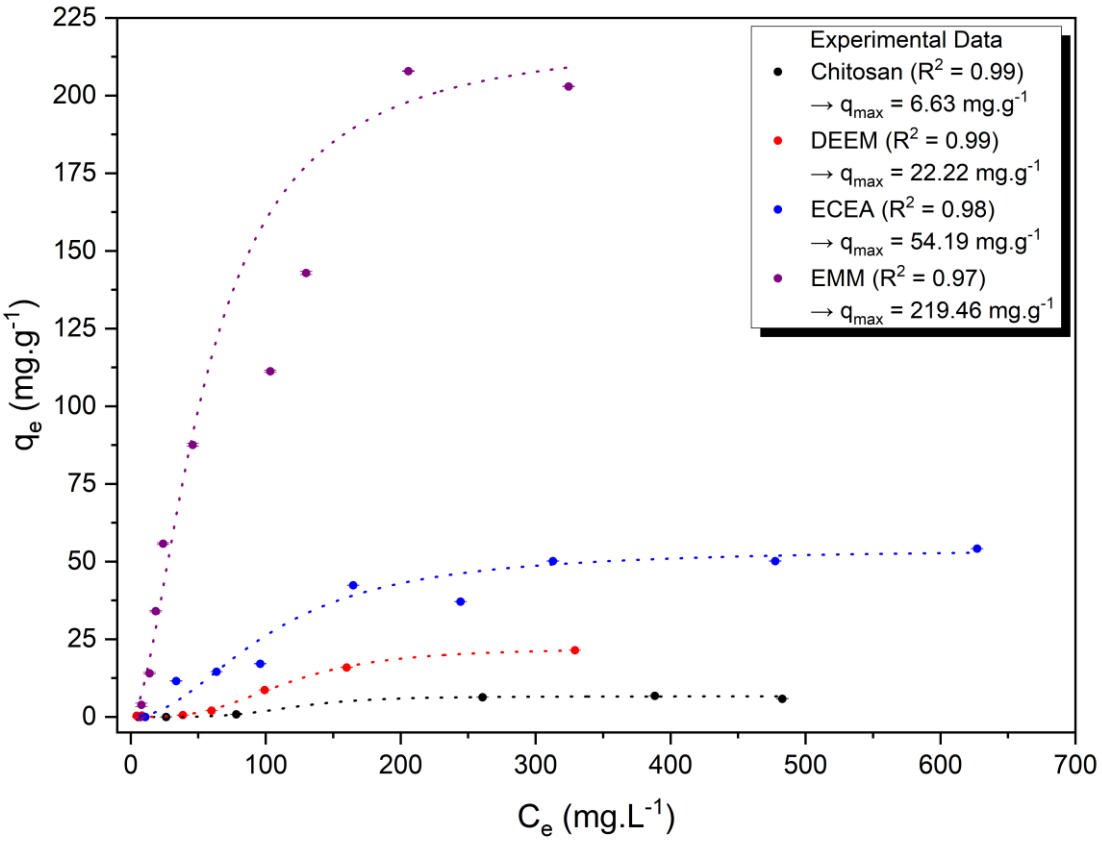

Figure 2 - Adsorption isotherms of sodium diclofenac onto pristine chitosan and its derivatives. Symbols represent experimental data, and dotted lines correspond to Sips model fitting.

The Sips model provided the best overall description of the equilibrium data, with higher correlation coefficients compared to the Langmuir and Freundlich models. Notably, the Langmuir model significantly overestimated q_{max} values for the modified materials, suggesting deviation from ideal monolayer behavior and the presence of energetic heterogeneity. The superior fitting (higher R^2) of the Sips model supports the existence of non-uniform adsorption sites (Sips, 1948), particularly for the chemically modified derivatives. The isotherm parameters obtained from non-linear fitting are summarized in Table 1.

Table 1 - Isotherm parameters obtained from non-linear fitting of Langmuir, Freundlich, and Sips models for sodium diclofenac adsorption onto pristine and modified chitosan derivatives.

Material	Langmuir Equation			Freundlich Equation			Sips Equation			
	q_{max}	K_L	R^2	*n*	K_F	R^2	q_{max}	*n*	K_S	R^2
	$mg.g^{-1}$	$L.mg^{-1}$	-	-	$mg^{1-1/n}.L^{1/n}.g^{-1}$	-	$mg.g^{-1}$	-	$(L.mg^{-1})^{1/n}$	-
Chitosan	17.03	0.0017	0.856	1.25	0.0579	0.819	6.63	4.367	0.0082	0.990
DEEM	85.89	0.0011	0.918	1.10	0.1184	0.907	22.22	3.148	0.0086	0.997
ECEA	78.29	0.0042	0.943	1.70	1.3652	0.875	54.19	2.042	0.0097	0.980
EMM	276.27	0.0108	0.954	2.02	12.665	0.883	219.47	1.712	0.0178	0.973

A clear quantitative correlation between the degree of substitution (DS) and adsorption capacity was observed (Figure 3). Increasing DS from 0.29 (DEEM) to 0.73 (ECEA) and 0.91 (EMM) resulted in a progressive, non-linear increase in q_{max}. While DEEM exhibited only a moderate enhancement relative to pristine chitosan, the transition from ECEA to EMM produced a substantial amplification of adsorption capacity, indicating that adsorption performance correlates strongly with functional group density rather than morphological factors. This trend is further supported by the progressive increase in the Sips affinity constant (K_S), which nearly doubled for EMM compared with the other materials, indicating enhanced interaction strength in addition to increased site availability. Such behavior is consistent with the higher density of electron-withdrawing substituents at larger DS values, which may promote more pronounced intramolecular charge transfer (ICT) within the conjugated enaminic segments, thereby increasing the polarity of the local environment and strengthening ion–dipole interactions with the diclofenac carboxylate. (Giraldo; Fajardo; Piraján, 2025; Murphy et al., 2023; Pereira; Gehlen, 2007; Tarai et al., 2020).

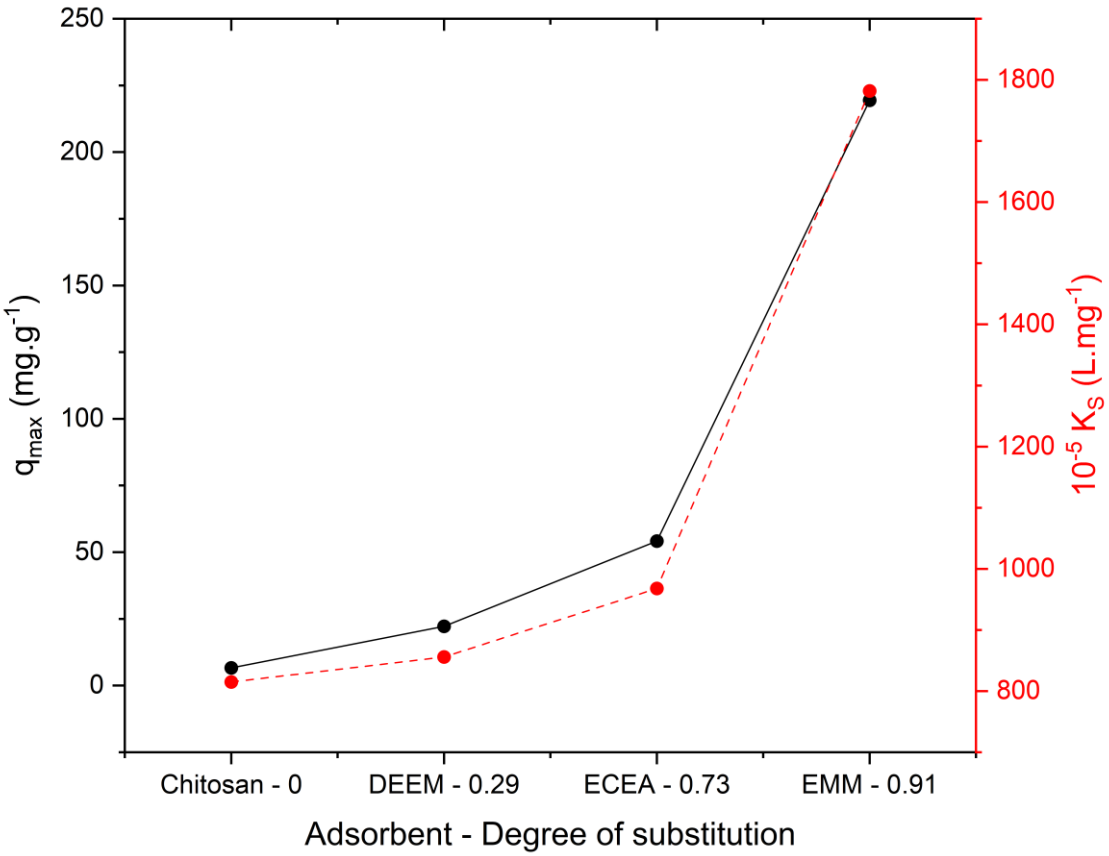

Figure 3 - Correlation between degree of substitution (DS) and adsorption parameters. (left-black-line) Maximum adsorption capacity (q_{max}) obtained from Sips model fitting. (right-red-dashed) Sips affinity constant (K_S) as a function of DS. Lines are provided as visual guides.

Beyond quantitative capacity differences, the shape of the adsorption isotherms also evolved with chemical modification. According to Giles classification, pristine chitosan and DEEM exhibited S-type (S-2) behavior, characterized by low initial affinity and cooperative adsorption at higher concentrations. In contrast, ECEA and EMM displayed L-type (L-2) isotherms, indicating higher affinity at low equilibrium concentrations and adsorption behavior approaching Langmuir-like characteristics. This transition from S-type to L-type behavior reflects a fundamental change in the adsorption regime induced by functionalization (Giles et al., 1960).

The shift in isotherm type suggests that the introduction of electron-withdrawing substituents modifies the interfacial environment of chitosan, enhancing its intrinsic affinity toward the anionic diclofenac species. For pristine chitosan and lightly substituted DEEM, adsorption appears to require a threshold surface coverage before significant uptake occurs. Conversely, for ECEA and especially for EMM, adsorption is favored

even at low concentrations, indicating stronger primary interactions between the adsorbent surface and pharmaceutical molecule.

9.4.3. Kinetic analysis and surface-controlled adsorption behavior

The adsorption kinetics of sodium diclofenac onto pristine and modified chitosan materials (represented in Figure 4) further elucidate the role of functional group density on adsorption behavior. Kinetic profiles were monitored up to 120 min, with equilibrium conditions confirmed after 24 h for isothermal experiments. Distinct differences in adsorption rate and kinetic modeling were observed among the materials.

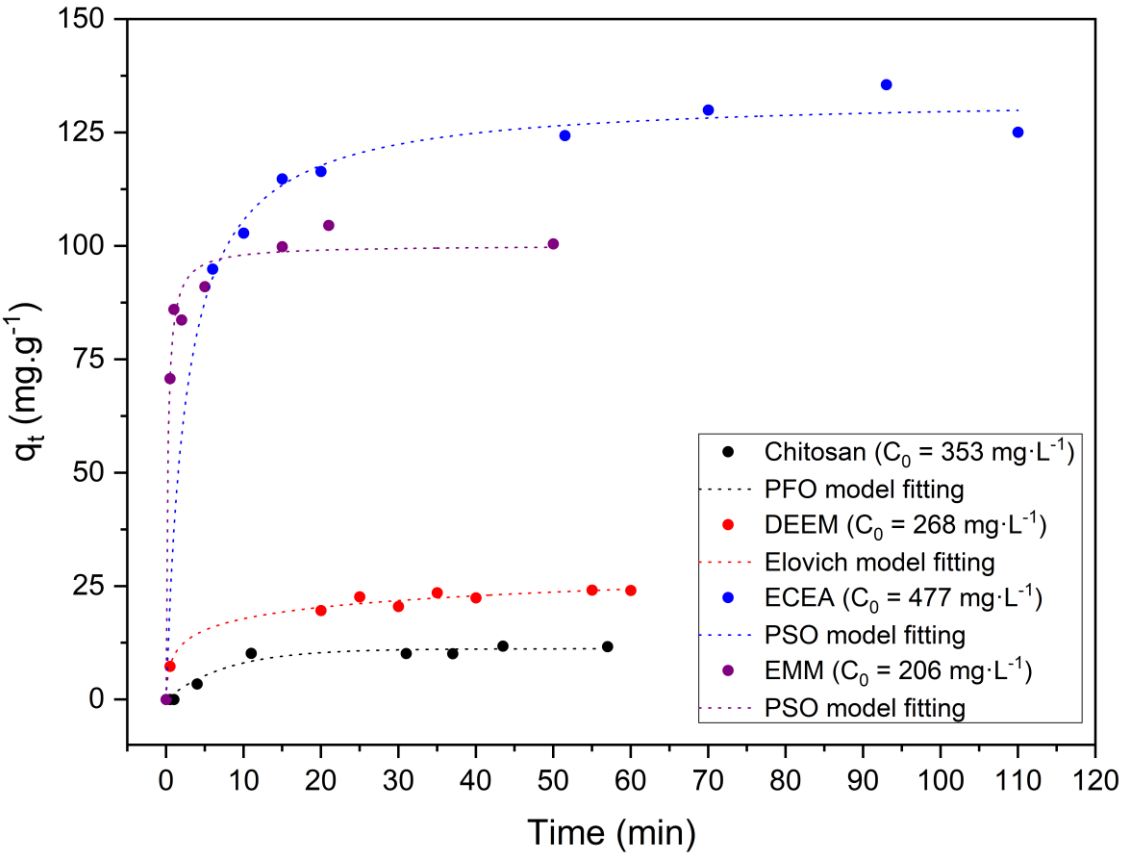

Figure 4 - Adsorption kinetics of sodium diclofenac onto pristine and modified chitosan derivatives. Symbols represent experimental data, and solid lines correspond to the best-fitting kinetic model for each material (PFO for chitosan, PSO for ECEA and EMM, and Elovich for DEEM).

Pristine chitosan and DEEM exhibited slower adsorption profiles, reaching equilibrium at approximately 60 min without a pronounced rapid initial uptake phase. In contrast, ECEA and especially EMM displayed faster adsorption rates, with EMM reaching equilibrium within approximately 50 min and ECEA within 120 min. The modified materials with higher DS presented a more defined initial adsorption stage,

indicating enhanced affinity at early contact times. It should be noted that the higher q_t values observed for ECEA at certain time intervals are partially associated with the higher initial concentration used in the kinetic experiment, which was more than twice that employed for EMM. As adsorption capacity is directly influenced by the available amount of solute in solution, this difference in C_0 contributes to the larger instantaneous uptake observed for ECEA despite the stronger intrinsic affinity exhibited by the EMM derivative.

Among the evaluated kinetic models, the pseudo-second-order (PSO) model provided the best fit for ECEA and EMM, as evidenced by higher correlation coefficients and strong agreement between calculated and experimental equilibrium capacities. This behavior suggests that the adsorption rate is governed predominantly by surface interactions rather than by simple mass transfer processes (Blanchard; Maunaye; Martin, 1984). In contrast, pristine chitosan showed better agreement with the pseudo-first-order (PFO) model, indicating weaker and less specific interactions with diclofenac (Corbett, 1972).

The Elovich model, typically associated with energetically heterogeneous surfaces, also showed strong fitting for the modified materials, particularly DEEM and EMM. This observation supports the presence of distributed active sites generated by chemical modification. However, the intraparticle diffusion model (Weber-Morris) exhibited comparatively low correlation coefficients, especially for ECEA and EMM, indicating that intraparticle diffusion is not the rate-limiting step under the experimental conditions (Singh et al., 2016). The kinetic parameters and fitting coefficients are presented in Table 2.

Table 2 - Kinetic parameters obtained from pseudo-first-order (PFO), pseudo-second-order (PSO), and Elovich models for sodium diclofenac adsorption onto pristine and modified chitosan derivatives.

Material	C_0	**PFO Equation**			**PSO Equation**			**Elovich Equation**		
		k_1t	q_e	R^2	q_e	k_2t	R^2	alfa	*beta*	R^2
		min^{-1}	$mg.g^{-1}$	-	$mg.g^{-1}$	$g.mg^{-1}.min^{-1}$	-	$mg.g^{-1}.min^{-1}$	$g.mg^{-1}$	-
Chitosan	353.12	0.128	11.19	0.945	13.39	0.009	0.930	2.147	0.292	0.903
DEEM	268.37	0.789	22.43	0.965	23.27	0.036	0.974	46.975	0.273	0.988
ECEA	477	0.196	126.04	0.977	132.94	0.003	0.993	8632.90	0.085	0.987
EMM	206.78	2.498	95.99	0.959	100.14	0.046	0.986	1571213.78	0.154	0.983

The progressive dominance of the PSO model with increasing DS reinforces the hypothesis that adsorption is controlled by surface interactions whose strength increases with functional group density. The higher *K* values observed for EMM further indicate enhanced interaction kinetics, consistent with the increased Sips affinity constant obtained from equilibrium modeling (Ezzati, 2020; Mahmoodi; Fattahi; Motevassel, 2021).

9.4.4. Mechanistic interpretation: role of electron-withdrawing substituents and ion-dipole stabilization

The equilibrium and kinetic results consistently indicate that adsorption performance is predominantly governed by the chemical nature and density of the introduced substituents rather than by surface charge or morphological factors. Although pristine chitosan possesses residual protonable amine groups, the zeta potential values at pH 7 were close to neutral for all materials, with EMM even exhibiting a slightly negative surface charge. Nevertheless, EMM showed the highest adsorption capacity and affinity. This lack of direct correlation between surface charge and adsorption performance suggests that classical electrostatic attraction is not the dominant mechanism under the investigated conditions (Gkika et al., 2023).

At pH 7, sodium diclofenac exists predominantly in its deprotonated carboxylate form ($-COO^-$). Therefore, stabilization of the anionic species at the polymer interface must arise from interactions other than simple Coulombic attraction. The progressive introduction of ester and nitrile groups provides a rational explanation for the observed behavior. Both functionalities exhibit electron-withdrawing character via inductive effects (–I), modifying the local electronic distribution along the biopolymer backbone. More importantly, nitrile groups possess a relatively high dipole moment, generating localized polar domains within the material (Misra; Bhattacharyya, 2018).

As the degree of substitution increases, the density of these polar domains becomes progressively higher. For DEEM, the presence of diester substituents moderately increases local polarity. For ECEA, the combination of one ester and one nitrile group per substituent further enhances dipolar character. For EMM, the incorporation of two nitrile groups per substituent results in the highest density of strongly polarized sites. This systematic increase in dipolar functionality parallels the observed

increase in adsorption capacity and Sips affinity constant (Gkika et al., 2023; Marqvorsen; Brinkø; Jensen, 2020; Zhang et al., 2019b).

The interaction between the carboxylate group of diclofenac and the dipolar nitrile-containing surface can be described as ion-dipole stabilization (Kaczmarek-Kędziera, 2020) (represented in Figure 5). In this context, the negatively charged carboxylate moiety is stabilized by the localized electric field generated by adjacent polar groups within the polymer matrix (Hammer et al., 2003). This stabilization does not arise from a positively charged nitrile or ester group. Instead, the electronic polarization originates from the conjugated enaminic framework formed between the chitosan amine and the electron-withdrawing substituents. In this system, amine nitrogen acts as an electron donor through its lone pair, whereas the nitrile/ester functionality acts as a strong electron acceptor. The resulting donor-acceptor arrangement within the π-conjugated segment promotes resonance-assisted intramolecular charge transfer (RAICT), which redistributes electron density along the conjugated backbone and generates localized partial positive character on the carbon framework adjacent to the amine (Pereira; Garcia Ferreira; Gehlen, 2005; Tarai et al., 2020). These polarized domains can stabilize the diclofenac carboxylate through oriented ion-dipole interactions even in the absence of a globally positive surface charge, which is consistent with the zeta potential results. The enhanced K_S values observed for EMM therefore not only reflect an increase in the number of available adsorption sites but also stronger local interaction fields arising from the more pronounced ICT associated with higher substitution density. The relevance of this conjugation-driven polarization is further supported by observations that disruption of the enaminic double bond suppresses the ICT character in these systems, indicating that the charge redistribution depends on the integrity of the π-conjugated donor–acceptor framework. (Giraldo; Fajardo; Piraján, 2025; Pereira; Gehlen, 2007).

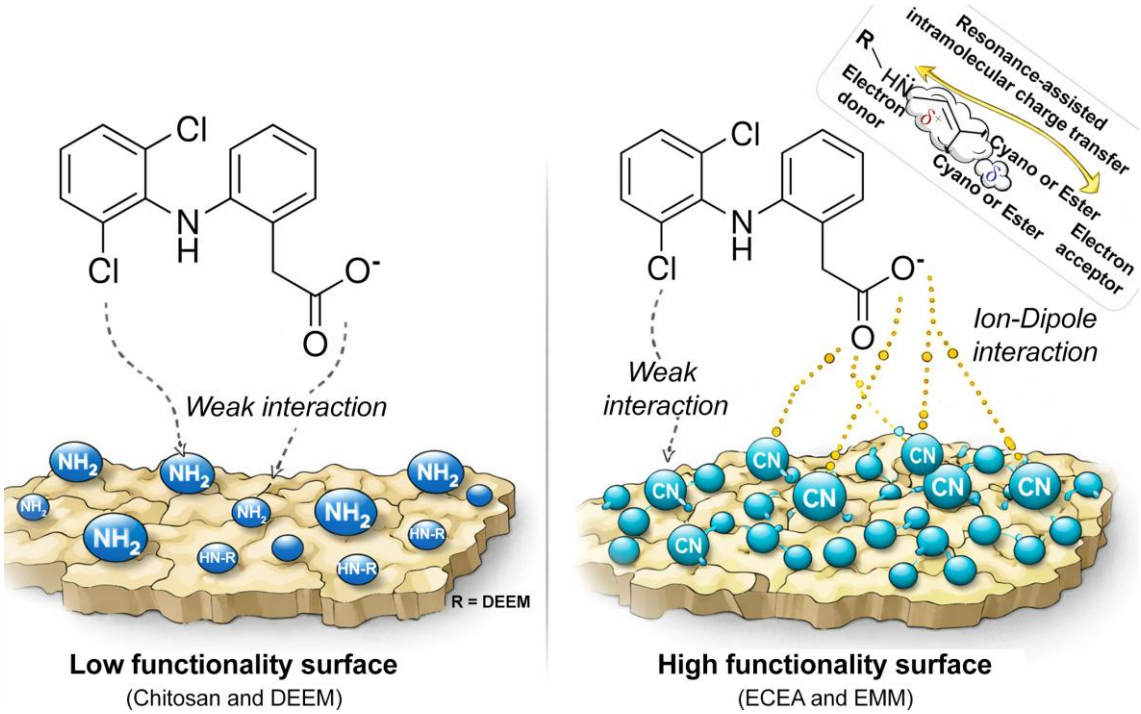

Figure 5 - Proposed adsorption mechanism of sodium diclofenac onto nitrile-modified chitosan derivatives. The progressive increase in functional group density enhances local dipolar interactions, promoting ion-dipole stabilization of the carboxylate group.

The transition from S-type to L-type isotherms with increasing DS supports this mechanistic interpretation. S-type behavior, observed for pristine chitosan and DEEM, suggests low initial affinity and possible cooperative effects at higher concentrations. In contrast, the L-type isotherms obtained for ECEA and EMM indicate stronger intrinsic affinity at low equilibrium concentrations, consistent with the presence of more energetically favorable interaction sites generated by higher densities of electron-withdrawing substituents (Inglezakis; Poulopoulos; Kazemian, 2018; Nicolle; Journot; Gerber-Lemaire, 2021; Shimizu; Matubayasi, 2023).

9.4.5. Integrated adsorption mechanism and performance correlation

The combined equilibrium, kinetic, and surface charge analyses allow a comprehensive interpretation of the adsorption mechanism governing diclofenac uptake onto the modified chitosan materials.

First, the absence of a direct correlation between zeta potential and adsorption capacity indicates that classical electrostatic attraction does not play a dominant role under the investigated conditions. At pH 7, all materials exhibited near-neutral surface charge, and the most efficient adsorbent (EMM) even displayed a slightly negative zeta potential. If Coulombic interactions between protonated amine groups and diclofenac

carboxylate were the primary driving force, higher adsorption would be expected for more positively charged surfaces. The experimental results clearly contradict this scenario. Therefore, electrostatic interactions can be considered secondary under these conditions.

Second, the strong correlation between the degree of substitution (DS) and the adsorption performance demonstrates that functional group density is the principal governing parameter. The progressive increase in DS from 0.29 (DEEM) to 0.73 (ECEA) and 0.91 (EMM) produced a marked and non-linear increase in adsorption capacity, culminating in an experimental q_e of 207.88 $mg \cdot g^{-1}$ for EMM. This enhancement occurred in the absence of significant morphological changes, reinforcing the conclusion that chemical modification of the biopolymer backbone is responsible for the improved performance.

Third, both isotherm modeling and kinetic behavior consistently support a surface-controlled mechanism driven by enhanced interaction strength. The Sips affinity constant increased with DS, and the transition from S-type to L-type isotherms reflects a shift from cooperative, low-affinity adsorption to a regime characterized by strong intrinsic affinity at low equilibrium concentrations. Additionally, the dominance of the pseudo-second-order model for the highly substituted materials and the poor fitting of the intraparticle diffusion model confirm that adsorption is governed primarily by surface interactions rather than diffusion limitations.

Taken together, the results indicate that the progressive incorporation of electron-withdrawing ester and nitrile groups increases the density of polar sites capable of stabilizing the diclofenac carboxylate via ion-dipole interactions. As DS approaches near-saturation (EMM, DS = 0.91), the interfacial environment becomes sufficiently enriched in dipolar functionalities to substantially enhance both adsorption capacity and affinity. The mechanism can therefore be described as a chemically driven, surface-controlled process in which ion-dipole stabilization predominates over classical electrostatic attraction (Kaczmarek-Kędziera, 2020).

This integrated interpretation establishes functional group density as the key descriptor governing adsorption performance in the present system and provides a rational framework for understanding the progressive enhancement observed from pristine chitosan to the dinitrile-modified derivative. Consistently, under the investigated conditions, the EMM derivative achieved removal efficiencies of up to 70%, whereas

pristine chitosan exhibited negligible removal (<3%), as can be seen in Table 3. This marked contrast further confirms that adsorption performance is primarily governed by chemical functionalization rather than by intrinsic properties of the native biopolymer.

Table 3 - Maximum removal efficiency of sodium diclofenac for pristine and modified chitosan derivatives under the investigated conditions.

Material	C_0 (mg.g^{-1})	Removal
Chitosan	353.12	2.38%
DEEM	268.37	9.06%
ECEA	477	32.31%
EMM	206.78	70%

To contextualize the adsorption performance of the synthesized materials, the maximum adsorption capacity obtained in this work was compared with values reported in the literature for diclofenac adsorption using various adsorbents. As summarized in Table 4, the EMM derivative exhibits competitive adsorption capacity compared with previously reported materials.

Table 4 - Comparison of adsorption capacity for diclofenac removal using chitosan-based and other reported adsorbents.

Adsorbent	Type	pH	q_{max}	Main interaction	References
COF/chitosan aerogels	Hybrid framework composite	7.0	557.1	Electrostatic	Li et al., (2026a)
Chitosan/amino silica–PVA grafted	Polymer–inorganic composite	5.0	493.8	Hydrogen bonds and electrostatic	Lu et al., (2020a)
Magnetic amine-functionalized chitosan	Magnetic composite	4.5	469.5	Hydrogen bonds and electrostatic	Liang et al., (2019)
Chitosan/cellulose functionalized with ethylenediamine	Biopolymer composite	4.5	444.4	Hydrogen bonds and acid-base	Hu et al., (2019)
Low-MW crosslinked chitosan	Crosslinked polymer	7.0	358.3	Hydrogen bonds and π-π	Riegger et al., (2018)
Medium-MW crosslinked chitosan	Crosslinked polymer	7.0	305.3	Hydrogen bonds and π-π	
Chitosan/MCC@PEI hydrogel beads	Polymer composite hydrogel	6.0	274.8	Electrostatic and hydrogen bonding	Wang et al., (2026a)
Crosslinked chitosan-epichlorohydrin	Crosslinked polymer	5.0	253.3	Hydrogen bonds and electrostatic	Lu et al., (2020b)
Magnetic quaternary chitosan–siliceous network	Magnetic inorganic composite	6.0	240.4	Electrostatic	Soares et al., (2019)
Glutaraldehyde-modified silica/chitosan	Polymer–silica composite	6.7	237.8	Covalent bonds	Machado et al., (2022)

Chitosan/EMM	**Chemically modified polymer**	7.0	219.5	Ion-dipole	This work
Magnetic chitosan ($ZnFe_2O_4$)	Magnetic composite	4.0	188.6	Hydrogen bonds and electrostatic	Dos Santos et al., (2019)
Chitosan/amino-hydroxyapatite composite	Polymer–mineral composite	6.0	139.5	Hydrogen bonds, electrostatic, and van der Waals forces	Pereira et al., (2020)
Zwitterionic chitosan grafted	Grafted polymer	4.0	120.0	Electrostatic	Malesic-Eleftheriadou et al., (2021)
Chitosan/*trans*-aconitic acid	Crosslinked polymer	4.0	84.56	Electrostatic	(Tzereme et al., 2019)
Chitosan/itaconic acid	Crosslinked polymer	4.0	67.12	Electrostatic	
Chitosan/succinic anhydride	Crosslinked polymer	4.0	64.49	Electrostatic	
Chitosan/maleic anhydride	Crosslinked polymer	4.0	47.07	Electrostatic	

An important aspect highlighted in Table is that many of the reported adsorbents rely on complex architectures such as composites, crosslinked networks, or multi-component systems to achieve high adsorption capacities. In contrast, the materials developed in this work are obtained through direct chemical modification of the chitosan backbone without the incorporation of inorganic fillers, nanomaterials, or polymeric blends. Despite this structural simplicity, the EMM derivative exhibits competitive adsorption performance, indicating that tuning the electronic environment of the polymer through functional group incorporation can be an effective strategy for enhancing adsorption. Moreover, these chemically modified chitosan derivatives may also serve as versatile platforms for the development of more complex materials, including composite systems or copolymeric architectures prepared through subsequent incorporation of inorganic phases or synthetic monomers.

9.5. CONCLUSION

The present study demonstrates that the adsorption performance of chitosan toward sodium diclofenac is strongly governed by the density and nature of chemically introduced functional groups. Progressive modification with diester, ester–nitrile, and dinitrile substituents resulted in a systematic increase in the degree of substitution (DS), reaching 0.91 for the EMM derivative. This near-saturation functionalization led to a dramatic enhancement in adsorption capacity, with a maximum experimental q_e of 207.88 $mg.g^{-1}$, representing an approximately 30-fold increase compared to pristine chitosan 6.63 $mg.g^{-1}$.

Equilibrium modeling revealed that the Sips equation provided the most accurate description of the adsorption behavior, and a clear transition from S-type to L-type isotherms was observed as DS increased. The progressive rise in the Sips affinity constant further confirmed that functionalization enhances not only the number of adsorption sites but also the interaction strength between the adsorbent and diclofenac molecules.

Kinetic analysis indicated a shift toward pseudo-second-order behavior for the highly substituted materials, while intraparticle diffusion was not identified as the rate-limiting step. In addition, the absence of correlation between zeta potential and adsorption capacity demonstrated that classical electrostatic attraction is not the dominant interaction mechanism at pH 7.

Comparison with previously reported adsorbents shows that the EMM derivative achieves competitive adsorption capacity despite its relatively simple structure, being obtained through direct chemical modification of chitosan without the need for composite architectures or inorganic additives. These findings highlight that tuning the electronic environment of the polymer backbone through controlled functionalization can significantly enhance adsorption performance.

Overall, the results indicate that diclofenac adsorption in this system is governed by a surface-controlled mechanism primarily driven by ion-dipole stabilization between the diclofenac carboxylate and the dipolar electron-withdrawing substituents introduced into the chitosan backbone. The strong correlation observed between functional group density and adsorption performance further identifies the degree of substitution as the key parameter controlling diclofenac uptake. These insights provide a rational basis for the design of chemically modified biopolymer adsorbents targeting the removal of anionic pharmaceutical contaminants from aqueous environments.

9.6. ACKNOWLEDGMENT

The authors acknowledge financial support from the Coordination for the Improvement of Higher Education Personnel (CAPES, Finance Code 001) through a doctorate scholarship. The authors also thank the Financiadora de Estudos e Projetos (FINEP) and the Federal University of São Carlos (UFSCar) for providing research infrastructure and laboratory facilities. Additionally, the authors acknowledge Grenoble INP – Pagora for hosting the research internship carried out through the CAPES PDSE program, which contributed to the development of this work.

10. CONCLUSÕES GERAIS

Esta tese teve como objetivo desenvolver e investigar derivados funcionalizados de quitosana obtidos por meio de reações de substituição nucleofílica vinílica com diferentes derivados alcoximetilênicos, bem como avaliar como a natureza eletrônica e a densidade dos grupos substituintes introduzidos influenciam as propriedades estruturais e o desempenho adsorptivo do material na remoção de contaminantes orgânicos em meio aquoso.

Inicialmente, foi demonstrada a viabilidade da modificação química da quitosana por meio da reação com etoximetilenomalononitrila, contendo grupos dinitrila. Esse estudo estabeleceu as bases da estratégia sintética adotada nesta tese, permitindo avaliar parâmetros fundamentais da reação, como o meio reacional, a razão molar entre reagente e unidades repetitivas da quitosana e o tempo de reação. Os resultados obtidos evidenciaram que a reação de substituição nucleofílica vinílica constitui uma rota eficiente para a funcionalização da quitosana, possibilitando a introdução de novos grupos funcionais diretamente na cadeia polimérica e alcançando elevados graus de funcionalização, com valores de grau de substituição de até 0,91.

Na sequência, foram investigadas novas rotas de modificação da quitosana utilizando diferentes derivados alcoximetilênicos contendo grupos funcionais com distintas características eletrônicas. A reação com Dietiletoximetilenomalonato levou à obtenção de um derivado contendo grupos diéster, enquanto a reação com Etil 2-ciano-3-etoxiacrilato resultou na formação de um derivado contendo grupos éster-nitrila. Para esses sistemas, a otimização das condições reacionais foi conduzida por meio de planejamento experimental, permitindo identificar as variáveis mais relevantes para o controle do grau de funcionalização do polímero. Os materiais obtidos foram amplamente caracterizados, evidenciando modificações significativas nas propriedades estruturais e físico-químicas da quitosana após a introdução dos diferentes substituintes.

A partir dos derivados obtidos, foi possível investigar de forma sistemática a relação entre natureza eletrônica dos grupos funcionais introduzidos e comportamento adsorptivo do material. Nos estudos de adsorção envolvendo o corante cristal violeta, observou-se que a modificação química da quitosana promoveu alterações significativas nas propriedades interfaciais do material, influenciando a afinidade entre o adsorvente e o corante em solução aquosa. Os resultados indicaram que a introdução de substituintes

contendo grupos eletronegativos contribui para modificar o ambiente eletrônico da superfície do polímero, favorecendo interações intermoleculares responsáveis pelo processo de adsorção.

De forma complementar, os estudos envolvendo a adsorção do fármaco diclofenaco permitiram avaliar a influência da densidade de grupos funcionais na eficiência do processo adsorptivo. Os resultados demonstraram que o aumento do grau de substituição ao longo da cadeia polimérica está diretamente relacionado ao aumento da capacidade de adsorção e da afinidade entre o material adsorvente e o contaminante, atingindo valores máximos da ordem de 219 mg g^{-1} para diclofenaco. De maneira semelhante, nos estudos com o corante cristal violeta, foram observadas elevadas capacidades de adsorção, alcançando valores da ordem de 383 mg g^{-1}, evidenciando a forte interação entre o material funcionalizado e moléculas com caráter catiônico. Esse comportamento reforça a importância da densidade e da natureza dos grupos funcionais introduzidos na determinação das propriedades adsorptivas do material.

De maneira geral, os resultados obtidos nesta tese demonstram que a modificação química da quitosana por meio de reações de substituição nucleofílica vinílica constitui uma estratégia eficiente para o desenvolvimento de novos materiais adsorventes baseados em biopolímeros. A introdução controlada de substituintes contendo grupos diéster, éster-nitrila e dinitrila permitiu modular as propriedades estruturais e interfaciais do material, evidenciando a forte relação entre estrutura química e desempenho adsorptivo.

Além disso, este trabalho contribui para o avanço do conhecimento sobre a aplicação de reações de substituição nucleofílica vinílica na modificação de biopolímeros, bem como para a compreensão dos efeitos da natureza eletrônica e da densidade de grupos funcionais sobre o comportamento adsorptivo de materiais poliméricos. Dessa forma, os resultados apresentados demonstram que derivados funcionalizados de quitosana obtidos por meio dessa abordagem sintética constituem materiais promissores para aplicações em processos de tratamento de água, especialmente na remoção de contaminantes orgânicos emergentes.

Como perspectivas futuras, destaca-se a possibilidade de investigar a aplicação desses materiais na remoção de outras classes de contaminantes orgânicos, bem como avaliar seu desempenho em sistemas mais complexos, como efluentes reais. Estudos

envolvendo a regeneração e reutilização dos materiais adsorventes também são relevantes para avaliar sua viabilidade em aplicações práticas de tratamento de água.

Além disso, a presença de grupos funcionais introduzidos ao longo da cadeia da quitosana abre novas possibilidades para modificações químicas adicionais. Esses materiais podem atuar como plataformas versáteis para o desenvolvimento de novos sistemas poliméricos, permitindo, por exemplo, a realização de reações de reticulação (crosslinking), enxertia de cadeias poliméricas (grafting) ou processos de polimerização iniciados por radicais livres. Tais estratégias podem levar à obtenção de materiais com arquiteturas mais complexas e propriedades ajustáveis, ampliando significativamente o campo de aplicação desses derivados de quitosana.

Dessa forma, os resultados apresentados nesta tese não apenas contribuem para o desenvolvimento de novos materiais adsorventes baseados em biopolímeros, mas também indicam que a modificação da quitosana por meio de reações de substituição nucleofílica vinílica constitui uma plataforma promissora para futuras investigações no desenvolvimento de materiais poliméricos funcionalizados.

11. REFERÊNCIAS

ABDULHAMEED, Ahmed Saud *et al.* Production of sustainable adsorbent of crosslinked chitosan-oxalate and modified mango (Mangifera indica L.) seed for highly efficient adsorption of crystal violet dye: Water treatment and biomass valorization. **Biomass and Bioenergy**, v. 199, p. 107889, ago. 2025.

ADHIKARI, Hari Sharan *et al.* Pyridine-Based NNS Tridentate Chitosan Thiosemicarbazones and Their Copper(II) Complexes: Synthesis, Characterization, and Anticancer Activity. **ACS Omega**, v. 7, n. 35, p. 30978–30988, 6 set. 2022.

ADHIKARI, Hari Sharan; GARAI, Aditya; YADAV, Paras Nath. Synthesis, characterization, and anticancer activity of chitosan functionalized isatin based thiosemicarbazones, and their copper(II) complexes. **Carbohydrate Research**, v. 526, p. 108796, abr. 2023.

AHARONI, C.; TOMPKINS, F. C. Kinetics of Adsorption and Desorption and the Elovich Equation. *In*: *[S.l.: S.n.]*. p. 1–49.

AHMAD, Rais; EJAZ, Mohammad Osama. Efficient adsorption of crystal violet (CV) dye onto benign chitosan-modified l-cysteine/bentonite (CS-Cys/Bent) bionanocomposite: Synthesis, characterization and experimental studies. **Dyes and Pigments: An International Journal**, v. 216, n. 111305, p. 111305, 2023.

AHMED, S. F. *et al.* Recent developments in physical, biological, chemical, and hybrid treatment techniques for removing emerging contaminants from wastewater. **Journal of Hazardous Materials**, v. 416, p. 125912, 15 ago. 2021.

AIJAZ, Shaikh Aliya; SHAFI AND, Zaryab; SHAHID, Mohammad. Magnetized phyto-adsorbents for industrial dye removal: functionalization and mechanistic insights for sustainable wastewater remediation. **RSC Advances**, v. 16, n. 1, p. 758–777, 22 dez. 2025.

ALAMRI, Abdullah Ali *et al.* Synthesis of Schiff bases based on Chitosan, thermal stability and evaluation of antimicrobial and antitumor activities. **Scientific Reports**, v. 15, n. 1, p. 892, 6 jan. 2025.

ALESSANDRETTI, Ingridy *et al.* Removal of diclofenac from wastewater: A comprehensive review of detection, characteristics and tertiary treatment techniques. **Journal of Environmental Chemical Engineering**, v. 9, n. 6, p. 106743, 1 dez. 2021.

AMJLEF, Asma *et al.* Adsorptive properties investigation of natural sand as adsorbent for methylene blue removal from contaminated water. **Nanotechnology for Environmental Engineering**, v. 6, n. 2, p. 26, 11 ago. 2021.

ATHAVALE, Rujuta *et al.* Tuning the surface charge properties of chitosan nanoparticles. **Materials Letters**, v. 308, p. 131114, 1 fev. 2022.

AUS DER BEEK, Tim *et al.* Pharmaceuticals in the environment—Global occurrences and perspectives. **Environmental Toxicology and Chemistry**, v. 35, n. 4, p. 823–835, 14 dez. 2015.

BELPAIRE, Claude *et al.* Toxic textile dyes accumulate in wild European eel Anguilla anguilla. **Chemosphere**, v. 138, p. 784–791, nov. 2015.

BENETTAYEB, Asmaa *et al.* Chitosan Nanoparticles as Potential Nano-Sorbent for Removal of Toxic Environmental Pollutants. **Nanomaterials**, v. 13, n. 3, p. 447, 21 jan. 2023.

BENJAMIN, Daniel J. *et al.* Redefine statistical significance. **Nature Human Behaviour 2017 2:1**, v. 2, n. 1, p. 6–10, 1 set. 2017.

BERRADI, Mohamed *et al.* Textile finishing dyes and their impact on aquatic environs. **Heliyon**, v. 5, n. 11, p. e02711, nov. 2019.

BLANCHARD, G.; MAUNAYE, M.; MARTIN, G. Removal of heavy metals from waters by means of natural zeolites. **Water Research**, v. 18, n. 12, p. 1501–1507, jan. 1984.

BLANK, Carrine E.; HINMAN, Nancy W. Cyanobacterial and algal growth on chitin as a source of nitrogen; ecological, evolutionary, and biotechnological implications. **Algal Research**, v. 15, p. 152–163, 1 abr. 2016.

BRATSKAYA, Svetlana *et al.* Chitosan Gels and Cryogels Cross-Linked with Diglycidyl Ethers of Ethylene Glycol and Polyethylene Glycol in Acidic Media. **Biomacromolecules**, v. 20, n. 4, p. 1635–1643, 8 abr. 2019.

BRUGNEROTTO, J. *et al.* An infrared investigation in relation with chitin and chitosan characterization. **Polymer**, v. 42, n. 8, p. 3569–3580, 1 abr. 2001.

CAÑAS, Ana Isabel; DELGADO, Jean Paul; GARTNER, Carmiña. Biocompatible scaffolds composed of chemically crosslinked chitosan and gelatin for tissue engineering. **Journal of Applied Polymer Science**, v. 133, n. 33, 5 set. 2016.

CAO, Yan *et al.* New chitosan Schiff base and its nanocomposite: Removal of methyl green from aqueous solution and its antibacterial activities. **International Journal of Biological Macromolecules**, v. 192, p. 1–6, dez. 2021.

CASTILLO, Andrés M.; PATINY, Luc; WIST, Julien. Fast and accurate algorithm for the simulation of NMR spectra of large spin systems. **Journal of Magnetic Resonance**, v. 209, n. 2, p. 123–130, 1 abr. 2011.

CHAO, An-Chong *et al.* Enzymatic grafting of carboxyl groups on to chitosan — to confer on chitosan the property of a cationic dye adsorbent. **Bioresource Technology**, v. 91, n. 2, p. 157–162, 2004.

CHATTERJEE, S. *et al.* Chitosan from Mucor rouxii: production and physico-chemical characterization. **Process Biochemistry**, v. 40, n. 1, p. 395–400, jan. 2005.

CHEN, Qizhou *et al.* Progress in Research of Chitosan Chemical Modification Technologies and Their Applications. **Marine Drugs**, v. 20, n. 8, p. 536, 21 ago. 2022.

CHEN, Sung-Ching *et al.* A novel pH-sensitive hydrogel composed of N,O-carboxymethyl chitosan and alginate cross-linked by genipin for protein drug delivery. **Journal of Controlled Release**, v. 96, n. 2, p. 285–300, abr. 2004.

CHRISTIAN, Gary D.; PURDY, William C. The residual current in orthophosphate medium. **Journal of Electroanalytical Chemistry (1959)**, v. 3, n. 6, p. 363–367, jun. 1962.

CORBETT, John F. Pseudo first-order kinetics. **Journal of Chemical Education**, v. 49, n. 10, p. 663, 1 out. 1972.

CORPUS, R. M. B. *et al.* Emerging pollutants in waste water: Challenges and advancements in treatment technology. **IOP Conference Series: Earth and Environmental Science**, v. 1372, n. 1, p. 012037, 1 jul. 2024.

CRINI, Grégorio; LICHTFOUSE, Eric. Advantages and disadvantages of techniques used for wastewater treatment. **Environmental Chemistry Letters**, v. 17, n. 1, p. 145–155, 31 mar. 2019.

CROISIER, Florence; JÉRÔME, Christine. Chitosan-based biomaterials for tissue engineering. **European Polymer Journal**, v. 49, n. 4, 2013.

CUNHA, Ana G. *et al.* What Is the Real Value of Chitosan's Surface Energy? **Biomacromolecules**, v. 9, n. 2, p. 610–614, 1 fev. 2008.

CZECHOWSKA-BISKUP, Renata *et al.* Determination of Degree of Deacetylation of Chitosan. *In*: Warsow: 2011.

DAUGHTON, C. G.; TERNES, T. A. Pharmaceuticals and personal care products in the environment: agents of subtle change? **Environmental Health Perspectives**, v. 107, n. suppl 6, p. 907–938, dez. 1999.

DAVID, Grégoire *et al.* Exploring the potential of gas-phase esterification to hydrophobize the surface of micrometric cellulose particles. **European Polymer Journal**, v. 115, p. 138–146, 1 jun. 2019.

DELEZUK, Jorge Augusto de Moura; PAVINATTO, Adriana; CAMPANA FILHO, Sergio Paulo. Effects of chitosan characteristics on its thermal stability. **Brazilian Journal of Thermal Analysis**, v. 3, n. 3–4, p. 36–39, 30 dez. 2014.

DESBRIÈRES, Jacques; GUIBAL, Eric. Chitosan for wastewater treatment. **Polymer International**, v. 67, n. 1, p. 7–14, 25 jan. 2018.

DOS SANTOS, Juliana M. N. *et al.* Alternative synthesis for ZnFe2O4/chitosan magnetic particles to remove diclofenac from water by adsorption. **International Journal of Biological Macromolecules**, v. 131, p. 301–308, 2019.

DRABCZYK, Anna *et al.* Physicochemical investigations of chitosan-based hydrogels containing Aloe vera designed for biomedical use. **Materials**, v. 13, n. 14, 1 jul. 2020.

EBRAHIMZADEH, Farzaneh. N-Alkylation of Amines Utilizing Magnetic Nano Chitosan Functionalized with EDTA/Co(II). **Letters in Organic Chemistry**, v. 22, n. 2, p. 147–153, fev. 2025.

EL KNIDRI, Hakima *et al.* Extraction, chemical modification and characterization of chitin and chitosan. **International Journal of Biological Macromolecules**, v. 120, p. 1181–1189, 1 dez. 2018.

EL-ARABY, Abir *et al.* Chitosan, chitosan derivatives, and chitosan-based nanocomposites: eco-friendly materials for advanced applications (a review). **Frontiers in Chemistry**, v. 11, p. 1327426, 4 jan. 2023.

EZZATI, Rohollah. Derivation of Pseudo-First-Order, Pseudo-Second-Order and Modified Pseudo-First-Order rate equations from Langmuir and Freundlich isotherms for adsorption. **Chemical Engineering Journal**, v. 392, p. 123705, jul. 2020.

FIRMANSYAH, Mochamad Lutfi; ALWAN, Yousef; ULLAH, Nisar. A comprehensive review on the adsorptive removal of pharmaceutical pollutants: Occurrence, toxicology, molecular simulation and mechanistic insights. **Talanta Open**, v. 12, 1 dez. 2025.

FOO, K. Y.; HAMEED, B. H. Insights into the modeling of adsorption isotherm systems. **Chemical Engineering Journal**, v. 156, n. 1, p. 2–10, jan. 2010.

FOWKES, Frederick M. Dispersion Force Contributions to Surface and Interfacial Tensions, Contact Angles, and Heats of Immersion. *In*: *[S.l.: S.n.]*. p. 99–111.

FRASER-REID, B. O.; TATSUKA, K.; THIEM, J. **Glycoscience**. Berlin, Heidelberg: Springer Berlin Heidelberg, 2008.

FREUNDLICH, Herbert.; HELLER, Wilfried. The Adsorption of cis - and trans-Azobenzene. **Journal of the American Chemical Society**, v. 61, n. 8, p. 2228–2230, 1 ago. 1939.

GATIAL, Anton *et al.* The vibrational and NMR spectra, conformations and ab initio calculations of aminomethylene, propanedinitrile and itsN-methyl derivatives. **Structural Chemistry**, v. 7, n. 1, p. 17–36, fev. 1996.

GILES, C. H. *et al.* Studies in adsorption. Part XI. A system of classification of solution adsorption isotherms, and its use in diagnosis of adsorption mechanisms and in measurement of specific surface areas of solids. **Journal of the Chemical Society (Resumed)**, p. 3973, 1960.

GIRALDO, Liliana; FAJARDO, Carlos A. Guerrero; PIRAJÁN, Juan Carlos Moreno. Innovative chitosan/graphene oxide composites: A thermodynamic and calorimetric

approach to pharmaceutical waste removal from water. **Results in Engineering**, v. 25, p. 103697, mar. 2025.

GKIKA, Despina A. *et al.* Modified chitosan adsorbents in pharmaceutical simulated wastewaters: A review of the last updates. **Carbohydrate Polymer Technologies and Applications**, v. 5, p. 100313, jun. 2023.

HAJ, Nadia Q.; MOHAMMED, Mohsin O.; MOHAMMOOD, Luqman E. Synthesis and Biological Evaluation of Three New Chitosan Schiff Base Derivatives. **ACS Omega**, v. 5, n. 23, p. 13948–13954, 16 jun. 2020.

HAMEED, Abdul Zubar *et al.* Chitosan: A Sustainable Material for Multifarious Applications. **Polymers**, v. 14, n. 12, p. 2335, 9 jun. 2022.

HAMMER, Nathan I. *et al.* Dipole-bound anions of carbonyl, nitrile, and sulfoxide containing molecules. **The Journal of Chemical Physics**, v. 119, n. 7, p. 3650–3660, 15 ago. 2003.

HAN, Guijuan *et al.* Sulfonated chitosan and phosphorylated chitosan coated polylactide membrane by polydopamine-assisting for the growth and osteogenic differentiation of MC3T3-E1s. **Carbohydrate Polymers**, v. 229, p. 115517, fev. 2020.

HEMMAMI, Hadia *et al.* Chitosan, Its Derivatives, Sources, Preparation Methods, and Applications: A Review. **Journal of the Turkish Chemical Society Section A: Chemistry**, v. 11, n. 1, p. 341–364, 4 fev. 2024.

HEMMATI, Vahid; KARIMI, Gholamreza; MOWLA, Dariush. High-efficiency removal of methyl orange from wastewaters using polyimide/chitosan-MoS2-UiO-66 nanofiber adsorbents. **Scientific Reports**, v. 16, n. 1, p. 2929, 17 dez. 2025.

HEUX, L. *et al.* Solid State NMR for Determination of Degree of Acetylation of Chitin and Chitosan. **Biomacromolecules**, v. 1, n. 4, p. 746–751, 1 dez. 2000.

HU, Dalin *et al.* Adsorption of diclofenac sodium on bilayer amino-functionalized cellulose nanocrystals/chitosan composite. **Journal of Hazardous Materials**, v. 369, p. 483–493, maio 2019.

HU, Ke-Jin *et al.* Rapid extraction of high-quality chitosan from mycelia of Absidia Glauca. **Journal of Food Biochemistry**, v. 23, n. 2, p. 187–196, jun. 1999.

HUANG, Jianying *et al.* Synthesis of sulfonated chitosan and its antibiofilm formation activity against E. coli and S. aureus. **International Journal of Biological Macromolecules**, v. 129, p. 980–988, 15 maio 2019.

HUQ, Tanzina *et al.* Sources, production and commercial applications of fungal chitosan: A review. **Journal of Bioresources and Bioproducts**, v. 7, n. 2, p. 85–98, 1 maio 2022.

IMGHARN, Abdelaziz *et al.* Synthesis and characterization of polyaniline-based biocomposites and their application for effective removal of Orange G dye using adsorption in dynamic regime. **Chemical Physics Letters**, v. 778, p. 138811, set. 2021.

INGLEZAKIS, Vassilis J.; POULOPOULOS, Stavros G.; KAZEMIAN, Hossein. Insights into the S-shaped sorption isotherms and their dimensionless forms. **Microporous and Mesoporous Materials**, v. 272, p. 166–176, dez. 2018.

ISLAM, Touhidul *et al.* Synthetic Dyes for Textile Colouration: Process, Factors and Environmental Impact. **Textile & Leather Review**, v. 5, p. 327–373, 8 ago. 2022.

JAFERNIK, Karolina *et al.* Chitosan-Based Nanoparticles as Effective Drug Delivery Systems—A review. **Molecules 2023, Vol. 28, Page 1963**, v. 28, n. 4, p. 1963, 18 fev. 2023.

KACZMAREK-KĘDZIERA, Anna. Gas Phase Computational Study of Diclofenac Adsorption on Chitosan Materials. **Molecules**, v. 25, n. 11, p. 2549, 30 maio 2020.

KAZACHENKO, Aleksandr S. *et al.* Synthesis optimization, DFT and physicochemical study of chitosan sulfates. **Journal of Molecular Structure**, v. 1245, p. 131083, 5 dez. 2021.

KIM, Tae-Young; PARK, Seung-Shik; CHO, Sung-Yong. Adsorption characteristics of Reactive Black 5 onto chitosan beads cross-linked with epichlorohydrin. **Journal of Industrial and Engineering Chemistry**, v. 18, n. 4, p. 1458–1464, jul. 2012.

KOU, Shijie Gabriel; PETERS, Linda M.; MUCALO, Michael R. Chitosan: A review of sources and preparation methods. **International Journal of Biological Macromolecules**, v. 169, p. 85–94, 1 fev. 2021.

KOWANGA, David K.; NYAIRO, Wilfrida N. A review on decontamination of aqueous systems using chitosan-derived adsorbents. **Discover Environment 2025 3:1**, v. 3, n. 1, p. 237-, 17 nov. 2025.

KOZBIAL, Andrew *et al.* Study on the Surface Energy of Graphene by Contact Angle Measurements. **Langmuir**, v. 30, n. 28, p. 8598–8606, 22 jul. 2014.

LANGMUIR, Irving. The adsorption of gases on plane surfaces of glass, mica and platinum. **Journal of the American Chemical Society**, v. 40, n. 9, p. 1361–1403, 1 set. 1918.

LEHOCKÝ, Marián. Environmental Applications of Chitosan Derivatives and Chitosan Composites. **Polymers 2025, Vol. 17, Page 2583**, v. 17, n. 19, p. 2583, 24 set. 2025.

LI, Chen *et al.* Evaluation of chitosan-ferulic acid microcapsules for sustained drug delivery: Synthesis, characterizations, and release kinetics in vitro. **Journal of Molecular Structure**, v. 1227, p. 129353, 5 mar. 2021a.

LI, Chong *et al.* A numerical solution to the effects of surface roughness on water–coal contact angle. **Scientific Reports 2021 11:1**, v. 11, n. 1, p. 1–12, 11 jan. 2021b.

LI, Hao-Ze *et al.* Novel cationic covalent organic framework/chitosan aerogels for enhanced adsorption of diclofenac sodium: Performance and mechanism. **Separation and Purification Technology**, v. 380, n. 135551, p. 135551, 2026a.

LI, Jianghua *et al.* Chitosan-Based Nanomaterials for Drug Delivery. **Molecules : A Journal of Synthetic Chemistry and Natural Product Chemistry**, v. 23, n. 10, 16 out. 2018.

LI, Xueyan *et al.* Constructing dual mechanisms for efficient Cr(VI) remediation: An organic-inorganic synergistic modification strategy for chitosan-sodium alginate composites. **Colloids and Surfaces A: Physicochemical and Engineering Aspects**, v. 734, p. 139350, abr. 2026b.

LIAKOS, Efstathios V. *et al.* Chitosan Adsorbent Derivatives for Pharmaceuticals Removal from Effluents: A Review. **Macromol**, v. 1, n. 2, p. 130–154, 11 maio 2021.

LIANG, Xue Xue *et al.* Efficient adsorption of diclofenac sodium from aqueous solutions using magnetic amine-functionalized chitosan. **Chemosphere**, v. 217, p. 270–278, 2019.

LIU, Bingzhi *et al.* A novel carboxyl-rich chitosan-based polymer and its application for clay flocculation and cationic dye removal. **The Science of the Total Environment**, v. 640–641, p. 107–115, 2018.

LIU, Rui; GUO, Qing-Wei; YANG, Wein-Duo. Chitosan-promoted synthesis of high-performance hybrid MoS2/N-doped carbon electrode materials for flexible supercapacitors. **Journal of Electroanalytical Chemistry**, v. 999, p. 119551, dez. 2025.

LIU, Yonglin *et al.* Multiple removal mechanism of EDTA-Enteromorpha-Chitosan-based hydrogel for organic/inorganic cation-anion complex pollution. **International Journal of Biological Macromolecules**, v. 339, p. 149953, jan. 2026.

LU, Ming Zhu *et al.* Recent Advances in Alkenyl sp2 C–H and C–F Bond Functionalizations: Scope, Mechanism, and Applications. **Chemical Reviews**, v. 122, n. 24, p. 17479–17646, 28 dez. 2022.

LU, Yuqing *et al.* PEI-modified core-shell/bead-like amino silica enhanced poly (vinyl alcohol)/chitosan for diclofenac sodium efficient adsorption. **Carbohydrate Polymers**, v. 229, n. 115459, p. 115459, 2020a.

LU, Yuqing *et al.* Fabrication of cross-linked chitosan beads grafted by polyethylenimine for efficient adsorption of diclofenac sodium from water. **International Journal of Biological Macromolecules**, v. 145, p. 1180–1188, 2020b.

LUAN, Fang *et al.* Preparation and Characterization of Quaternized Chitosan Derivatives and Assessment of Their Antioxidant Activity. **Molecules**, v. 23, n. 3, p. 516, 26 fev. 2018.

MA, Guiping *et al.* Synthesis and properties of photosensitive chitosan derivatives(1). **International Journal of Biological Macromolecules**, v. 46, n. 5, p. 558–561, jun. 2010.

MABUZA, Major Melusi; MAHLOBO, Mandlenkosi George Robert. Adsorption Equilibria and Systematic Thermodynamics Analysis of Carbon Dioxide Sequestration on South African Coals Using Nonlinear Three-Parameter Models: Sips, Tóth, and Dubinin–Astakhov. **Energies**, v. 18, n. 10, p. 2646, 20 maio 2025.

MACHADO, Thaís Strieder *et al.* Synthesis of glutaraldehyde-modified silica/chitosan composites for the removal of water-soluble diclofenac sodium. **Carbohydrate Polymers**, v. 277, n. 118868, p. 118868, 2022.

MACIEL, Vinicius *et al.* Electrostatic Self-Assembled Chitosan-Pectin Nano- and Microparticles for Insulin Delivery. **Molecules**, v. 22, n. 10, p. 1707, 12 out. 2017.

MAHMOODI, Hossein; FATTAHI, Moslem; MOTEVASSEL, Mohsen. Graphene oxide–chitosan hydrogel for adsorptive removal of diclofenac from aqueous solution: preparation, characterization, kinetic and thermodynamic modelling. **RSC Advances**, v. 11, n. 57, p. 36289–36304, 2021.

MALEKI, Gisoo; WOLTERING, Ernst J.; MOZAFARI, M. R. Applications of chitosan-based carrier as an encapsulating agent in food industry. **Trends in Food Science & Technology**, v. 120, p. 88–99, 1 fev. 2022.

MALESIC-ELEFTHERIADOU, Neda *et al.* Simultaneous removal of anti-inflammatory pharmaceutical compounds from an aqueous mixture with adsorption onto chitosan zwitterionic derivative. **Colloids and Surfaces. A, Physicochemical and Engineering Aspects**, v. 619, n. 126498, p. 126498, 2021.

MANZO-VALENCIA, Sandra *et al.* Arsenate Adsorption from Aqueous Solutions Using Chitosan/Fe-Nanoparticles Composite Microspheres. **ChemistrySelect**, v. 9, n. 14, 12 abr. 2024.

MARQVORSEN, Mikkel H. S.; BRINKØ, Anne; JENSEN, Henrik H. On the electron withdrawing nature of ethers in glycosylation chemistry. **Carbohydrate Research**, v. 487, p. 107886, jan. 2020.

MASSOUDINEJAD, Mohamadreza; RASOULZADEH, Hassan; GHADERPOORI, Mansour. Magnetic chitosan nanocomposite: Fabrication, properties, and optimization for adsorptive removal of crystal violet from aqueous solutions. **Carbohydrate Polymers**, v. 206, p. 844–853, 2019.

MATHIAS, Samir Leite *et al.* Synthesis of a chitosan derivative via conjugate addition-elimination with diethylethoxymethylenemalonate and its physicochemical properties. **Reactive and Functional Polymers**, v. 208, p. 106167, mar. 2025a.

MATHIAS, Samir Leite *et al.* Optimized One-Pot reaction and characterization of a cyanoethoxyethylated chitosan. **International Journal of Biological Macromolecules**, v. 310, n. 143500, maio 2025b.

MCMURRY, John E. **Organic Chemistry**. 9th. ed. *[S.l.]*: Cengage Learning, 2015.

MEI, Ju *et al.* Comparative study of the dicyanovinyl-functionalized 1,1-dimethyl-2,3,4,5-tetraphenylsilole derivatives on their structures, properties, and applications in thiol detection. **Dyes and Pigments**, v. 141, p. 366–378, jun. 2017.

MERZENDORFER, Hans. Insect chitin synthases: a review. **Journal of Comparative Physiology B**, v. 176, n. 1, p. 1–15, 2 jan. 2006.

MILATA, V. *et al.* Gould-Jacobs reaction of 6-amino-2,3-diphenylquinoxaline. **Monatshefte für Chemie - Chemical Monthly**, v. 126, n. 12, p. 1349–1358, dez. 1995.

MISRA, Ramprasad; BHATTACHARYYA, S. P. **Intramolecular Charge Transfer**. *[S.l.]*: Wiley, 2018.

MOLANDER, Gary A.; SINGARAM, Bakthan; BROWN, Herbert C. Conjugate addition-elimination in the reaction of B-1-alkenyl-9-borabicyclo[3.3.1]nonanes with 4-methoxy-3-buten-2-one. A convenient new route to conjugated dienones. **The Journal of Organic Chemistry**, v. 49, n. 25, p. 5024–5025, 1 dez. 1984.

MONIKA *et al.* Towards the critical understanding of selected vibrational features in biologically important dicyano aromatic conjugated molecules: Importance of electron donating/withdrawal groups and geometry associated with dicyano group. **Spectrochimica Acta Part A: Molecular and Biomolecular Spectroscopy**, v. 224, p. 117419, jan. 2020.

MOONEY, E. F.; WINSON, P. H. Nitrogen Magnetic Resonance Spectroscopy. **Annual Reports on NMR Spectroscopy**, v. 2, n. C, p. 125–152, 1 jan. 1969.

MURPHY, Orla P. *et al.* A Review on the Adsorption Isotherms and Design Calculations for the Optimization of Adsorbent Mass and Contact Time. **ACS Omega**, v. 8, n. 20, p. 17407–17430, 23 maio 2023.

NA, Ha-Na *et al.* Synthesis of O-carboxylated low molecular chitosan with azido phenyl group: Its application for adhesion prevention. **Macromolecular Research**, v. 18, n. 10, p. 1001–1007, 23 out. 2010.

NANDA, Biswarup *et al.* Acylated chitosan anchored paclitaxel loaded liposomes: Pharmacokinetic and biodistribution study in Ehrlich ascites tumor bearing mice. **International Journal of Biological Macromolecules**, v. 122, p. 367–379, fev. 2019.

NASAB, Shima Ghanavati *et al.* Decolorization of crystal violet from aqueous solutions by a novel adsorbent chitosan/nanodiopside using response surface methodology and artificial neural network-genetic algorithm. **International Journal of Biological Macromolecules**, v. 124, p. 429–443, 2019.

NICOLLE, Laura; JOURNOT, Céline M. A.; GERBER-LEMAIRE, Sandrine. Chitosan Functionalization: Covalent and Non-Covalent Interactions and Their Characterization. **Polymers**, v. 13, n. 23, p. 4118, 26 nov. 2021.

NIEMCZYK, Agata *et al.* Biofunctional catheter coatings based on chitosan-fatty acids derivatives. **Carbohydrate Polymers**, v. 225, p. 115263, dez. 2019.

ONJIA, Antonije. **Chemometric Approach to the Experiment Optimization and Data Evaluation in Analytical Chemistry**. 1. ed. Belgrade: Faculty of Technology and Metallurgy, 2016. v. 1

ONYEKACHUKWU, Erwin *et al.* Low-Cost Adsorbents for the Removal of Pharmaceuticals from Surface Waters. **Water**, v. 17, n. 17, p. 2619, 4 set. 2025.

OWENS, D. K.; WENDT, R. C. Estimation of the surface free energy of polymers. **Journal of Applied Polymer Science**, v. 13, n. 8, p. 1741–1747, 9 ago. 1969.

PAL, Anjali; PAN, Satyajit; SAHA, Sandip. Synergistically improved adsorption of anionic surfactant and crystal violet on chitosan hydrogel beads. **Chemical Engineering Journal (Lausanne, Switzerland: 1996)**, v. 217, p. 426–434, 2013.

PAL, Sucharita *et al.* Biomimetic aerogels with hierarchical honeycomb architecture for superior CO2 adsorption, selectivity, and structural integrity. **Communications Materials**, v. 6, n. 1, p. 130, 2 jul. 2025.

PAULA, Haroldo C. B. *et al.* Eco-friendly synthesis of an alkyl chitosan derivative. **International Journal of Biological Macromolecules**, v. 163, p. 1591–1598, 15 nov. 2020.

PEREIRA, M. B. B. *et al.* Amino hydroxyapatite/chitosan hybrids reticulated with glutaraldehyde at different pH values and their use for diclofenac removal. **Carbohydrate Polymers**, v. 236, n. 116036, p. 116036, 2020.

PEREIRA, Robson Valentim; GARCIA FERREIRA, Ana Paula; GEHLEN, Marcelo Henrique. Excited-State Intramolecular Charge Transfer in 9-Aminoacridine Derivative. **The Journal of Physical Chemistry A**, v. 109, n. 27, p. 5978–5983, 1 jul. 2005.

PEREIRA, Robson Valentim; GEHLEN, Marcelo Henrique. Polymerization and Conformational Transition of Poly(methacrylic Acid) Probed by Electronic Spectroscopy of Aminoacridines. **Macromolecules**, v. 40, n. 6, p. 2219–2223, 20 mar. 2007.

PEREIRA, Robson V *et al.* A new route to produce chitosan derivatives: nucleophilic vinylic substitution with ethoxymethylenemalononitrile. **Polymer International**, v. 72, n. 3, p. 376–382, 22 mar. 2023.

PETRIE, Bruce *et al.* Fate of drugs during wastewater treatment. **TrAC Trends in Analytical Chemistry**, v. 49, p. 145–159, set. 2013.

PIEGAT, Agnieszka *et al.* Antibacterial Activity of N,O-Acylated Chitosan Derivative. **Polymers**, v. 13, n. 1, p. 107, 29 dez. 2020.

PRABAHAR, Kousalya; UDHUMANSHA, Ubaidulla; QUSHAWY, Mona. Optimization of Thiolated Chitosan Nanoparticles for the Enhancement of in Vivo Hypoglycemic Efficacy of Sitagliptin in Streptozotocin-Induced Diabetic Rats. **Pharmaceutics**, v. 12, n. 4, p. 300, 26 mar. 2020.

QASEMI, Elham; ANBIA, Mansoor; REZAIE, Marzie. Synergetic effect of heteroatoms doping and functional groups of graphene-chitosan magnetic nanocomposite on enhancement of heavy metal sorption. **Reactive and Functional Polymers**, v. 214, p. 106283, set. 2025.

QIN, Jiao *et al.* Adsorption behavior of crystal violet from aqueous solutions with chitosan–graphite oxide modified polyurethane as an adsorbent. **Journal of Applied Polymer Science**, v. 132, n. 17, 2015.

QIU, Tianyang *et al.* Development of 3D-Printed Sulfated Chitosan Modified Bioresorbable Stents for Coronary Artery Disease. **Frontiers in Bioengineering and Biotechnology**, v. 8, 19 maio 2020.

RAFIQUE, Ammara *et al.* Chitosan functionalized poly(vinyl alcohol) for prospects biomedical and industrial applications: A review. **International journal of biological macromolecules**, v. 87, p. 141–154, 1 jun. 2016.

RAVI, Seenu *et al.* Covalent organic polymer/chitosan multifunctional granular aerogels for diclofenac sodium removal from water. **Chemical Engineering Journal**, v. 492, p. 152334, jul. 2024.

RIEGGER, Benjamin R. *et al.* Chitosan nanoparticles via high-pressure homogenization-assisted miniemulsion crosslinking for mixed-matrix membrane adsorbers. **Carbohydrate Polymers**, v. 201, p. 172–181, 2018.

RODRIGUEZ-NARVAEZ, Oscar M. *et al.* A review on emerging water contaminants and the application of sustainable removal technologies. **Case Studies in Chemical and Environmental Engineering**, v. 6, p. 100219, 1 dez. 2022.

ROUT, Prangya R. *et al.* Treatment technologies for emerging contaminants in wastewater treatment plants: A review. **Science of the Total Environment**, v. 753, 20 jan. 2021.

RUIZ-HERRERA, José; SENTANDREU, Rafael. Fungal Cell Wall Synthesis and Assembly. *In*: **Current Topics in Medical Mycology**. 3. ed. Florida: Boca Raton, 1989. p. 168–217.

SALAMA, Ahmed; HESEMANN, Peter. Guanylated chitosan derivatives for the adsorption of anionic dyes: Performance and mechanism. **International Journal of Biological Macromolecules**, v. 311, n. Pt 2, 1 jun. 2025.

SALEHI, Ehsan *et al.* Advances in nanocomposite and nanostructured chitosan membrane adsorbents for environmental remediation: A review. **Desalination**, v. 527, p. 115565, abr. 2022.

SALEHI, Ehsan; DARAEI, Parisa; ARABI SHAMSABADI, Ahmad. A review on chitosan-based adsorptive membranes. **Carbohydrate Polymers**, v. 152, p. 419–432, 5 nov. 2016.

SANTILLI, Arthur A.; BRUCE, William F.; OSDENE, T. S. Enamine Derivatives of Malonic Acid with Pharmacologic Activities. **Journal of Medicinal Chemistry**, v. 7, n. 1, p. 68–72, 1 jan. 1964.

SCHATZ, Christophe *et al.* Formation of Polyelectrolyte Complex Particles from Self-Complexation of N-Sulfated Chitosan. **Biomacromolecules**, v. 6, n. 3, p. 1642–1647, 1 maio 2005.

SEGAL, L. *et al.* An Empirical Method for Estimating the Degree of Crystallinity of Native Cellulose Using the X-Ray Diffractometer. **Textile Research Journal**, v. 29, n. 10, p. 786–794, 1959.

SELVAKUMAR, N.; BARSHILIA, Harish C.; RAJAM, K. S. Effect of substrate roughness on the apparent surface free energy of sputter deposited superhydrophobic polytetrafluoroethylene coatings: A comparison of experimental data with different theoretical models. **Journal of Applied Physics**, v. 108, n. 1, 1 jul. 2010.

SHAGDAROVA, Balzhima; ZHUIKOVA, Yulia; IL'INA, Alla. Adsorbent Materials Based on Modified Chitosan for Purification of Aqueous Media from Pharmaceutical Residues, Primarily Antibiotics. **Polymers**, v. 17, n. 19, p. 2601, 26 set. 2025.

SHEHAB, Mohammed Ahmed *et al.* Recent progress in adsorptive removal of different contaminants by chitosan-based aerogel. **RSC Advances**, v. 15, n. 36, p. 29727–29742, 2025.

SHIBATA, Masayuki; KUNTZLEMAN, Thomas S. Intermolecular Interactions: Dipole–Dipole, Dipole–Induced Dipole, and London Dispersion Forces. **Journal of Chemical Education**, v. 86, n. 12, p. 1469, 1 dez. 2009.

SHIMIZU, Seishi; MATUBAYASI, Nobuyuki. Cooperativity in Sorption Isotherms. **Langmuir**, v. 39, n. 39, p. 13820–13829, 3 out. 2023.

SHUKLA, Sudheesh K. *et al.* Chitosan-based nanomaterials: A state-of-the-art review. **International Journal of Biological Macromolecules**, v. 59, p. 46–58, 2013.

SHUKLA, Sushil Kumar *et al.* Removal of crystal violet by Cu-chitosan nano-biocomposite particles using Box–Behnken design. **Journal of Environmental Chemical Engineering**, v. 9, n. 5, p. 105847, out. 2021.

SILVERSTEIN, R. M. *et al.* **Spectrometric Identification of Organic Compounds**. *[S.l.]*: Wiley, 2014.

SINGH, Devendra Kumar *et al.* Modeling of adsorption behavior of the amine-rich GOPEI aerogel for the removal of As(III) and As(V) from aqueous media. **RSC Advances**, v. 6, n. 61, p. 56684–56697, 2016.

SIPS, Robert. On the Structure of a Catalyst Surface. **The Journal of Chemical Physics**, v. 16, n. 5, p. 490–495, 1 maio 1948.

SIRVIÖ, Juho Antti *et al.* Aqueous Modification of Chitosan with Itaconic Acid to Produce Strong Oxygen Barrier Film. **Biomacromolecules**, v. 22, n. 5, p. 2119–2128, 10 maio 2021.

SOARES, Sofia F. *et al.* Magnetic quaternary chitosan hybrid nanoparticles for the efficient uptake of diclofenac from water. **Carbohydrate Polymers**, v. 203, p. 35–44, 2019.

SONG, Zhaoping *et al.* Application of Chitin/Chitosan and Their Derivatives in the Papermaking Industry. **Polymers**, v. 10, n. 4, p. 389, 1 abr. 2018.

SUDARSHAN, Shanmugam *et al.* Impact of textile dyes on human health and bioremediation of textile industry effluent using microorganisms: current status and future prospects. **Journal of Applied Microbiology**, v. 134, n. 2, 16 fev. 2023.

SUN, Xiaojie *et al.* A composite sponge based on alkylated chitosan and diatom-biosilica for rapid hemostasis. **International Journal of Biological Macromolecules**, v. 182, p. 2097–2107, jul. 2021.

TARAI, Arup *et al.* ICT and AIE Characteristics Two Cyano-Functionalized Probes and Their Photophysical Properties, DFT Calculations, Cytotoxicity, and Cell Imaging Applications. **Molecules 2020, Vol. 25, Page 585**, v. 25, n. 3, p. 585, 29 jan. 2020.

TENG, Wee Lin *et al.* Concurrent production of chitin from shrimp shells and fungi. **Carbohydrate Research**, v. 332, n. 3, p. 305–316, jun. 2001.

TERKULA IBER, Benedict *et al.* A Review of Various Sources of Chitin and Chitosan in Nature. **Journal of Renewable Materials**, v. 10, n. 4, p. 1097–1123, 2022.

TZEREME, Areti *et al.* Chitosan Grafted Adsorbents for Diclofenac Pharmaceutical Compound Removal from Single-Component Aqueous Solutions and Mixtures. **Polymers**, v. 11, n. 3, p. 497, 14 mar. 2019.

VAKILI, Mohammadtaghi *et al.* Application of chitosan and its derivatives as adsorbents for dye removal from water and wastewater: A review. **Carbohydrate Polymers**, v. 113, p. 115–130, nov. 2014.

VIENO, Niina; SILLANPÄÄ, Mika. Fate of diclofenac in municipal wastewater treatment plant — A review. **Environment International**, v. 69, p. 28–39, ago. 2014.

VILAR JUNIOR, José Carlos *et al.* Physicochemical and Antibacterial Properties of Chitosan Extracted from Waste Shrimp Shells. **International Journal of Microbiology**, v. 2016, n. 1, p. 5127515, 1 jan. 2016.

VITHALKAR, Sarika H.; JUGADE, Ravin M. Adsorptive removal of crystal violet from aqueous solution by cross-linked chitosan coated bentonite. **Materials Today: Proceedings**, v. 29, p. 1025–1032, 2020.

WANG, Hongyu *et al.* Efficient removal of diclofenac sodium from water by chitosan/microcrystalline cellulose@polyethyleneimine hydrogel beads: Adsorption performance and mechanism study. **Journal of Environmental Sciences (China)**, v. 159, p. 480–489, 2026a.

WANG, Liang *et al.* Removal of Pb2+ from wastewater using composite microspheres based on chitosan crosslinked with aminated silica. **International Journal of Biological Macromolecules**, v. 337, p. 149580, jan. 2026b.

WANG, Lingshuang *et al.* Tissue adhesives based on chitosan for skin wound healing: Where do we stand in this era? A review. **International Journal of Biological Macromolecules**, v. 258, p. 129115, 1 fev. 2024.

WANG, Wenqian *et al.* Chitosan Derivatives and Their Application in Biomedicine. **International Journal of Molecular Sciences**, v. 21, n. 2, 2 jan. 2020.

WANG, Xuan *et al.* Progresses in lignin, cellulose, starch, chitosan, chitin, alginate, and gum/carbon nanotube (nano)composites for environmental applications: A review. **International Journal of Biological Macromolecules**, v. 241, p. 124472, 30 jun. 2023.

WARREN-VEGA, Walter M. *et al.* A Current Review of Water Pollutants in American Continent: Trends and Perspectives in Detection, Health Risks, and Treatment Technologies. **International Journal of Environmental Research and Public Health**, v. 20, n. 5, p. 4499, 1 mar. 2023.

WEBER, Walter J.; MORRIS, J. Carrell. Kinetics of Adsorption on Carbon from Solution. **Journal of the Sanitary Engineering Division**, v. 89, n. 2, p. 31–59, abr. 1963.

XIAO, Xue *et al.* Analysis of trace malachite green, crystal violet, and their metabolites in zebrafish by surface-coated probe nanoelectrospray ionization mass spectrometry. **Talanta**, v. 217, p. 121064, set. 2020.

XU, Kaimeng *et al.* Novel flexible, strong, thermal-stable, and high-barrier switchgrass-based lignin-containing cellulose nanofibrils/chitosan biocomposites for food packaging. **Industrial Crops and Products**, v. 179, p. 114661, 1 maio 2022.

YAN, Han *et al.* Removal of various cationic dyes from aqueous solutions using a kind of fully biodegradable magnetic composite microsphere. **Chemical Engineering Journal (Lausanne, Switzerland: 1996)**, v. 223, p. 402–411, 2013.

YANG, Dongxue *et al.* Functionalized chitosan electrospun nanofiber membranes for heavy-metal removal. **Polymer**, v. 163, p. 74–85, 1 fev. 2019.

YEUL, Vijay S.; RAYALU, Sadhana S. Unprecedented Chitin and Chitosan: A Chemical Overview. **Journal of Polymers and the Environment**, v. 21, n. 2, p. 606–614, 14 jun. 2013.

YU, Chen; KECEN, Xiao; XIAOSAI, Qu. Grafting Modification of Chitosan. **Biopolymer Grafting: Synthesis and Properties**, p. 295–364, 1 jan. 2018.

ZAINOL ABIDIN, Nurul Alyani *et al.* The Potential of Insects as Alternative Sources of Chitin: An Overview on the Chemical Method of Extraction from Various Sources. **International Journal of Molecular Sciences**, v. 21, n. 14, p. 4978, 15 jul. 2020.

ZDZIENNICKA, Anna *et al.* Components and parameters of liquids and some polymers surface tension at different temperature. **Colloids and Surfaces A: Physicochemical and Engineering Aspects**, v. 529, p. 864–875, set. 2017.

ZHANG, Shu *et al.* Curdlan sulfate–O-linked quaternized chitosan nanoparticles: potential adjuvants to improve the immunogenicity of exogenous antigens via intranasal vaccination. **International Journal of Nanomedicine**, v. Volume 13, p. 2377–2394, abr. 2018.

ZHANG, Songhong *et al.* Chromatographic separation of ovalbumin by novel chitosan and poly(butyl methacrylate) nanogels-based anion-exchange cryogels. **Journal of Chromatography A**, v. 1758, p. 466188, set. 2025.

ZHANG, Ying *et al.* N-alkylated chitosan/graphene oxide porous sponge for rapid and effective hemostasis in emergency situations. **Carbohydrate Polymers**, v. 219, p. 405–413, set. 2019a.

ZHANG, Yuecheng *et al.* Dicyanovinyl substituted push–pull chromophores: effects of central C=C/phenyl spacers, crystal structures and application in hydrazine sensing. **Physical Chemistry Chemical Physics**, v. 21, n. 6, p. 3218–3226, 2019b.

ZHAO, Dongying *et al.* Biomedical Applications of Chitosan and Its Derivative Nanoparticles. **Polymers**, v. 10, n. 4, p. 462, 23 abr. 2018a.

ZHAO, Jiangbin *et al.* Chitosan adsorbent reinforced with citric acid modified β-cyclodextrin for highly efficient removal of dyes from reactive dyeing effluents. **European Polymer Journal**, v. 108, p. 212–218, 1 nov. 2018b.